15th German Ferrofluid Workshop

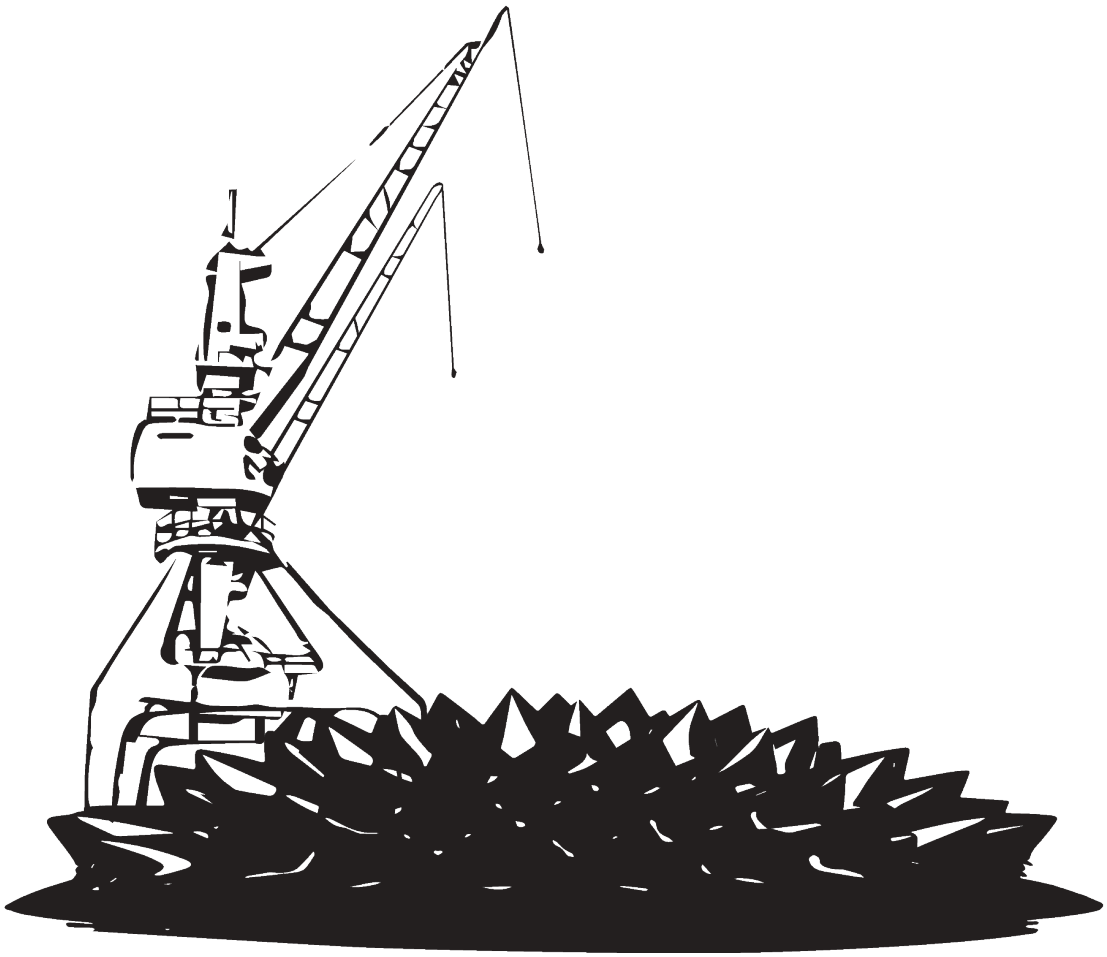

Rostock, June 15th - 17th, 2015

Program of the 15th Ferrofluid Workshop 2015

Rostock, June 15th – 17th 2015

Monday, June 15th

Tuesday, June 16th

Theoretical Methods

10:00 Coffee Break

Imaging and Applications

13:30 Guided city tour/Meeting of the Ferrofluidverein Deutschland e.V.

Experimental Methods

17:00 Postersession

20:00 Dinner

Wednesday, June 17th

Experimental Methods

12:30 Closing

Poster:

Preparation and Characterization

Experimental Methods

Imaging and Applications

Theoretical Methods

Biomedical Applications

Core-Shell Hybrid Materials by Producing a Protein Corona Around Magnetic Nanoparticles

A. Weidner[1], C. Gräfe[2], M. v.d. Lühe[3,4], H. Remmer[5], J.H. Clement[2,4], D. Eberbeck[6], D. Fischer[4,7], F. Ludwig[5], R. Müller[8], F.H. Schacher[3,4], F. von Eggeling[4,8,9], S. Dutz[1*]

[1] *Institute of Biomedical Engineering and Informatics (BMTI), Technische Universität Ilmenau*
[2] *Klinik für Innere Medizin II, Abteilung Hämatologie und Internistische Onkologie, Universitätsklinikum Jena*
[3] *Institute of Organic and Macromolecular Chemistry, Friedrich-Schiller-University Jena*
[4] *Jena Center for Soft Matter (JCSM), Friedrich-Schiller-University Jena*
[5] *Institut für Elektrische Messtechnik und Grundlagen der Elektrotechnik, Technische Universität Braunschweig*
[6] *Physikalisch-Technische Bundesanstalt, Berlin*
[7] *Institute of Pharmacy, Department of Pharmaceutical Technology, Friedrich-Schiller-University Jena*
[8] *Leibniz Institute of Photonic Technology (IPHT), Jena*
[9] *Institute of Physical Chemistry, Friedrich-Schiller-University & ENT Department, University Hospital Jena*

** Corresponding author: silvio.dutz@tu-ilmenau.de*

Introduction

When nanomaterials (e.g. magnetic nanoparticles; MNP) are exposed to the blood circulation, a protein corona consisting of various components is formed immediately. The composition of the corona as well as their amount bound to the particle surface is dependent on different factors, e.g. particle size and surface charge [1, 2]. The actual composition of the formed protein corona might be of major importance for cellular uptake of magnetic nanoparticles [3, 4]. The aim of our experiments is to analyze the formation of the protein corona during *in vitro* serum incubation in dependence of incubation time and temperature as well as to investigate the biocompatibility of serum coated MNP.

Methods

MNP were prepared following the alkaline precipitation route and coated with different shells (amino-dextran, dextran, carboxymethyl-dextran, polyethylenimine, poly-*tert*-butoxycarbonylamino acrylic acid). The obtained core/shell nanoparticles were incubated in fetal calf serum (FCS) for defined times and temperatures within a water bath with the desired temperature to generate the protein corona on the surface of the particles. Before, during, and after the incubation the physical properties of the particles were determined by a variety of methods (e.g. MRX - magnetorelaxometry, zeta-potential, VSM – vibrating sample magnetometry, TGA - thermogravimetric analysis, and TEM – transmission electron microscopy). Additionally, the incubated nanoparticles were applied to a TBS (Tris-buffered saline) polyacrylamide gradient gel under denaturing conditions and protein bands were visualized by silver staining. The effect of incubated particles on cell viability was tested for human brain micro vascular endothelial cells (HBMEC) by the CellTiter Glo™ Cell Viability Assay and for long term viability up to 96 h by real time cell analysis (RTCA).

Results

The MRX measurements showed that immediately (seconds) after the contact of MNP and FCS a protein corona is formed on the surface of the coated MNP. This formation led to an increase of particle size and a slight agglomeration of the particles, which was relatively constant during the first minutes of incubation. A longer incu-

bation (from hours to days) resulted in a stronger agglomeration of the FCS incubated MNP.
Since the zeta potential of FCS incubated MNP varies as a function of particle shell and incubation temperature, it is clearly demonstrated, that surface charge of particle shell as well as incubation temperature have an influence on the composition of the corona.

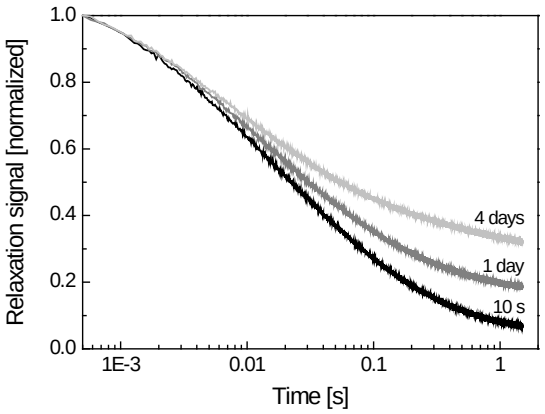

Fig. 1: Temporal evolution of the MRX signal after adding 140 µL FCS to 10 µL DEAE coated MNP suspension for incubation times up to 4 days, curves are normalized to be '1' for time point 0.5 ms.

Quantitative analysis (gel electrophoresis) of serum incubated particles revealed a relatively constant amount of bound proteins during the first minutes of serum incubation. After a longer incubation (> 10 min) a considerably higher amount of surface proteins was determined for incubation temperatures below 40 °C. For incubation temperatures above 50 °C, the influence of time was less significant which might be attributed to an immediate denaturation of proteins during incubation. Overall, the analysis of the molecular weight distribution of proteins found in the corona revealed a clear influence of incubation time and temperature on corona composition.
The solid fraction of the protein corona on the surface of incubated MNP was determined to be about 9 % by mass by means of VSM and TGA.
Cell toxicity assays revealed no cytotoxic effect for coated MNP [5] and serum incubated MNP. Long term viability assays (RTCA) showed that the protein corona is able to mask the cytotoxic effect of polyethylenimine (PEI) coating for about two days.

Conclusion

We found very interesting results regarding the influence of particle coating as well as incubation temperature and incubation time on protein corona formation. The protein corona shows no cell irritating effects and may mask cytotoxic effects of core/shell particles. Due to the possibility of heating by magnetic losses (additionally to the external heating) magnetic nanoparticles are very interesting model particles for ongoing investigations.

Acknowledgements

This work was supported by Deutsche Forschungsgemeinschaft (DFG) via SPP 1681 (FKZ: DU 1293/4-1, EG 102/6-1, SCHA1640/7-1, CL202/3-1, MU 2382/4-1, TR 408/8-1, LU800/4-1). PEI coated MNP were kindly provided by chemicell, Berlin/Germany.

References

[1] S. Tenzer et al., *Nanoparticle Size Is a Critical Physicochemical Determinant of the Human Blood Plasma Corona: A Comprehensive Quantitative Proteomic Analysis*, ACS Nano 5/9: 7155-67, 2011

[2] M. Mahmoudi, A.M. Abdelmonem, S. Behzadi, J.H. Clement, S. Dutz, et al., *Temperature: The "Ignored" Factor at the NanoBio Interface*, ACS Nano 7/8: 6555-6562, 2013

[3] X. Jiang et al., *Quantitative Analysis of the Protein Corona on FePt Nano-particles formed by Transferring Binding*, J. R. Soc. Interface 7 (Suppl1): S5-S11, 2010

[4] A. Lesniak et al., *Serum Heat Inactivation affects Protein Corona Composition and Nanoparticle uptake*, Biomaterials 31(36): 9511-8, 2010

[5] M. v.d. Lühe, U. Günther, A. Weidner, C. Gräfe, J.H. Clement, S. Dutz, F.H. Schacher. *SPION@Polydehydroalanine Hybrid Particles*, RSC Advances 5: 31920-9, 2015

High energy crosslinking of gelatin ferrogels towards a thermally stable composite

Emilia I. Wisotzki[1], Dietmar Eberbeck[2], Stefan G. Mayr[1,2,3]

[1] *Leibniz Institute of Surface Modification (IOM), Permoserstr. 15, 04318 Leipzig, Germany*
[2] *Physikalisch-Technische Bundesanstalt, Abbestr. 2-12, 10587 Berlin, Germany*
[3] *Faculty of Physics and Earth Science, Leipzig University, Linnéstr. 5, 04103 Leipzig, Germany*
[4] *Translational Center for Regenerative Medicine, Philipp-Rosenthal-Str. 55, 04103 Leipzig, Germany*

From a biomedical point of view, there is significant interest in ferrogels as magnetically responsive materials with potential applications from drug delivery systems to actuators. For such applications, it is critical to understand the coupling and interactions between the magnetic nanoparticles (MNPs) and surrounding matrix. Molecular interactions can lead to the formation of aggregates and dramatically alter the magnetic response [1], while insufficient binding could lead to undesirable particle losses from the composite with time. Here, superparamagnetic iron oxide MNPs were integrated into gelatin, selected for its well-established record of use in biological applications. High energy electron irradiation was investigated as a reagent-free crosslinking method [2] to thermally stabilize the ferrogels.

Magnetic response in gelatin

The magnetic response of the MNPs was investigated using magnetic particle spectroscopy (MPS) and magnetorelaxometry (MRX). From these techniques, the magnetic behavior was monitored at a range of temperatures across the sol-gel transition, near 34°C for gelatin. As deduced from these obtained spectra, the mean effective magnetic size of the particles decreased, while the anisotropy energy distribution broaded in comparison to the same MNPs immobilized in a freeze dried sugar matrix. This response suggests the formation of aggregates in the presence of gelatin.
Below the gelation point, the magnetorelaxation was roughly similar to that of particles in a freeze dried matrix, which is dominated by Néel relaxation processes. Once the gel was soluble, the relaxation spectra were strongly influenced by Brownian relaxation and the MNPs appeared more easily magnetized in low fields. The gel-sol transition was accompanied by a jump in the characteristic relaxation time with respect to increasing temperature, shown in Fig. 1. Interestingly, prior to this macroscopic melting, the relaxation accelerated. This result provides evidence of the onset of local mobility of the MNPs and was not observed in crosslinked samples that do not melt at this temperature.

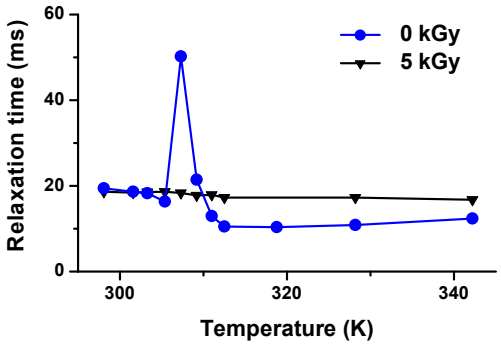

Figure 1: Relaxation times with temperature of untreated and 5 kGy irradiated gelatin ferrogels.

Formation of aggregates

Using dynamic light scattering (DLS), trace amounts of gelatin were added to an aqueous solution of MNPs to monitor changes to the average particle diameter. Overall, the formation of multiparticle clusters appeared at significantly lower concentrations than required to form a network. These aggregates were visualized with scanning electron microscopy.

Particle stability during crosslinking

High energy electron irradiation was investigated as a method to confine and stabilize MNPs in the gelatin hydrogel. During irradiation, the hydrogels gave off significant amounts of liquid. This byproduct was investigated for the release of magnetic particles. Around 1% of the total particle content was lost during crosslinking, even when the overall structural weight was reduced by 40%. Therefore, particles appear tightly bound to the network before irradiation, as previously indicated in the magnetic response of the untreated gelatin ferrogel.

Long-term thermal stability

Samples were heated above the network melting point to 37°C in simulated body fluid (SBF) for 7 days. Without crosslinking, gelatin was soluble at this temperature. From the crosslinked gels, a maximum of 3% of the MNPs were released. The majority of the particle loss came from submersion in the first 24 hours. As seen in fig. 2, gels were highly stable after this point.

Effect of crosslinking on magnetic response

Irradiated ferrogels were subjected to MPS and MRX measurements across the previous sol-gel transition temperature. Below the melting point, irradiated samples did not show any significant differences in the magnetic response compared to the uncrosslinked gelatin matrices. However, above this temperature, crosslinked samples demonstrated a high degree of stability in the magnetic response, as demonstrated in Fig. 1.

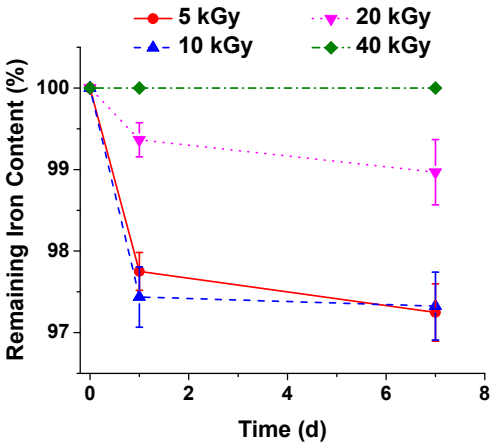

Figure 2: MNPs released from ferrogel with time in SBF at 37°.

Acknowledgments

This research is supported by the Deutsche Forschungsgemeinschaft (DFG) *via* the Schwerpunktprogramm 1681 “Feldgesteuerte Partikel-Matrix-Wechselwirkungen: Erzeugung, skalenübergreifende Modellierung und Anwendung magnetischer Hybrid-Materialien.”

References

[1] D. Eberbeck, F. Wiekhorst, U. Steinhoff and L. Trahms. J. Phys.: Condens. Matter 18:S2829-S2846, 2006.

[2] E. I. Wisotzki, M. Hennes, C. Schuldt, F. Engert, W. Knolle, U. Decker, J. A. Käs, M. Zink and S. G. Mayr. J. Mater. Chem. B, 2:4297-4309, 2014.

Magnetic Microgel Particles

Marcus U. Witt[1], Sebastian Backes[1], Eric Roeben[2], Annette Schmidt[2], Regine von Klitzing[1]

[1] *Technische Universität Berlin, Stranski-Laboratorium für Physikalische und Theoretische Chemie, Straße des 17. Juni 124, 10623 Berlin,Germany*
[2] *Department für Chemie, Institut für Physikalische Chemie, Universität zu Köln, Luxemburger Str. 116, 50939K öln, Germany*

Introduction

Research on multifunctional microgels is of increasing interest. Microgels made of poly(N-isopropylacrylamide) (PNIPAM) show a fast response to outer stimuli such as temperature or pH.
The microgel particles are swelling in water and exhibit a Volume Phase Transition Temperature (VPTT) above which the particles are shrinking in size and the polymer mesh density increases.
With the adsorption of magnetic nanoparticles ($CoFe_2O_4$)(MNP) into the gel structure the gel becomes responsive to an external magnetic field. Recent research was mainly focused on core/shell structured magnetic microgels (MMG) [1].
We will show a broader distribution of MNP inside the gel and first response measurements of adsorbed MMG to an external magnetic field.

Sample Preparation

PNIPAM microgels are synthesized with a surfactant free precipitation polymerization according to Pelton and Chibante [2].
The MNP are synthesized with the thermal decomposition of $Fe(acac)_3$ and $Co(acac)_2$ according to Sun et al. [3].
The two components (microgel and MNP) are mixed at room temperature (swollen gel) and at pH=10 (stabilized MNP).

Results

Fig.1 shows the distribution of MNP inside the gel as imaged by transmission electron microscopy. The MNP are well adsorbed inside the polymer network.

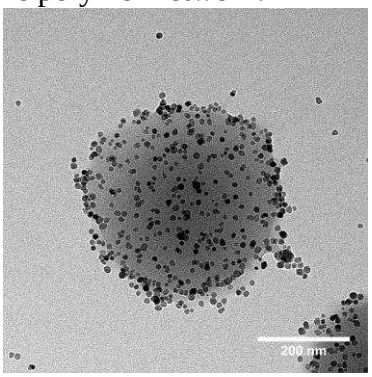

Figure 1. TEM picture of magnetic microgle particle.

Zeta potential measurements have shown that the temperature response known from pure microgels is preserved for MMG.
Measurements on individually adsorbed MMG with an applied external magnetic field are performed with an MFP-3D AFM (Asylum Research) with the Variable Field Module 2 (VFM2) extension The VFM2 applies a homogenous magnetic field up to 0.375 T to the sample. The results are shown in Fig. 2. The adsorbed MMG are stretched parallel to the field direction while the height decreases, leading to an overall anisotropic volume loss.

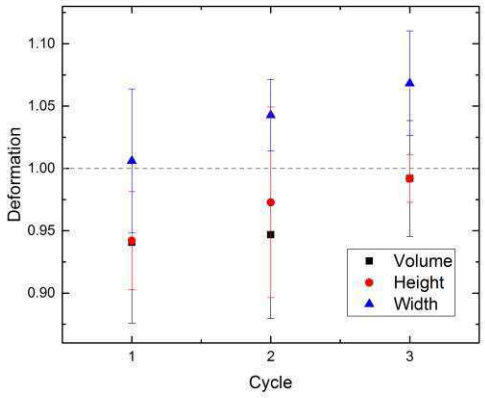

Figure 2. Change of volume, height and width during three cycles in each of which the magnetic field was ramped up from 0 T to 0.375 T.

Outlook

A remaining topic is to increase the number of adsorbed MNP inside the gel and tune the strength of the interaction between the gel and the MNP. By increasing the interaction strength, we hope to create a higher response to magnetic field.

Acknowledgments

The authors thank the DFG for funding via the priority program "Feldgesteuerte Partikel-Matrix-Wechselwirkungen: Erzeugung, skalenübergreifende Modellierung und Anwendung magnetischer Hybridmaterialien" (SPP1681).

References

[1] Städele, V., Gasser, U., Dietsch, H. (2012). *Soft Matter*, *8*(16), 4427.

[2] R. Pelton, P. Chibante (1986), *Colloids Surf.*, 20, 247-256

[3] Sun, S., Zeng, H., Robinson, D. (2003). *Journal of the American Chemical Society*, *4*(1), 126–132.

Synthesis and Characterization of Mesogen-Hybridized Magnetic Nanoparticles

I. Appel[1], S. Behrens[1]

[1]Institut für Katalyseforschung und-technologie; Karlsruher Institut für Technologie (KIT), Postfach 3640, 76021 Karlsruhe

Liquid crystals (LCs) are manifold used in electro-optical devices (e.g. liquid crystalline displays; LCD) due to their anisotropic, crystal-like physical properties that are easily controlled by weak electric fields due to their dynamic, fluid-like behavior.
As postulated by Brochard and de Gennes in 1970, the magnetic susceptibility of LCs can strongly be increased by the integration and stabilization of magnetic nanoparticles (MNP) [1]. While the integration of the MNP in the LC phase was realized soon after prediction together with interesting magneto-optical properties [2], the long-term stabilization and aggregation have remained a current challenge [3].
Here, we address the development of a new synthetic strategy for mesogen-hybridized MNPs.

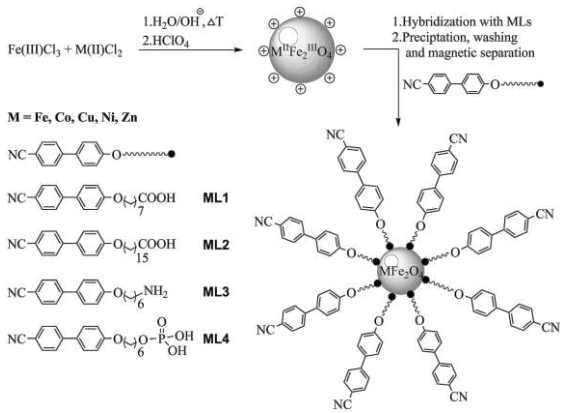

Figure 1 Functionalization of magnetic nanoparticles with mesogenic ligands.

In a first step, a series of electrostatically stabilized, spherical ferrite MNPs were synthesized with sizes in the range of 10 nm, by using a modified protocol by Massart et al. [4]. The ferrite NPs were successively hybridized with mesogenic ligands (MLs) [5], bearing functional groups for nanoparticle binding (figure 1) and eventually purified by washing and magnetic separation. IR-spectra of the NPs demonstrated the successful binding of the MLs to the surface of the nanoparticles.
The hybrid materials were characterized by differential scanning calorimetry and polarized optical microscopy (POM). POM images of the MLs (ML1, ML2 and ML3) and the hybridized MNPs in ML (e.g. $CuFe_2O_4$@ML4 in ML4) revealed the birefringent character of the ligands and the hybrid materials. No aggregates were detected by POM investigations.
A successful strategy for the hybridization of MNP with mesogenic molecules has been developed, resulting in hybridized materials with mesomorphic characteristics at higher temperatures. Future studies will concern the behavior of these hybrid materials in magnetic fields. This strategy appears a promising route not only to stabilize and organize MNPs but also to modulate the mesomorphism of the hybrid materials.

Acknowledgments

The financial support by the DFG via SPP1681 and the experimental support of Lukas Ahrens are gratefully acknowledged.

References

[1] Brochard, F.; de Gennes, P. G., Journal de Physique **1970,** 31 (7), 691-708.
[2] Chen, S.-H.; Amer, N., Physical Review Letters **1983,** 51 (25), 2298-2301.
[3] Podoliak, N.; Buchnev, O.; Buluy, O.; D'Alessandro, G.; Kaczmarek, M.; Reznikov, Y.; Sluckin, T. J., Soft Matter **2011**, 7, 4742-4749.
[4] Massart, R., IEEE Transactions on Magnetics **1981**, 17 (2), 1247-1248.
[5] Saliba, S.; Mingotaud, C.; Kahn, M. L.; Marty, J. D., Nanoscale **2013,** 5 (15), 6641-61.

Self-assembled ferrogels containing magnetic nanocubes

S. Metzke[1], J. Seliger[1], S. Prévost[1,2], M. Gradzielski[1]

[1] *Physikalische Chemie / Molekulare Materialwissenschaften, Institut für Chemie, Technische Universität Berlin, Straße des 17. Juni 124. D-10623 Berlin.*
[2] *Now at Soft Matter Structure, ESRF – The European synchrotron, 71 avenue des Martyrs, F-38000 Grenoble.*

Thermoresponsive aqueous ferrogels with cubic magnetic nanoparticles (MNPs) incorporated in a self-assembled network built by low molecular weight gelators, are studied primarily by Small Angle Scattering together with rheology and magnetometry, to understand the inter-play between the living network and NPs, and enable control of the response to mechanical stress, temperature and magnetic field.

Background

Most ferrogels result from the addition of polymeric gelators in large amounts to an existing ferrofluid. [1] The resulting ferrogels are in fact composed of pockets or blobs of the original ferrofluid encapsulated by domains of polymer molecules at the colloidal scale. Such systems do not exhibit any significant synergistic response.

Goal

Using a silica shell to stabilize NPs in water, and creating the gel network via self-assembly of small surfactant molecules that interact with functionalized NPs, enables the construction of more elaborated ferrofluids that can quickly respond to stimuli due to the small size of the gelator that reorganizes immediately. Modifying the surface of the silica shell by hydrophobic modification or by grafting amino acids to it, allows to control the charge of NPs and their interaction with the gel network via H-bonds and/or hydrophobic interactions (strength and number of junctions). Small Angle Scattering (SANS, SAXS) is used to get a detailed picture of the arrangement of the particles and of the gel fibers at the nanometer-scale while Time-Resolved SAS will show the dynamics of such systems (relaxation time and pathway of particles and network).

Low molecular weight gelators

A new class of gels discovered within this project is based on mixing fatty acids with basic amino-acids, with an emphasis on oleic acid (C18:1COOH) and L-arginine. Such gels are eco-friendly, non-toxic, cheap and present attractive rheological and temperature-dependent properties.

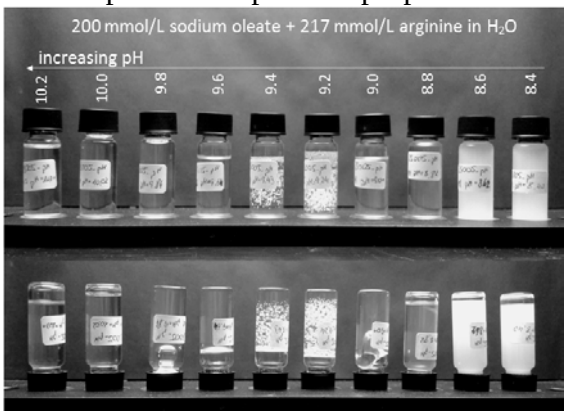

Fig. 1: 200 mM sodium oleate with 217 mM L-arginine under pH-variation.

The formation of a vesicle gel in these systems is already a very interesting finding by itself, and even more so as by variation of pH one can rather directly switch to a viscoelastic network based on Na oleate in worm-like micelles, where similar worm-like micelles can also be formed by increasing the ionic strength of Na oleate solutions (Figs. 1 and 2). In particular the ability to change easily by pH the gel structure in the oleate/arginine system is a very elegant way of tuning the gel structure and properties and this renders this system very interesting and suitable for our future preparation and investigation of ferrogels.

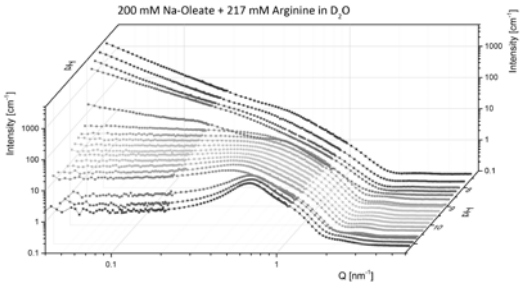

Fig. 2: SANS measurement of a Na-oleate and arginine mixture in terms of pH.

Nanocubes

Highly monodisperse Fe_3O_4, $CoFe_2O_4$ (hard ferrite), $Mn_{0.5}Zn_{0.5}Fe_2O_4$ (soft ferrite) nanocubes in a size range of 7 to 17 nm (edge length) corresponding to 10 to 29 nm space diagonal were synthesized using a thermal decomposition route [2] resulting in a large scale reaction (2-3 g NP / synthesis). Such monodisperse nanoparticles are required for detailed investigations (SAS) and commercial ferrofluids and not suitable due to their high polydispersity (Fig. 3).

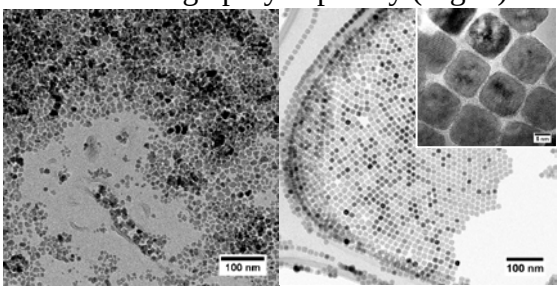

Fig. 3: TEM of magnetite nanoparticles (left: commercial, right: synthesized).

Silica Shell

However, in order to enhance and control the colloidal stability as well as having the ability to integrate these hydrophobic magnetic nanoparticles into an hydrogel network, it is required that they become surrounded by a protective shell that subsequently can easily be modified chemically – as it is best the case for silica shells.
A silica coating [3] is obtained by hydrolyzing TEOS in the presence of arginine, thus resulting in NPs functionalized by amino acids. Particles are water dispersible and the homogeneous shell thickness can be tuned between 4 and 13 nm.

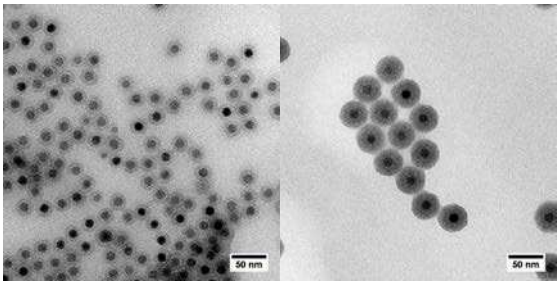

Fig. 4: TEM of Fe_3O_4@SiO_2 nanoparticles.

Ferrogels

The aim is to combine the nanocubes and gels to self-assembled ferrogels, whose properties cannot only be controlled by pH, temperature and composition, but also by a possible hydrophobic modification of the silica shell resulting in a versatile system.

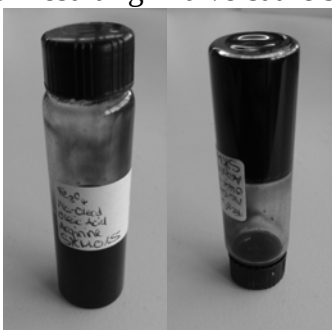

Fig. 5: Photo of an as prepared ferrogel.

Future Perspectives

Dynamic SAS experiments with and without magnetic field will be done together with magnetometry measurements in order to thoroughly characterize the dynamic properties of these ferrogels.

Acknowledgments

This work is supported by DFG PR1473/1 within the Priority Program SPP1681.

References

[1] M. Krekhova and G. Lattermann J. Mat. Chem. 18, 2842-2848 (2008).
[2] J. Park, K. An, Y. Hwang, J.G. Park, H.J. Noh, J.Y. Kim, J.H. Park, N.M. Hwang, and T. Hyeon Nat. Mater. 3, 891-895 (2004).
[3] H. L. Ding, Y. X. Zhang, S. Wang, J. M. Xu, S. C. Xu, and G. H. Li Chem. Mater. 24, 4572-4580 (2012).

Hindered nematic alignment of hematite spindles in viscoelastic matrices

A. Nack, J. Seifert, C. Passow, J. Wagner

Universität Rostock, Dr.-Lorenz-Weg 1, 18059 Rostock

Spindle-shaped hematite particles align with their long axis perpendicular to the direction of an external magnetic field [1]. We compare the orientational distribution functions (ODF) of hematite spindles in aqueous suspension and in hydrogel matrices at the same number densities.

The ODFs are determined by means of Small Angle X-ray Scattering in dependence on the flux-density and the direction of the scattering vector $\mathbf{Q}$ with respect to the direction of an external field. Since the electron density of hematite is significantly larger than the one of water or poly(N-isopropylacrylamid), the scattered intensity is dominated by the iron oxide particles.

In diluted suspensions and hydrogel-composites, where particle-particle interactions can be neglected, the orientation of the spindles is random in absence of an external field resulting in an isotropic scattering pattern. With increasing flux density, the anisotropy of the scattering patterns rises. Both, for aqueous suspensions and hydrogels, this field-induced isotropic-nematic transition is completely reversible within several to several ten seconds.

Depending on the viscoelastic properties of the hydrogel matrices which are tuned via the volume fraction of the polymer and its crosslinking density [2], the anisotropy of the scattering pattern is less pronounced for composites than for suspensions in Newtonian liquids. The stronger the elastic modulus of the hydrogel is, the more hindered is the field-induced nematic alignment of the particles. In Fig. 1, false color representations of the intensity scattered by an aqueous suspension and a hydrogel containing the same number density of identical hematite particles are compared.

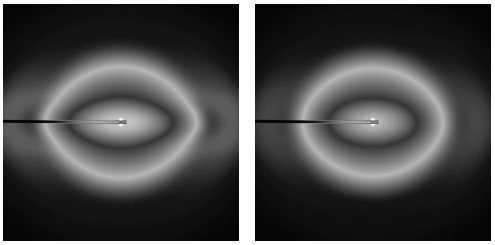

Fig. 1: SAXS false-color plot of a HEM suspension (left) and a HEM-pNIPAM composite (right) at B=1.5 T.

The scattered intensity detected by a CCD camera is sector-averaged in 72 sectors with an acceptance of $\Delta\vartheta = 2.5°$. The ODFs are obtained from least-squares fits of the scattered intensity as a function of the modulus and the direction of the scattering vector $\mathbf{Q}$ with respect to the direction $\hat{\mathbf{B}}$ of the magnetic field.

To quantify the aligning of hematite particles, the nematic order parameter

$$S_2 = \frac{1}{2}\langle 3\cos^2\vartheta_P - 1\rangle$$

is calculated from the ODF. In aqueous suspensions, at a flux density of $B = 1.0\,\mathrm{T}$ nearly a complete alignment of the spindles can be achieved with an order parameter close to $S_2 = -1/2$. With increasing elastic modulus of the hydrogel matrix, the decay of the order parameter

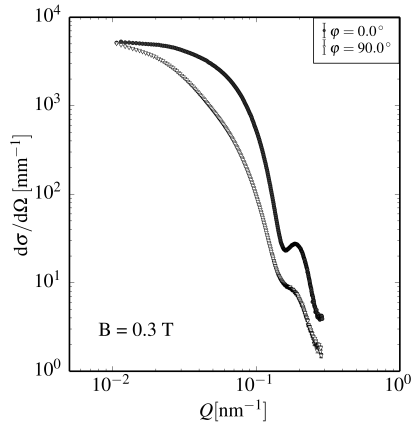

Fig. 2: Sector averaged mean intensities for $\vartheta_{\mathbf{Q}} = 0°$ and 90° of SAXS experiments of an aquous HEM suspension.

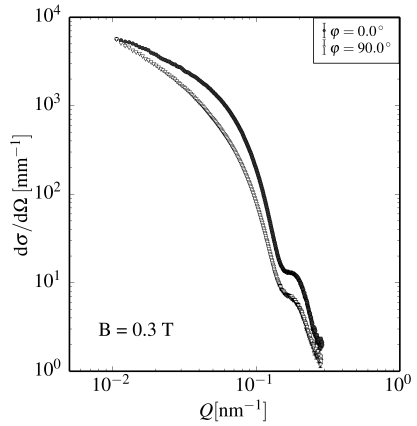

Fig. 3: Sector averaged mean intensities for $\vartheta_{\mathbf{Q}} = 0°$ and 90° of SAXS experiments of a HEM-pNIPAM-composite.

with increasing flux density is less pronounced. The reversibility of the field-induced isotropic-nematic transition indicates, that this effect is not related to the Newtonian viscosity of the hydrogel but to the elastic modulus of the polymer network. An increased Newtonian viscosity would only slow down the systems response to the external stimulus. By rotation of the spindle-shaped particles the polymer network of the hydrogel matrix is deformed causing a torque opposite to the torque induced by the magnetic field. Ocillatory shear experiments in presence of an external magnetic field confirm at small deformations the structural response of the composites to an external field. Particles rotate in the vorticity of the shear gradient. The particles orientational arrest in presence of an external field leads to strongly increasing strorage moduli with rising flux density. The anisotropic magnetic particles behave as field-dependend crosslinkers of the polymer matrix.

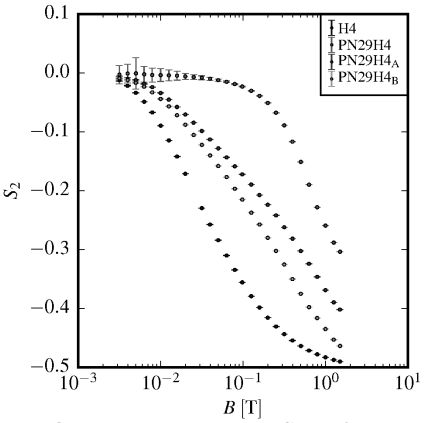

Fig. 4: Order parameter S_2 of HEM suspension and HEM-pNIPAM composites with varying volume fractions ($\varphi(PN29)$=0.050, $\varphi(\mathrm{PN29})_A$=0.025, $\varphi(\mathrm{PN29})_B$=0.017).

Acknowledgments

We acknowledge the European Synchrotron Radiation Facility (ESRF) for providing beamtime at the beamlines ID02 and ID10 as well as the DFG for financial support within the priority program SPP 1681.

References

[1] Märkert et al. *Journal of Applied Crystallography*, 2011, 44, 441-447

[2] Hu et al. *Angewandte Chemie Internation Edition*, 2003, 42, 4799-4802

Dynamic Magnetic Measurements of $CoFe_2O_4$ Nanoparticles in Aqueous Gelatin Solutions

H. Remmer[1], E. Roeben[2], A. Tschöpe[3], A. M. Schmidt[2], and F. Ludwig[1]

[1] *Institut für Elektrische Messtechnik und Grundlagen der Elektrotechnik, Technische Universität Braunschweig*
[2] *Department für Chemie, Institut für Physikalische Chemie, Universität zu Köln*
[3] *Experimentalphysik, Universität des Saarlandes*

* *Corresponding author: h.remmer@tu-bs.de*

Introduction

Bacri et al. [1] proposed already in 1985 to determine the nanoscale viscosity by measuring the Brownian time constant of magnetic nanoparticles (MNP). Whereas the situation is rather clear for Newtonian fluids, only a few studies aiming at a nanoscale rheometry of non-Newtonian fluids [2] and viscoelastic matrices have been performed. Here we investigate the temporal evolution of the gelation process of aqueous gelatin solutions analogous to recent experiments which were based on the magneto-optical detection of the dynamics of Ni nanorods during gelation [3]. By contrast, magnetically blocked $CoFe_2O_4$ MNP are used as probe particles in the present study. The $CoFe_2O_4$ MNP are dispersed in aqueous gelatin suspensions with contents of gelatin between 2.5 wt% and 10 wt%. The measured ac susceptibility (ACS) data were analyzed according to a theoretical model by Raikher et al. [4] assuming a viscous and an elastic term in parallel (Voigt-Kelvin model) and describing the dependence of the complex susceptibility on viscosity and shear modulus of the matrix.

Methods

The $CoFe_2O_4$ single-core MNP have a core diameter of 15 nm (TEM) and hydrate shells. Because of their large magnetocrystalline anisotropy they are magnetically blocked and their dynamics in a Newtonian liquid are dominated by Brownian relaxation which is directly proportional to the viscosity. ACS measurements of these nanoparticles in DI water provide a hydrodynamic diameter of about 18 nm.

The ACS measurements presented here were performed with our fluxgate based RMF setup described in detail in [5] with a frequency range between 2 Hz and 9 kHz and ac field amplitude of 200 µT and which allows sample heating from room temperature up to 70°C. To generate a sinusoidal excitation field, only one of the two orthogonal Helmholtz coils is powered.

The gelatin sol was equilibrated in the measurement setup at 40°C for one hour and then cooled to 23°C. ACS measurements were performed every 30 min on the first day and then every 24 hours.

Results

The ACS spectra of the sample with 2.5 wt% gelatin show a continuous shift of the maximum of the imaginary part to lower frequencies with increasing gelation time (Fig. 1). As can be seen in Fig. 2, for the sample with 5 wt%, the maximum first shifts to lower frequencies but at long gelation times a shift to higher frequencies takes place. Besides the shift of the maximum position of the imaginary part, a significant broadening is observed. The peaks of the samples with 7.5 wt% and 10 wt% are outside the measurement window before achieving 23°C because of their higher viscosities.

The measured spectra of the imaginary part of the complex susceptibility were fitted

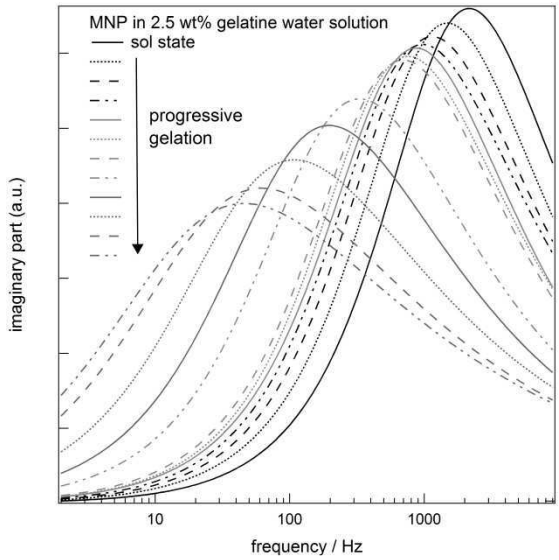

Fig. 1: Imaginary part of ACS spectra for the sample with 2.5 wt% gelatin.

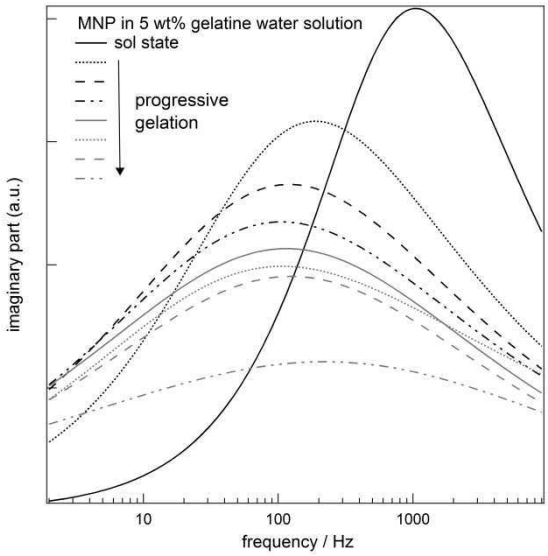

Fig. 2: Imaginary part of ACS spectra for the sample with 5 wt% gelatin.

with the model by Raikher et al. [4] extended by lognormal distributions of the hydrodynamic particle diameter and the local viscosity. The distribution of the hydrodynamic diameters was estimated from measurements of the gelatin sol at 40°C and independent rheological measurements of the sol viscosity. It was found that the mean hydrodynamic diameters of the particles were significantly larger (36 nm and 47 nm for 2.5 wt% and 5 wt% gelatin, respectively) than the value obtained for the aqueous sample presumably caused by a gelatin adsorbate layer. The obtained temporal evolution of the viscosity and shear modulus data shows a qualitatively similar trend for both concentrations of gelatin despite their different trends in the ACS spectra.
Magnetorelaxometry measurements on the same samples indicate a continuous increase of the characteristic time constant with increasing gelation time.

Conclusion

Blocked $CoFe_2O_4$ nanoparticles are well suited for the nanoscale rheological investigation of non-Newtonian fluids and viscoelastic media. The temporal evolution of the gelation process of aqueous gelatin solutions measured applying AC susceptometry was analyzed with the Voigt-Kelvin model providing viscosity and shear modulus of the viscoelastic matrix versus gelation time. The behavior over the time was found to be different and depending of gelatin concentration. Macrorheological reference measurements are in progress.

Acknowledgements

Financial support by the Deutsche Forschungsgemeinschaft, DFG Priority Program 1681 is acknowledged (LU800/4-1, SCHM1747/10-1, TS62/4-1).

References

[1] J.-C. Bacri et al., „Ferrofluid viscometer", J. Phys. Lett. 46, 1199-1205 (1985)

[2] E. Roeben et al., „Magnetic particle nanorheology", Colloid Polym. Sci. 292, 2013-2023 (2014)

[3] A. Tschöpe et al., „Nanoscale rheometry of viscoelastic soft matter by oscillating field magneto-optical transmission using ferromagnetic nanorod colloidal probes", J. Appl. Phys. 116, 184305-1 – 10 (2014)

[4] Y. L. Raikher et al., „Dynamic susceptibilities of an assembly of dipolar particles in an elastic environment", Phys. Rev. E 63, 031402-1 – 10 (2001)

[5] J. Dieckhoff et al., "Fluxgate based detection of magnetic nanoparticle dynamics in a rotating magnetic field", Appl. Phys. Lett. 99, 112501-1-3 (2011)

Magnetic Particle Nanorheology

E. Roeben, L. Kibkalo, U. K. Deiters, A. M. Schmidt

Department Chemie, Institut für Physikalische Chemie, Universität zu Köln, Luxemburger Str. 116, D-50939 Köln, email: annette.schmidt@uni-koeln.de

Motivation

Static and dynamic rheology is an established methodology for the investigation of the flow and deformation properties of viscoelastic complex materials like polymers.

In the context of nanostructured materials and composites, there is an increasing interest to study the material properties on the micro- or nanoscale and to investigate the interaction between the nanoscopic building blocks and the surrounding matrix in detail. Peculiar interest is paid to the relative size of the tracer particles and the structural length scale of the investigated material. In this respect, different tracer particle-based microrheological methods are developed, showing the additional advantage of a small sample volume and thus allowing the exploration of samples that cannot be produced in bulk quantities, like biological polymers or living cells.[1,2] A tracer-free method is based on dielectric spectroscopy, relating the complex dielectric function to the complex dynamic viscosity according to the Gemant-DiMarzio-Bishop model.[3]

Here, we demonstrate that by Magnetic Particle Nanorheology based on the complex dynamic susceptibility of ferromagnetic nanoscopic probes, the frequency-dependent interaction between the probe and its viscoelastic environment can be obtained in a broad frequency range.

Method

Ferromagnetic $CoFe_2O_4$-nanoparticles (d_{TEM} = 13.3 nm ± 1.9 nm) are used as tracer particles in model systems based on a) Newtonian fluids based on mixtures of ethylene glycol and triethylene glycol with water, b) aqueous polyethylene glycol (PEG) solutions and c) PEG-based dynamic networks. The samples are doped with the magnetic probe particles, and the dynamic response of the brownian particles is recorded by AC susceptometry (Fig. 1).

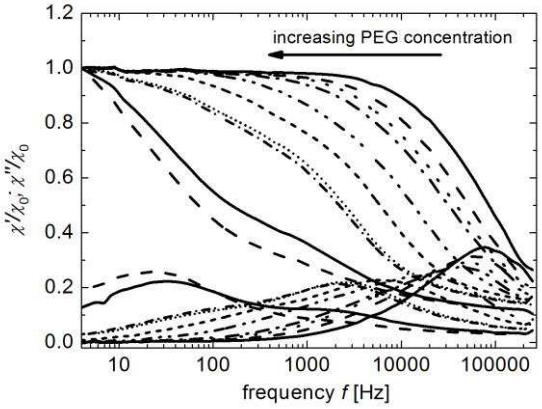

Fig. 1: AC susceptometry measurements of aqueous polyethylene glycol solutions (M_w = 35000 g·mol^{-1}) with different polymer concentration.

The collected frequency-dependent complex susceptibility data are treated using different theoretical approaches.[4]

Results and Discussion

By applying different methods including an extended Debye relaxation model and a modified version of the Gemant-DiMarzio-Bishop approach for the magnetic case, the experimental data can be fitted to receive frequency-dependent rheological properties including viscosity, loss moduli and storage moduli.

The approach is verified under employment of Newtonian fluids of different, frequency-independent viscosity. By comparing their nanorheological results to results from macroscopic rheology, a good correspondence is obtained.

The method is subsequently applied to aqueous PEG solutions, with a systematic variation of the concentration and the mo-

lar mass of the polymer. For each sample, the dynamic storage and loss modulus are calculated over a broad frequency range, and are used to determine characteristic relaxation times of the polymer systems (Fig. 2).

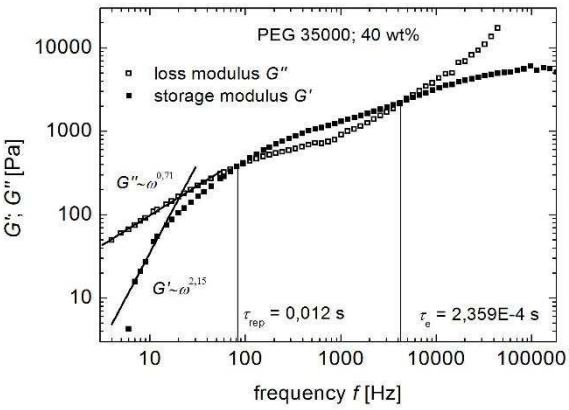

Fig. 2: Frequency-dependent loss and storage modulus calculated according to the modified Gemant-DiMarzio-Bishop approach for an aqueous solution of PEG (M_w = 35000 g·mol^{-1}, 40 mass-%).

By comparing the results with outcomes of conventional rheology, the validity and the limits of the nanorheological method are demonstrated [4]. The corresponding scaling of the relaxation times can be compared to the theoretical expectations [5] under consideration of the size-dependent particle diffusion in polymer solutions (Fig. 3).

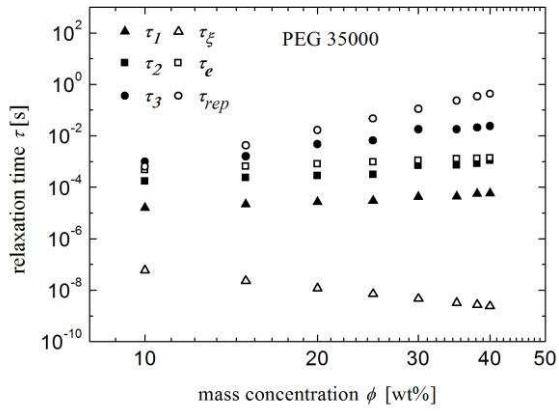

Fig. 3: Comparison between different relaxation times obtained from nanorheology and theoretical calculations [5] for aqueous solutions of PEG (M_w = 35000 g·mol^{-1}).

Acknowledgements

Financial support is acknowledged from DFG-SPP 1681 "Feldgesteuerte Partikel-Matrix-Wechselwirkungen". (SCHM1747/10-1)

References

[1] C. Wilhelm, J. Browaeys, A. Ponton, J.-C. Bacri, Physical Review E 67, 011504, **2003**

[2] P. A. Valberg, H. A. Feldmayn, Biophys J., 52, 551-561, **1987**

[3] E. A. DiMarzio, M. Bishop, J. Chem. Phys. 60, 3802-3811, **1974**

[4] E. Roeben, L. Roeder, S. Teusch, M. Effertz, U. K. Deiters, A. M. Schmidt, Colloid Polym. Sci., 292, 2013-2023, **2014**

[5] Cai L., Panyukov S., Rubinstein M. 44, Macromolecules, 44, 7853–7863, **2011**

Anisometry versus anisotropy: the consequences of competing directionality in systems of cube-like magnetic particles

Joe G. Donaldson[1], Sofia S. Kantorovich[1, 2]

[1] *Faculty of Physics, University of Vienna, Boltzmanngasse 5, 1090 Vienna, Austria*
[2] *Ural Federal University, Lenin av. 51, Ekaterinburg, 620083, Russia*

Systems whose magnetic responses can be finely tuned using control parameters, such as temperature and/or external magnetic field strength, are extremely desirable both in research and in an industrial setting. Magnetic nano/micro-particles – in particular, suspensions thereof – offer opportunities for this controllability to be realised. Traditional ferrofluids composed of spherical nanoparticles have been developed over many years to allow useful, magnetically controllable liquids to be developed.

Nowadays, in order to provide systems that respond in a different manner, modifications to the particle structure must be made. These changes can be in terms of the magnetic structure or indeed the particle shape. We have considered the effect of both. The manufacture of non-spherical magnetic particles, ranging from the nano- to microscopic regimes, is now a reliable technique of colloidal synthesis [1]. Cube-like particles are particularly monodisperse examples that, together with their favourable packing behaviour, makes them interesting to study [2,3,4].

We have used analytical theory in combination with molecular dynamics simulations to study the behaviour of permanently magnetised dipolar cubic particles. Most notably, we have elucidated the ground state microstructure of these particles for a number of different preferred magnetisation directions [5]. As well as detailing the zero-field magnetic properties of isolated clusters, we have also begun to address the effects of particle curvature on these structures [6,7]. In addition, we discuss the influence of the ground state structural motifs at finite temperatures through consideration of the resulting bulk thermodynamic/magnetic behaviour in dilute suspensions. The observed phenomena are a direct result of the fundamental relationship between the anisotropy of the magnetic interaction and the anisometric geometry of the particles.

Acknowledgments

The research has been partially supported by Austrian Science Fund (FWF): START-Projekt Y 627-N27, RFBR grant mol-a-ved 12-02-33106, the Ural Federal University stimulating programme and by the Ministry of Education and Science of the Russian Federation (Contract 02.A03.21.000, Project 3.12.2014/K).

References

[1] P. Tierno, Phys. Chem. Chem. Phys., 2014, 16, 23515
[2] M. V. Kovalenko et al, J. Am. Chem. Soc., 2007, 129, 6352
[3] E. Wetterskog et al, Sci. Technol. Adv. Mater., 2014, 15, 055010
[4] L. Rossi et al, Soft Matter, 2011, 7, 4139
[5] J. G. Donaldson and S. S. Kantorovich, Nanoscale, 2015, 7, 3217.
[6] R. D. Batten et al, Phys. Rev. E, 2010, 81, 061105.
[7] R. Ni et al, Soft Matter, 2012, 8, 8826.

Tunable material properties of ferrogels and magnetic elastomers and a step towards a scale-bridging description

G. Pessot[1], P. Cremer[1], R. Weeber[2], C. Holm[2], D. Y. Borin[3], S. Odenbach[3], H. Löwen[1], A. M. Menzel[1]

[1] *Institut für Theoretische Physik II: Weiche Materie, Heinrich-Heine-Universität Düsseldorf, D-40225 Düsseldorf, Germany*
[2] *Institute for Computational Physics, Universität Stuttgart, 70569 Stuttgart, Germany*
[3] *Technische Universität Dresden, Institute of Fluid Mechanics, D-01062 Dresden, Germany*

Introduction

Ferrogels and magnetic elastomers represent a fascinating class of composite materials, which are receiving growing attention because of their unique interplay of elastic and magnetic effects. Their reversible deformability under an external magnetic field, as well as the tunability of their elastic moduli, may result in innovative applications in many fields. In the present contribution we focus on the tunability of elastic moduli by magnetic interactions and adjust our mesoscopic model by comparison to a microscopic approach.

Elastic moduli and non-affinity

In the first part we consider a minimal 2D dipole-spring model with all the dipoles of equal magnitude and oriented along the same direction [1]. We show the dependence of the elastic modulus on increasing magnetic interactions for different magnetization directions and particle arrangements; a central role here is played by the relative orientation of the nearest neighbors. For increasingly disordered particle distributions we demonstrate that the often applied assumption of affine homogeneous deformations leads to increasing errors in the elastic moduli calculations. This becomes dramatically evident when we consider realistic particle distributions extracted from x-ray micro-tomography measurements on an actual experimental sample [2], see Fig. 1.

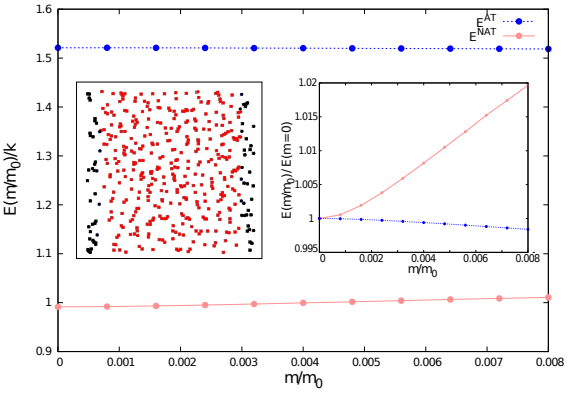

Figure 1: Elastic modulus (rescaled in the right inset) as a function of increasing magnetic interactions for a particle distribution extracted from a real experimental sample (left inset): the assumption of affine deformations (AT) leads to obviously incorrect results when compared to realistic non-affine deformations (NAT).

Building mesoscopic potentials

To check and improve our mesoscopic model potentials [1, 3, 4] we study a more microscopic minimal system of two mesoscopic particles connected by a coarse-grained polymer chain [5], see Fig. 2. Using molecular dynamics simulations we collect statistics on the mesoscopic particle configurations under thermal fluctuations of the whole system.

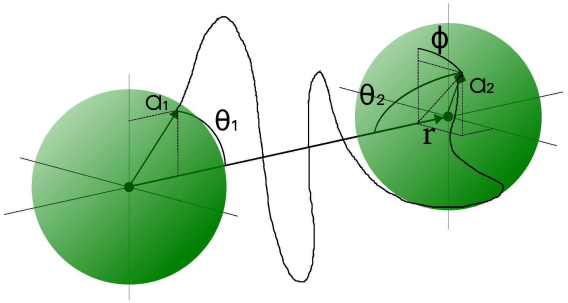

Figure 2: A simplified sketch of the geometry of the microscopic system.

From the resulting probability distribution, we obtain an effective pair potential between the mesoscopic particles as a function of their relative configuration. This effective potential contains the role of the fluctuating polymer chain, with the influence of its many microscopic degrees of freedom projected onto the configuration of the mesoscopic particles. On the one hand, we find a remarkably good agreement with some expressions in the literature, such as the FENE potential, or orientational memory terms introduced in Refs. [3, 4]. On the other hand, our strategy of scale-bridging guides us to additional coupling contributions in the effective potential and correlations not present in the mesoscopic model so far. For an illustrative example of such newly included effects, rotations of the mesoscopic particles lead to a wrapping of the polymer chain around them, decreasing their relative distance [5]. A three-dimensional model material can then be built up using the derived model potential as a pair interaction between the mesoscopic particles. The additional magnetic interactions between the particles can be included in a straightforward manner.

Conclusions and prospects

On the basis of a mesoscopic dipole-spring model we determine elastic moduli as a function of magnetic interactions. The influence of the particle distribution and the importance of non-affine deformations arises, especially in the modeling of realistic particle arrangements. Moreover, we derive mesoscopic pair potentials from microscopic simulation data with the scope of justifying and improving the existing models. In particular, explicit correlations so far missing in the mesoscopic models were included in this way.

Acknowledgments

We thank the Deutsche Forschungsgemeinschaft for support of this work through the priority program SPP 1681.

References

[1] G. Pessot, P. Cremer, D. Y. Borin, S. Odenbach, H. Löwen, and A. M. Menzel, *J. Chem. Phys.* **141**, 124904 (2014).

[2] D. Günther, D. Y. Borin, S. Günther, and S. Odenbach, *Smart Mater. Struct.* **21**, 015005 (2012).

[3] M. A. Annunziata, A. M. Menzel, and H. Löwen, *J. Chem. Phys.* **138**, 204906 (2013).

[4] M. Tarama, P. Cremer, D. Y. Borin, S. Odenbach, H. Löwen, and A. M. Menzel, *Phys. Rev. E* **90**, 042311 (2014).

[5] G. Pessot, R. Weeber, C. Holm, H. Löwen, and A. M. Menzel, *arXiv:1502.03707* (2015).

Modeling and numerical simulation of ferrogels using a magneto-mechanical continuum-based approach

A. Attaran[1], J. Brummund[1], T. Wallmersperger[1]

[1] Institut für Festkörpermechanik, Technische Universität Dresden

Ferrogels are magneto-sensitive polymers. Their fabrication was first reported in the late 90s [1, 2]. Ferrogels consist of a chemically cross-linked polymer network and magnetic nanoparticles (e.g. $CoFe_2O_4$ [3]).

In the course of preparation, parts of the magnetic particles are adhered to the polymer network. If no magnetic field is present in the process of preparation, the magnetic particles are randomly distributed within the ferrogel, leading to an isotropic material [4]. In ferrogels, there could also exist mobile magnetic particles which are not attached to the polymer network.

A comprehensive model for ferrogels consisting of a polymer network, fixed and mobile magnetic particles as well as a pore fluid has been developed by the authors in [5]. In [5] the corresponding field equations were derived using a continuum mechanical approach based on the multiphase, multicomponent nature of the ferrogels.

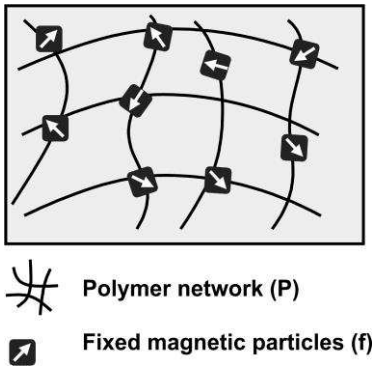

Figure 1. Microstructure of a ferrogel

In the present study a reduced version of this model is introduced. For this, only polymer network (P) and fixed magnetic particles (f) are considered, see Fig. 1. The interaction with the fluid is neglected. The magnetic particles are assumed to be of the hard magnetic type with given magnetization.

The field equations are numerically solved by using the Finite Element Method. For the purpose of this research a user defined element (UEL) was formulated and implemented in Abaqus commercial finite element package.

For the numerical investigation a rectangular strip of ferrogel (6mm × 1mm) was used. The ferrogel, as shown in Fig. 2 and Fig. 3, is fixed at one end and all other sides are free to move.

To verify the validity of the developed model, first a simple magneto-elastic problem was investigated. To study the magnetic stimulation of the ferrogel and its effect on the deformation of the sample, the coupled magneto-elastic problem was solved. For this approach different fundamental test cases have been performed:

In the first test case (Fig. 2), the ferrogel has a given magnetization in x-direction (m_x = 0.005 T kg^{-1} m^3). The magnetic induction vector of B = 0.1 T is applied also in x-direction. This results in an elongation of the sample in x-direction and a slight contraction in y-direction.

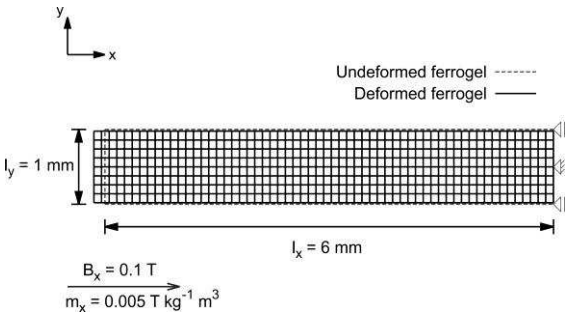

Figure 2. Test case 1: Deformation of a ferrogel in a magnetic field

In the second test case (Fig. 3) the ferrogel has a given magnetization in y-direction. The magnetic induction vector is set in y-direction. This leads to a small elongation of the sample in y-direction and a contraction in x-direction.

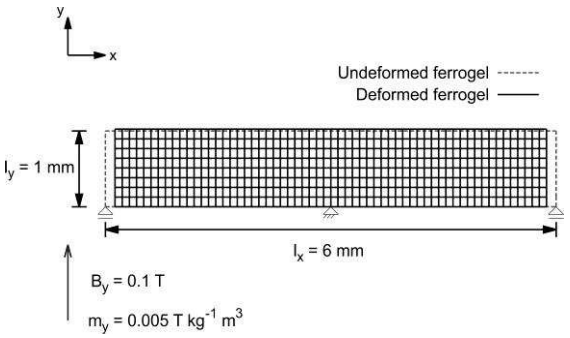

Figure 3. Test case 2: Deformation of a ferrogel in a magnetic field

Other test cases were also carried out in the present study. The results proved to be qualitatively in-line with previous experimental results [1].

Concluding, an approach for modeling the behavior of ferrogels – consisting of polymer network and fixed magnetic particles – under magnetic stimulation has been provided.

Acknowledgments

This research has been financially supported by the Deutsche Forschungsgemeinschaft in the framework of Priority Programme, SPP1681.

References

[1] M. Zrínyi, L. Barsi, and a. Büki, “Deformation of ferrogels induced by nonuniform magnetic fields,” The Journal of Chemical Physics, vol. 104, no. 21, p. 8750, 1996.

[2] M. Zrínyi, L. Barsi, and A. Büki, “Ferrogel: a new magneto-controlled elastic medium,” Polymer Gels and Networks, vol. 5, no. 5, pp. 415 – 427, 1997.

[3] L. Roeder, P. Bender, M. Kundt, A. Tschöpe, and A. M. Schmidt, “Magnetic and geometric anisotropy in particle-crosslinked ferrohydrogels,” Phys. Chem. Chem. Phys., vol. 17, pp. 1290–1298, 2015.

[4] E. Jarkova, H. Pleiner, H.-W. Müller, and H. R. Brand, “Hydrodynamics of isotropic ferrogels,” Phys. Rev. E, vol. 68, no. 4, p. 41706, 2003.

[5] J. Brummund, A. Attaran, and T. Wallmersperger, “Development of a continuum model for ferrogels.” submitted to Physical Review E, 2015.

Macroscopic magnetostriction of magnetorheological elastomers – extended finite element modeling and simulation

C. Spieler and M. Kästner

Institute of Solid Mechanics, Technische Universität Dresden, 01062 Dresden, Germany

Introduction

Magnetorheological elastomers (MRE) feature mechanical moduli that become strongly enhanced by an applied external magnetic field as well as the ability to generate magnetically induced deformations (magnetostriction) and mechanical actuation stresses. Typically, these materials represent a two-component system, in which micron-sized magnetizable particles are embedded in a cross-linked polymer network. Since the effective material behavior of MRE is essentially determined by the constitutive properties of the individual components and their geometrical arrangement in the composite, this contribution will apply a homogenization approach for coupled magnetomechanical problems.

Modeling

Starting from the properties of the magnetizable particles and the polymeric matrix, a weakly coupled model based on a continuum formulation of the heterogeneous microstructure is presented. The governing equations are solved with the extended finite element method (XFEM) that allows the use of non-conforming, structured meshes which do not have to be adapted to the particle-matrix interfaces [1]. This is advantageous if complex systems representing stochastic and structured particle distributions are considered. To study and understand the structure-property relations of isotropic and anisotropic MRE qualitatively, a linear magnetic material model and linear elasticity are adequate.

Simulation

While in [2] the coupled magnetomechanical behavior of an idealized microstructure is analyzed in terms of actuation stresses, here the focus is on the magnetostrictive strain and the mechanical stiffening of particle reinforced composites. In addition to irregular particle arrangements also regular lattice-based structures are modeled. This allows a comparison with analytic models based on dipol-dipol interactions and the assumption of affine deformations. The effective behavior of a representative volume element (RVE) is obtained by computational homogenization. Volume averages of the local field distributions $(\cdot)$ result in the corresponding macroscopic variables $\bar{(\cdot)}$.

Results and discussion

In Fig. 1 the computed effective magnetostrictive strain $\bar{\varepsilon}$ is presented for isotropic microstructures with varying volume content of magnetic particles φ [3]. The results are obtained for a horizontal and a vertical external magnetic field in terms of the strain parallel and perpendicular to the loading. Beside the isotropic behavior a mechanical stiffening is observed which dominates the magnetomechanical coupling above the volume content of approximately 27 %. This is in accordance with the findings in [4].
If a MRE is cross-linked under the action of an external magnetic field, the particles arrange into chain-like structures. A RVE of such an anisotropic microstructure is depicted in Fig. 2 (a). A horizontal magnetic loading causes an elongation of the structure

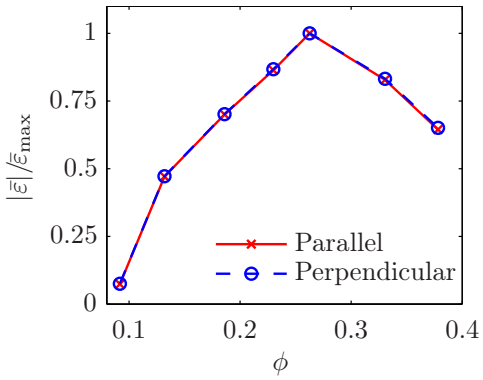

Figure 1: Absolute value of magnetostrictive strain normalized by its extremal value depending on the volume fraction [3].

under consideration, see Fig. 2 (b). This is due to the magnetomechanical interactions between neighboring particles. If the direction of the magnetic field is perpendicular to the particle chain, the RVE will contract, see Fig. 2 (c). The magnetostrictive strains are plotted in Fig. 2 (d). Red curves correspond to a horizontal magnetic loading and blue curves to a vertical. The anisotropic behavior of the RVE is obvious, which is also confirmed by the magnetization curves in Fig. 2 (e).

Acknowledgements

The present study is funded by the German Research Foundation (DFG), Priority Program (SPP) 1681, grant KA 3309/2-1.

References

[1] T. P. Fries and T. Belytschko, Int. J. Numer. Meth. Engng. 84: 253 – 304, 2010.

[2] C. Spieler et al., Acta Mech. 224: 2453 – 2469 , 2013.

[3] K. Zimmermann et al., Probl. Mech. 4: 23 – 41, 2014.

[4] L. C. Davis, J. Appl. Phys. 85: 3348 – 3351, 1999.

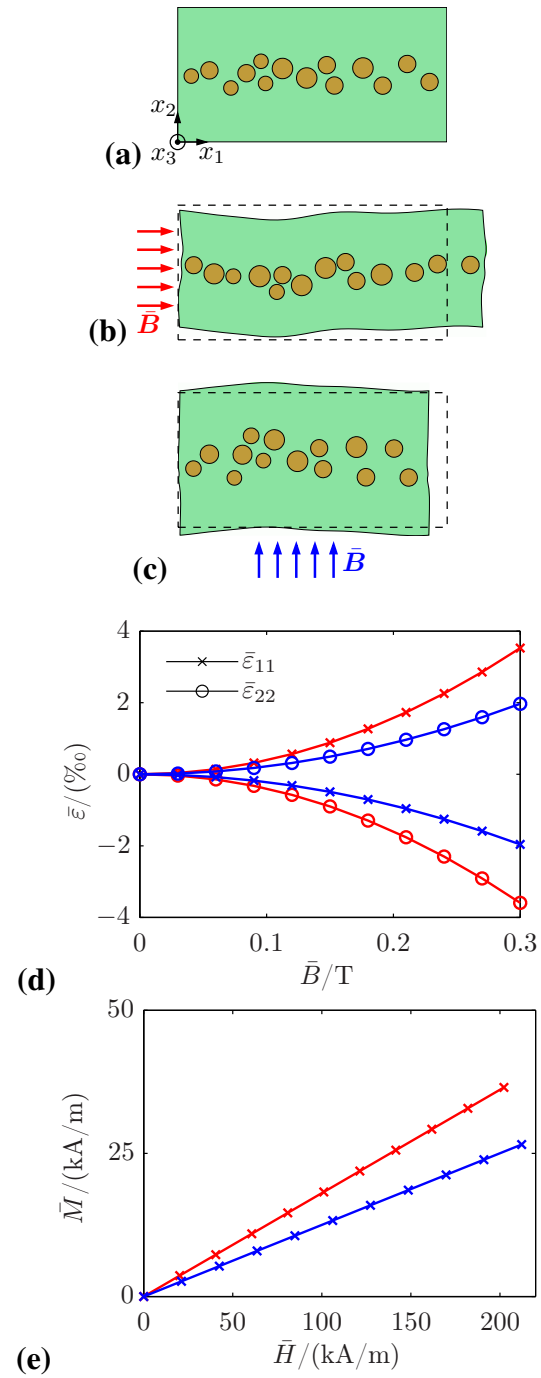

Figure 2: Anisotropic RVE: **(a)** unloaded structure; **(b)** deformed RVE under a horizontal and **(c)** a vertical magnetic field; **(d)** effective magnetostrictive strain; **(e)** macroscopic magnetization.

Quantitative comparison of Magnetorelaxometry models

A. Coene[1], G. Crevecoeur[1], J. Leliaert[1,2], L. Dupré[1]

[1]*Department of Electrical Energy, Systems and Automation, Ghent University, Zwijnaarde, Belgium*
[2]*Department of Solid State Sciences, Ghent University, Gent, Belgium*

Introduction

Magnetic nanoparticles (MNP) are increasingly employed in biomedical applications [1]. To improve the performance of these applications, it is of critical importance to develop accurate imaging techniques which allow a visualization of spatial MNP distributions in a non-destructive way. An example of such an imaging technique is magnetorelaxometry (MRX) [2]. In MRX, the MNP align their magnetic moment parallel to the direction of an externally applied magnetic field. After a certain time, the field is switched off and, due to thermal interactions, the MNP's alignment to the applied field relaxes. This is observed in sensitive magnetometers as a signal decaying towards zero. Using these measurements we can obtain the spatial MNP distribution by solving an inverse problem. This inverse problems requires a forward model which relates measurements to a spatial MNP distribution. The forward model is represented by a leadfield matrix. Based on [3], we apply a transformation approach on the leadfield which employs information theory parameters to compare different MRX models and setups. This transformation results in an improved reconstruction accuracy: where sources previously were shifted upward in the reconstruction process, they are now accurately reconstructed. Fig. 1 depicts an overview of the presented method.

Method

An MRX measurement is modeled as follows [4]:

$$\mathbf{B} = \mathbf{L} \cdot \mathbf{c} \tag{1}$$

$\mathbf{L}$ is the leadfield matrix with dimensions $S \times N$. These matrix elements are calculated from Biot-Savart's law and depend on parameters such as coil distance and orientation. $\mathbf{c}$ is a $N \times 1$ vector which contains the MNP amounts for the N voxels of the MNP sample. $\mathbf{B}$ consists of the measurement values of the S sensors. To recover the spatial MNP distribution an inverse problem is solved using the Moore-Penrose inverse of $\mathbf{L}$:

$$\mathbf{c}^* = \mathbf{L}^\dagger \cdot \mathbf{B} \tag{2}$$

Each MRX model is denoted as $\mathbf{L}_m$, $m = 1...M$. We consider each voxel n as a random variable (RV). Each column of $\mathbf{L}$ then has S observations of the RV. We compare the performance of each model, for a voxel n, by calculating the conditional entropy (H) and mutual information (MI) [3]. $H(\mathbf{Y}|\mathbf{X})$ expresses the amount of information needed to describe the outcome of RV $\mathbf{Y}$ given that the value of RV $\mathbf{X}$ is known. $MI(\mathbf{X}, \mathbf{Y})$ describes the information both RV's have in common. We use a sequential two-way approach, first, the model with the lowest H for voxel n, which is best suited for reconstructing this voxel, is given a weighting of 1. Secondly, the weighting value for the model having a higher H is calculated by minimizing the MI between both models, as dependent information can reduce the stability of the inverse solution [3]. The complete transformation is then:

$$\mathbf{T}(\mathbf{L}_m) = \mathbf{N}_m \cdot \mathbf{L}_m \cdot \mathbf{W}_m \cdot \mathbf{S}_m \tag{3}$$

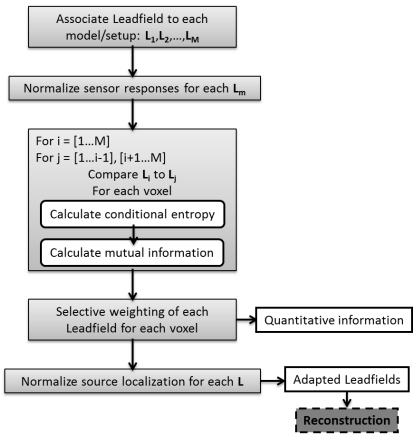

Figure 1: Quantitative comparison between different MRX models.

$\mathbf{W}_m$ is a diagonal matrix containing all the weights of model m for the N voxels, determined by calculating H and MI. $\mathbf{N}_m$ is a diagonal matrix which normalizes the sensor responses and $\mathbf{S}_m$ is a diagonal matrix which removes the impact of source orientation. The simulations are performed using an existing MRX setup of the Physikalisch-Technische Bundesanstalt (PTB), Berlin [4]. This setup consist out of 48 coils which can be activated sequentially. We calculate for each coil the resulting $\mathbf{L}_m$. When combining all $\mathbf{L}_m$, $m = 1...M$ into an single leadfield of dimensions $M.S \times N$, we obtain $\mathbf{L}_{seq}$, associated to a sequential activation of the setup (see [5]). We compare $\mathbf{L}_{seq}$ to $\mathbf{T}(\mathbf{L}_{seq})$. $\mathbf{T}(\mathbf{L}_{seq})$ consists of the M transformations of $\mathbf{L}_m$ (eq. (3)). Because H and MI only allow a comparison between two models, all comparisons (with the 47 other models) are averaged out to obtain one weighting matrix $\mathbf{W}_m$ for each model.

Results

Fig. 2 shows a reconstruction example in which a reconstruction of an MNP phantom is performed using $\mathbf{L}_{seq}$ and $\mathbf{T}(\mathbf{L}_{seq})$. The transformation results in an increased reconstruction accuracy for layers further away from the sensors (middle and bottom layer).

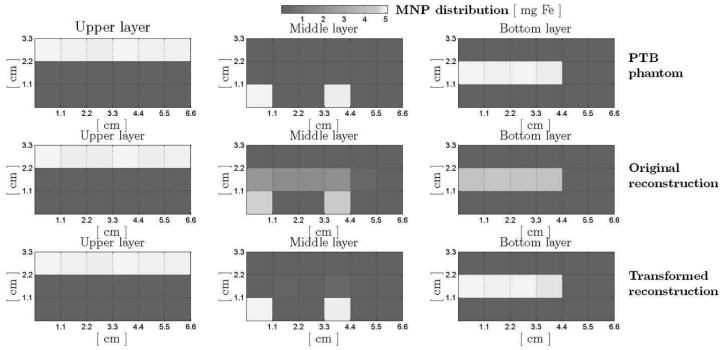

Figure 2: Reconstruction of MNP phantom using $\mathbf{L}_{seq}$ and $\mathbf{T}(\mathbf{L}_{seq})$.

This improved stability is also proven by investigating the condition numbers of $\mathbf{L}_{seq}$ and $\mathbf{T}(\mathbf{L}_{seq})$ which is 143 and 61 respectively. In the full paper we will also consider optimal voxel resolution and coil configuration based on the quantitative information associated to the MRX models.

Conclusion

We present a transformation for the leadfield matrix in MRX. Using information theory parameters it is possible to quantitatively compare different MRX models. This way a voxel-based weighting of these models is realized which is then used to increase the accuracy of MNP reconstructions.

References

[1] Pankhurst, Q. A., et al. J. Phys. D: Appl. Phys. 42.22 (2009): (10p).

[2] Flynn, E. R., and H. C. Bryant. Phys. Med. Biol. 50.6 (2005): 1273-93.

[3] Baillet, S., et al. IEEE Trans. Biomed. Eng. 46.5 (1999): 522-34.

[4] Coene, A., et al. IEEE Trans. Magn. 48.11 (2012): 2842-5.

[5] Liebl, M., et al. Phys. Med. Biol. 59.21 (2014): 6607-20.

Imaging characterization of magnetic nanoparticles for Magnetic Particle Imaging using offset field supported Magnetic Particle Spectroscopy

D. Schmidt[1], F. Palmetshofer[1], D. Heinke[2], D. Gutkelch[1], P. Radon[1], O. Posth[1], U. Steinhoff[1]

[1] Physikalisch-Technische Bundesanstalt, 10587 Berlin, Germany
[2] nanoPET Pharma GmbH, 10115 Berlin, Germany

Introduction

Magnetic Particle Spectroscopy (MPS) is a powerful tool for the characterization of magnetic nanoparticles as tracers for Magnetic Particle Imaging (MPI). So far the signal strength per mol iron is interpreted as a relative indicator for the imaging quality. The direct derivation of real imaging parameters from MPI such as the spatial resolution is time-consuming and requires a scanner. With our method of an offset field supported imaging characterization, we aim to derive absolute imaging parameters for the 1D case of MPI directly from MPS.

Method

MPS can be considered as a 0D MPI with the missing gradient field and therefore the field of view as the main difference between spectral analysis and imaging modality. In our method we describe the gradient field mathematically as a series of step functions. This enables us to sequentially measure each position in the field of view using an external offset field and therefore acquire the 1D system function using MPS. This has been shown already by [1] and was used by [2] to reconstruct MPI data showing better results than model based reconstruction and being faster than the MPI based system function acquisition. We applied this method to measure a very close-meshed system function of FeraSpin™ R and used these data to compose artificial particle distributions.

We then reconstructed the particle distribution in a mesh corresponding to the voxel grid from the artificial MPI signal for different noise levels using the Kaczmarz regularization to measure the distinguishability of particle clusters of different distances to each other.

Results

Figure 1 depicts the MPS measured system function for FeraSpin™ R for a magnetic field strength of $H = 12\text{mT}/\mu_0$. These measured spectra were used to generate artificial MPI signals corresponding to the defined particle distribution.

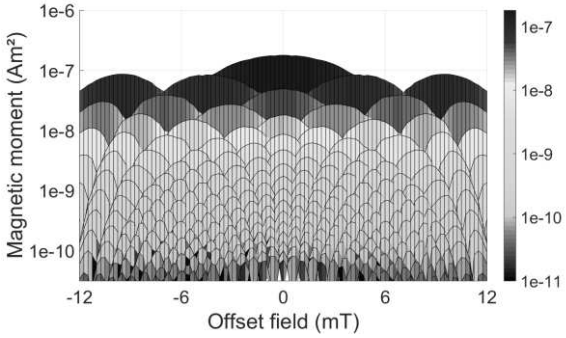

Figure 1. MPS acquired system function

This distribution can be seen in figure 2 (a) with a total simulated field of view of d = 19.2 mm and a maximum concentration of c = 5 mmol/L. Figure 2 (b) to (d) depict the reconstructed images for noise levels of A_{SD} = 1E-12 Am², A_{SD} = 3E-12 Am² and A_{SD} = 5E-12 Am² with SD being the standard deviation.

It can be seen that the noise level directly influences the distinguishability of the defined particle clusters and therefore lead to a decrease of the achievable resolution.

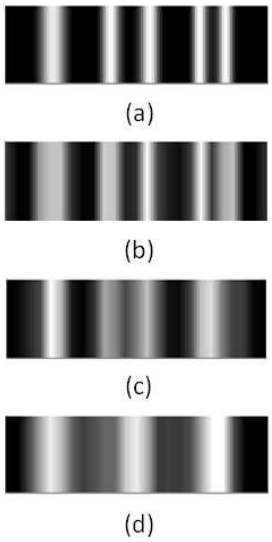

Figure 2. Defined particle distribution (a) and reconstruction results for various noise levels. (b): A_{SD} = 1E-12 Am², (c): A_{SD} = 3E-12 Am², (d): A_{SD} = 5E-12 Am²

While in figure 2 (b) the particle clusters with the smallest distance of 1.75 mm can be separated, the resolution decreases in (c) to 2.7 mm and in figure 2 (d) only the three main complexes can be resolved. This enables us to estimate the achievable resolution for every tracer we measure with this method.

Conclusion

In our work we presented a method to characterize magnetic nanoparticles as MPI tracers in a significantly shorter time than actual MPI measurements would require. This allows us to pre-characterize particles and their imaging performance in terms of voxel volume, concentration and tolerated noise level before actual MPI measurements with a phantom or an animal. Due to the higher throughput, this method might also lead to a better understanding of the relation between basic particle parameters and the imaging performance.

Acknowledgments

This work was supported by the German Federal Ministry of Economics and Technology grant No. KF2303711UW2 and KF2725002UW2 and by the EU FP7 research program “Nanomag” FP7-NMP-2013-LARGE-7
We also thank nanoPET Pharma GmbH for providing FeraSpin™ R for our research.

References

[1] **Gräser et al.**, “Determination of a 1D-MPI-System-Function using a Magnetic Particle Spectroscope”, 44. Jahrestagung der Deutschen Gesellschaft für Biomedizinische Technik im VDE, vol. 56, 2011

[2] **Grüttner et al.**, „ On the formulation of the image reconstruction problem in magnetic particle imaging”, Biomedizinische Technik/Biomedical Engineering, vol. 58, no. 6, 2013

Magnetic Biocomposites for Remote Melting

Mengbo Zhou[1], Tim Liebert[1], Robert Müller[2], Andrea Dellith[2], Thomas Heinze[1]

1 Institute of Organic Chemistry and Macromolecular Chemistry, Friedrich Schiller University of Jena, D-07743 Jena, Germany.
2 Leibniz-Institute of Photonic Technology e.V. (IPHT), Postfach 100239 D-07702 Jena, Germany.

The aim of this project is to develop a biocompatible hybrid material from a defined meltable polymer and functional nanoparticles, which can be softened under an induced alternating magnetic field (AMF) and allows in that way a release of active pharmaceutical ingredients. This could be a suitable alternative for swellable hydrogel composites embedded with magnetic particles as remote controlled biomaterials [1].

A new approach towards the fabrication of biocompatible composites suitable for remote melting is presented. For that purpose, fatty acid esters of dextran with adjustable melting points in the range of 30 to 140 °C were synthesized. Esterification of the polysaccharide by activation of the fatty acids with iminium chlorides guaranteed mild reaction conditions leading to high quality products as confirmed by FTIR- and NMR spectroscopy as well as by gel permeation chromatography [2]. A method for the preparation of magnetically responsive bionanocomposites was developed consisting of combined dissolution/suspension of the dextran ester and oleic acid hydrophobized magnetite nanoparticles (MNPs) in an organic solvent followed by homogenization with ultrasonication, casting of the solution, drying and melting of the composite for a defined shaping. This process leads to a uniform distribution of MNPs in nanocomposite as revealed by scanning electron and optical microscopy (Fig. 1) [3].

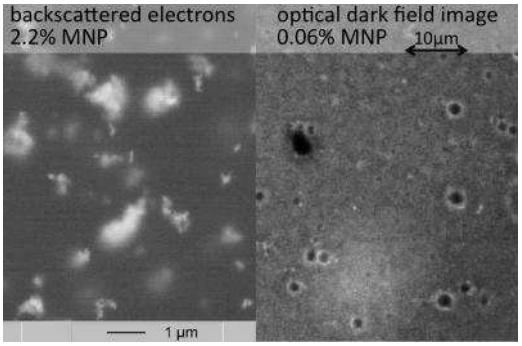

Fig.1: SEM (left) and optical image (right) of MNP in dextran ester polymer

DSC measurements were carried out to evaluate if embedment of particles modifies the thermal behavior of dextran esters. The first heating curve of dextran palmitic ester (DE9) and nanocomposite obtained with this sample (1 and 2 wt. % MNP) is shown in Fig. 2. These DSC measurements of the nanocomposites show the same signals with comparable intensities, which means the physical presence of the MNP does not affect the thermal behavior of dextran ester.

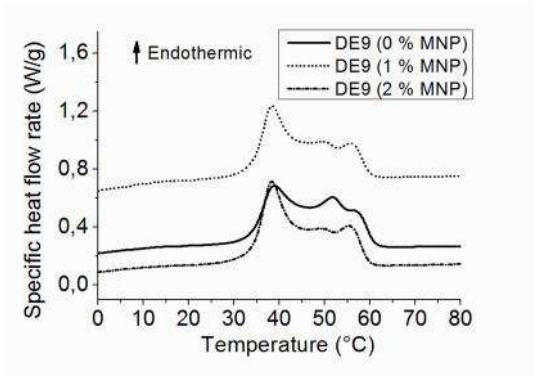

Fig. 2: Thermal behavior of dextran palmitic ester and nanocomposite illustrated by the DSC (solid line: DE9; point: DE9 with 1 wt. % MNP; dash-point: DE9 with 2 wt. % MNP)

Samples of different geometries were exposed to an alternating magnetic field (400 kHz, 20 kA/m). As shown in the Fig. 3, it took 160 s to heat such a disk-type sample of C8 (dextran palmitic ester with 2 wt. % MNP) above the melting temperature (40 - 50 °C) of the dextran ester. In case of a comparable sample of C9 (dextran myristic ester with 2 wt. % MNP), it took only 120 s (melting temperature 40 °C). After AMF was switched off, the nanocomposites were quickly cooled by air and the temperature dropped down under the melting temperature within 2 min. These data confirm that the material is in principle very well suitable for remote melting, e.g., in controlled release applications. In a further experiment, the nanocomposite was combined with gelatin (C10) to obtain a model system comparable to a biological surrounding. The specific absorption rate of the nanocomposite (10 wt. % in gelatin) was determined as 6.3 W/g with a fiberoptical sensor on a bulk shaped sample (Fig. 3), which was subjected to AMF (20 kA/m, 400 kHz). A plateau at 55 °C was found and lasted for about 80 s.

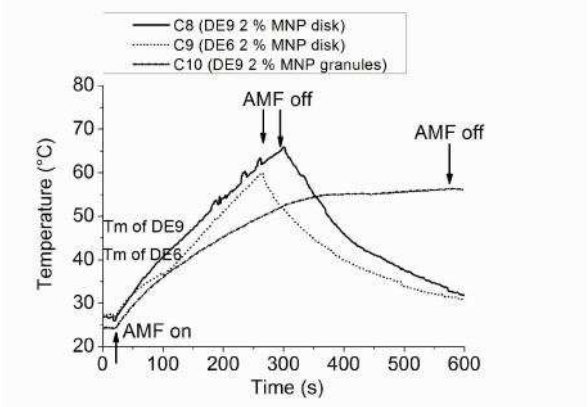

Fig. 3: Surface temperature by IR thermography of bionanocomposite disks (1400 µm thickness and radius of 8 mm) and nanocomposite granulesin gelatin subjected to continuous AMF

Microscopic investigations in molten state of the matrix allow the observation of the movement of single particles in the matrix that can be influenced by a superposition of a magnetic field gradient driven movement and convection by thermal gradient (Fig.4).

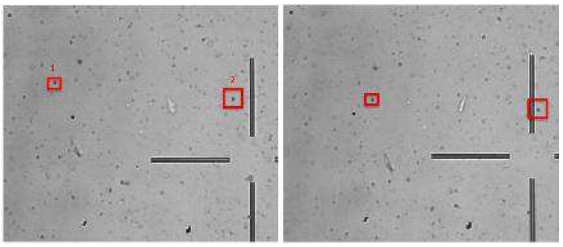

Fig.4: Single particle tracking (Fig. right after 45s) under external heating and static magnetic field gradient; particle velocity ca. 0.25 µm/s

Conclusion

It is shown that defined remote melting of biocompatible nanocomposites is possible for the first time. This may lead to a new class of magnetic remote control systems, which are suitable for controlled release applications or self-healing materials.

Acknowledgments

The financial support of the German Science Foundation (DFG, priority program SPP 1681, contracts HE2054/14-1 and MU2382/4-1) is acknowledged. We sincerely thank Dr. Grit Festag for GPC measurements and Mr. Renzo Paulus for DSC measurements in Jena Center for Soft Matter and Prof. I. Hilger (IDIR Jena) for providing the IR camera.

References

[1] N. S. Satarka, et al, Acta Biomater. 4, 11-16, 2008; T. Hoare, et al, Nano Lett. 11, 1395-1400, 2011

[2] T. Liebert et al, Biomacromolecules 12, 3107-3113, 2011

[3] M. Zhou et al, Biomacromolecules submitted in 2015

Ferrofluid based artificial tactile sensors

T.I. Volkova[1], S. Hermann[1], T. Kaufhold[1], V. Böhm[1], I. Zeidis[1], K. Zimmermann[1], V.A. Naletova[2]

[1] *Technische Universität Ilmenau, Department of Mechanical Engineering, Technical Mechanics Group, Ilmenau, D-98693, phone: +49-3677-69-2474, fax: +49-3677-69-1823, e-mail: tatiana.volkova@tu-ilmenau.de*
[2] *Faculty of Mechanics and Mathematics, Lomonosov Moscow State University, GSP-1, Leninskie Gory 1, 119991 Moscow, Russia*

Introduction

Vibrissae are long tactile hairs in the snout ('mystacial') and forelimb ('carpal') region of mammals. They grow from a special hair follicle, which is embedded in a capsule of blood [1]. The strongly innervated viscoelastic bearing of the vibrissa, so called follicle-sinus complex (FSC), is surrounded by several types of muscles allowing oscillations of the hair ('whisking').

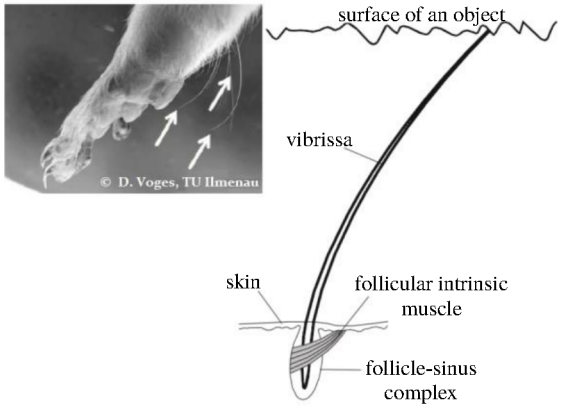

Fig.1 Triple of carpal vibrissae (arrows) at a forelimb of *Rattus norvegicus* [2] and the schematic drawing of a vibrissa sweeping past a rough surface

Vibrissae are specialized in spatial sensing and can be considered as a biological role model for tactile sensors [3]. The current paper presents a mechanical model of a vibrissa as a rigid rod with an attached paramagnetic body. The viscoelastic bearing of the vibrissa inside the FSC is modelled by a volume filled with ferrofluid (FF). An applied magnetic field exerts a force on the body immersed in FF [4,5,6]. To realize controlled oscillations of the mechanical vibrissa, it is necessary to know the dependence of this force on magnetic properties of the mediums and on the characteristics of the applied magnetic field.

Problem of a magnetic force calculation

A rigid body of paramagnetic material is submerged in a FF volume and placed in an external magnetic field $\vec{H}_0$, Fig. 2. Gravitation is not taken into account. In the stationary case the pressure and velocity of the fluid do not contribute to the electrodynamic problem of calculating the distorted magnetic field $\vec{H}$. Therefore, the magnetic force $\vec{F}_b$ acting on the body is determined by the terms associated with $\vec{H}$.

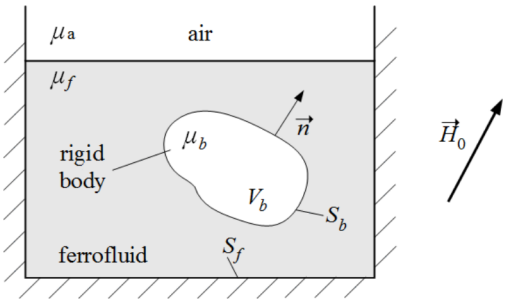

Fig.2 Body of paramagnetic material in a vessel filled with FF in an external magnetic field $\vec{H}_0$

If the FF occupies an infinite volume, in other words, the effect of the vessel walls on the magnetic field is neglected, the force $\vec{F}_b$ acting on the body is directed along the gradient of the applied magnetic field. When the non-uniform field $\vec{H}_0$ is so strong that the magnetization of the FF M_f is related to H_0 by $4\pi M_f / H_0 \ll 1$, the expression for $\vec{F}_b$ has the form [4]:

$$\vec{F}_b = V_b \left(M_b(H_0) - M_f(H_0) \right) (\vec{\nabla} H)_0. \quad (1)$$

Here V_b is the volume of the body, M_b the magnetization of the paramagnetic material, the index 0 denotes the strength of the undistorted magnetic field and its gradient at some point of the body.

Experimental evaluation

In order to measure the magnetic force acting on a body immersed in a FF volume, the setup shown in Fig. 3 is designed. The cuboid vessel (inner dimensions: 4×4×5.5 cm^3) and the rigid rod are made of aluminium. A quantity of 60 cm^3 of the oil-based FF (APG S12n) produced by FerroTec is used. The non-uniform applied magnetic field is generated by an NdFeB magnet (4×1×2 cm^3), which is moved by a linear actuator. The force $F_b(x)$ dependent on a distance x between the magnet and the center of the body is measured by a load cell on a lever arm, a = 4.2 cm, b = 9.5 cm.

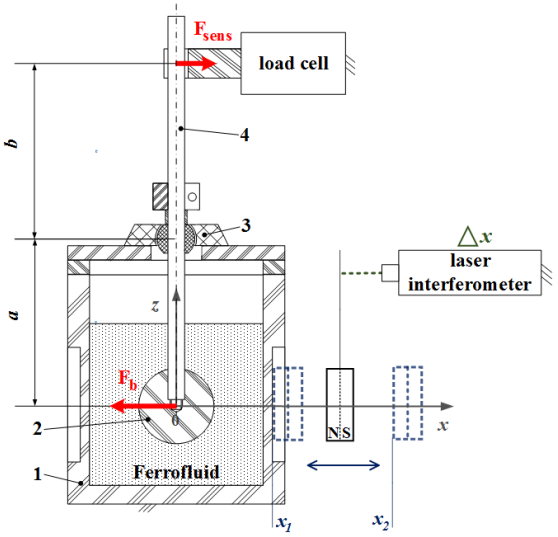

Fig. 3. Sketch of the setup: 1 – vessel, 2 – paramagnetic body, 3 – bearing, 4 – artificial vibrissa

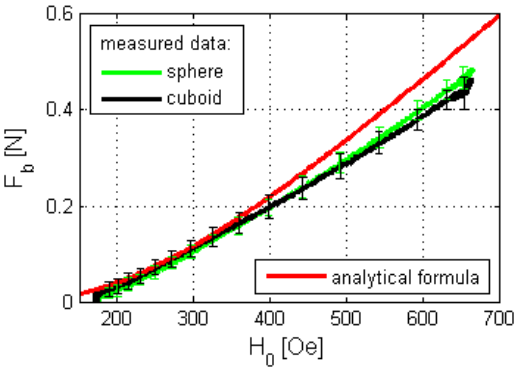

Fig. 4. Experimental results for aluminium bodies with $V_b = 4.19$ cm^3: a sphere of radius 1 cm and a cuboid of dimensions 2.5×0.96×1.75 cm^3. Analytical result given by equation (1)

Several pairs of aluminium bodies of the same volume but different shapes (spherical/cuboidal) are used to investigate the dependence of $F_b(H_0)$ on geometry of the body. It is shown that the magnetic force depends primarily on the volume of the body, Fig. 4. Although the FF volume in the experiment is bounded, the obtained results confirm the analytical formula (1).

To conclude, the magnetic force acting on a paramagnetic body immersed in a FF volume is measured in the non-uniform magnetic field of a permanent magnet. The controlled oscillations of the mechanical vibrissa may be realized by means of an external alternating magnetic field.

Acknowledgments

This work was supported by DFG with the research grant ZI 540/16-1 and as part of priority program 1681 grant ZI 540-17/1.

References

[1] J. Dörfl: The musculature of the mystacial vibrissae of the white mouse. J. Anat., 135 (1982) 1, pp. 147–154.

[2] M. Schmidt et al.: Technical, non-visual characterization of substrate contact using carpal vibrissae as a biological model: An overview. Proc. of the 58th International Scientific Colloquium, IWK 2014. Ilmenau, Germany, September 8-12, 2014.

[3] C. Behn, T. Schmitz, M. Fremerey, D. Voges, H. Witte, K. Zimmermann: Tasthaare für die Mechatronik - Modellbildung, Simulation und Adaptive Regelung. In: Tagungsunterlagen Mechatronik 2013, Seiten 7–12. Aachen, Deutschland, März 6-8, 2013.

[4] V.A. Naletova, I.A. Shkel: Force exerted on a body by a magnetic liquid in a nonuniform magnetic field. Magntohydrodynamics, 23 (1987) 2, pp. 173–176.

[5] A.S. Kvitantsev, V.A. Naletova, V.A. Turkov: Levitation of magnets and paramagnetic bodies in vessels filled with magnetic fluid. Fluid Dynamics, 37 (2002) 3, pp. 361–368.

[6] R.E. Rosensweig: Buoyancy and stable levitation of a magnetic body immersed in a magnetizable fluid. Nature, 210 (1966) 5036, pp. 613-614.

Comparing the coarsening dynamics of ferromagnetic networks

Armin Kögel[1], Reinhard Richter[1],
Elena Pyanzina[2,3], Sofia Kantorovich[2]

[1]*Experimentalphysik 5, Universität Bayreuth, 95440 Bayreuth, German,*
[2] *Ural Federal University, 620000 Ekaterinburg, Russia,*
[3] *Computergestützte Physik, Universität Wien, 95440 Vienna, Austria*

Introduction

Permanent magnetic dipoles may self-assemble to linear chains and rings, even without an externally applied magnetic field. This has been investigated for nano-sized particles in ferrofluids; see e.g. [1,2]. However, in this system the emerging structures and their dynamics are difficult to observe. Similar aggregates have also been observed in a mixture of glass beads and magnetized steel spheres, which are shaken in a vessel [3]. In our contribution we focus on the formation of transient networks in this system, when quenching the amplitude of the vibrations.

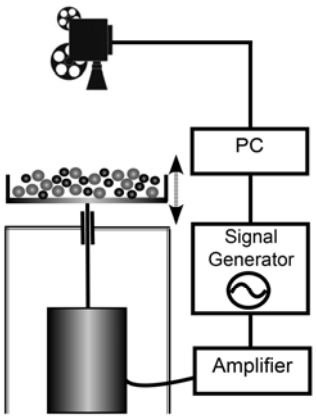

Figure1: Sketch of the experimental setup.

Experimental setup

Steel spheres with a diameter of 3mm are permanently magnetized in a homogeneous field of 1.15T. Consecutively they are filled together with glass spheres (diameter of 4mm) in a rectangular vessel which is vibrated by an electromagnetic shaker. As sketched in Fig.1, a long rod takes care that the alternating magnetic field generated in the shaker has no significant influence on the steel spheres. A personal computer controls the sinusoidal output of a signal generator, connected via an amplifier to the shaker. The beads are illuminated from below utilizing an electroluminescent display. The dynamics of the beads is recorded from above using a charge coupled device camera connected to the computer.

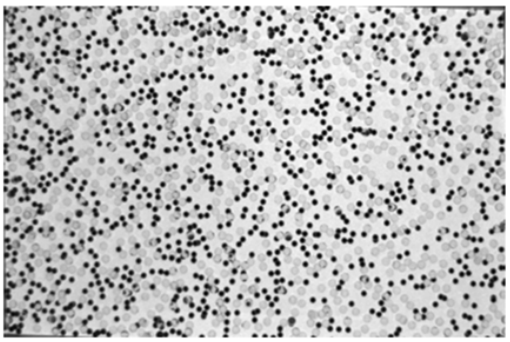

Figure 2: Gas-like state of shaken steel spheres (black) and glas spheres (grey).

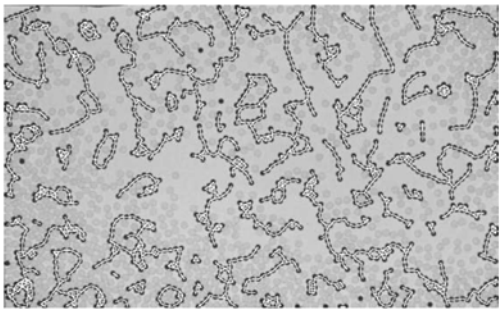

Figure 3: Formation of transient networks. Clusters detected by computer vision are marked by lines.

Experimental results

For large shaker amplitudes we observe a gas-like state of single steel and glass spheres, as shown in Fig.2. After a quench of the shaker amplitude to a lower value we record the assembly of steel spheres to

chains and networks, as shown in Fig. 3. Eventually compact clusters emerge. A movie of this transition can be found at [4]. Utilizing computer vision (cf. Fig. 3) we are extracting characteristic measures of the networks [5]. They comprise the average number of neighbors $\bar{k}$, the distributions of cluster size, and gyration radius, the characteristic path length and the efficiency of the network. Here we present as an example the average number of neighbors in Fig.4. We find that its evolution is well described by the logistic function

$$\bar{k}(t) = \bar{k}_{\max}\left(1 - \frac{1}{1+(t/t_0)^p}\right).$$

We discuss the evolution of the characteristic network measures in the context of a recently proposed model of *viscoelastic phase separation* [6]. In this model the dynamic asymmetry between the glass spheres and the magnetized steel spheres, with their enhanced shear viscosity, leads to phase separation and the formation of transient networks.

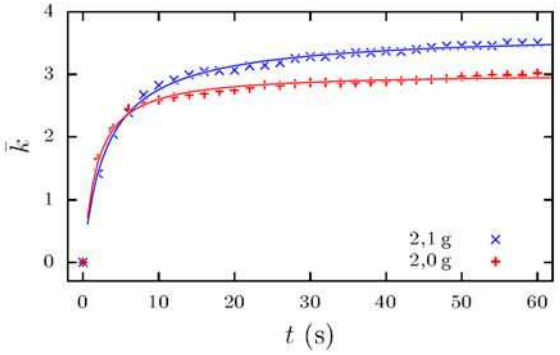

Figure 4: Evolution of the avg. number of next neighbors for different acceleration amplitudes.

Simulations

We employ Molecular Dynamics simulations in the software package ESPReSso, in order to understand, if the presence of nonmagnetic beads changes the self-assembly scenario. Even though, there is no possibility to directly compare the results of the coarse-grained model of the equilibrium behavior of dipolar soft spheres and soft spheres used in our simulations to the experimental data, one can see already using this 'toy'-model that the mixture exhibits a qualitatively different cluster distribution as shown in Fig.5.

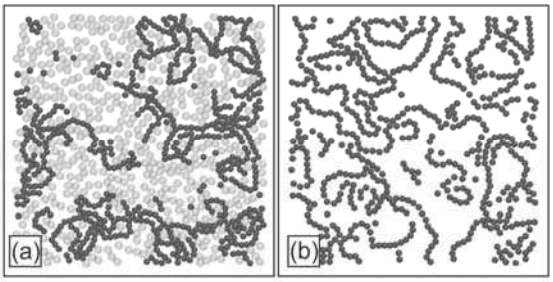

Figure 5: (a) Snapshot of a mixture of neutral and dipolar spheres with the experimental size-ratio and comparable area fraction; (b) pure dipolar system with the same parameters.

Acknowledgments

The authors would like to thank T. Müller for early support in particle detection, and R. Maretzki, I. Rehberg, E. Katifori and S. Kantorovich for discussion.

References

[1] P.G. De Gennes and A. Pincus, *Pair Correlations in a Ferromagnetic Colloid*, Phys. Kondens. Mater. **1**, 189 (1970).

[2] T. A. Prokopieva, V. A. Danilov, S. S. Kantorovich, Ch. Holm, *Ground state structures in ferrofluid monolayers*, Phys. Rev. E **80**, 031404 (2009).

[3] D. L. Blair, A. Kudrolli, *Clustering transitions in vibrofluidized magnetized granular materials*, Phys. Rev. E **67**, 021302 (2003).

[4] A movie can be accessed at http://www.youtube.com/watch?v=Tt82K6osdzM

[5] S. Boccaletti, V. Latorab, Y. Morenod, M. Chavezf, & D.-U.Hwanga, *Complex Networks: Structure and dynamics.* Physics Reports **424**, 175–308 (2006).

[6] H. Tanaka, *Viscoelastic phase separation*, J. Phys.: Condens. Matter. **12**, R207 (2000). H. Tanaka, Y. Nishikawa and T. Koyama, *Network-forming phase separation of colloidal suspensions*, J. Phys.: Condens. Matter. **17**, L143 (2005).

Quantitative Analysis of Gelatin Adsorption on Colloidal Nanorods by Magneto-Optical Relaxation Measurements

K. Birster, A. Tschöpe and R. Birringer

Universität des Saarlandes, FR 7.2 Experimentalphysik, 66123 Saarbrücken

Introduction

Nonspecific protein adsorption onto solid surfaces is a fundamental phenomenon with implications for nanotechnology, biomaterials, protein diagnostics and microrheology in biological systems. In the latter, adsorption of proteins on colloidal probe particles results in (i) an increase of the hydrodynamic volume of the particles and (ii) a reduction of the residual concentration of proteins in the bulk solution. The separation of these two effects is an important task which is addressed in the present study.
We demonstrate a method to quantify the amount of gelatin molecules adsorbed on the surface of nickel nanorods using dynamical magneto-optical measurements and a sequential depletion procedure. Furthermore we make use of the nanorod length as an experimental variable and the different scale-dependence of hydrodynamic size and microviscosity on the relaxation frequency to discriminate the two contributions.

Methods

Ferromagnetic nickel nanorods were synthesised by pulsed electrodeposition of nickel into a nanoporous AAO template [1, 2]. After dissolution of the oxide layer, the colloidal suspension was sterically and electrostatically stabilised using PVP as surfactant at pH 6.
The rotational motion of ferromagnetic nanorods driven by an external oscillating magnetic field is monitored through optical transmission measurements (OF-MOT) [3]. In

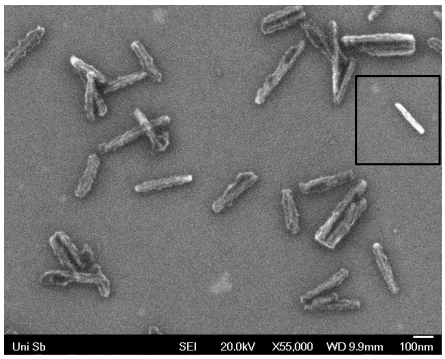

Figure 1: REM image of Ni nanorods with adsorbed gelatin shell and initial PVP-coated nanorod (square).

the Voigt–Kelvin model the characteristic relaxation frequency ω_c^0 in Newtonian fluids is a function of a geometry factor K, which depends essentially on average hydrodynamic length L and diameter D of the nanorods, and the viscosity η of the medium:

$$\omega_c^0 = \frac{1}{K(L,D)\eta}. \qquad (1)$$

An increasing hydrodynamic volume due to gelatin adsorption is accompanied by a decrease of the relaxation frequency compared to a measurement in pure water.
While the thickness of the adsorbate layer can be calculated from hydrodynamic models [4], their molecular density and thus the amount of gelatin adsorbed on the particle surface and of residual gelatin in the sol remains unknown. This information can be retrieved using a sequential depletion series. Starting point is a gelatin sol at a concentration of $c \simeq 5\,\mathrm{mg/dl}$. A fixed number of nanorods is dispersed in the sol and their

relaxation frequency ω_c^0 determined. After separation of the nanorods from the sol by centrifugation, fresh nanorods are dispersed in the supernatant and this procedure is repeated until the relaxation frequency returned to the value of nanorods in pure water. With the assumption that the gelatin forms a uniform adsorbated layer with constant density ρ, we can reconstruct the amount of free gelatin in solution at each intermediate step.

Results

Fig. 2 shows the shell volume of the adsorbed gelatin as a function of the free gelatin concentration in solution measured by the sequential depletion method. Data points were measured from right to left. In each step, the characteristic frequency increases, indicating a reduced adsorption volume. Hence, we notice that the adsorbed volume is a function of the free bulk concentration. Further dilution experiments show that adsorbed molecules are irreversibly bound to the particles surface.

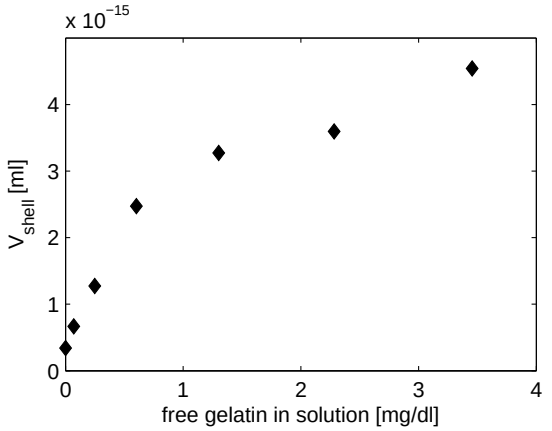

Figure 2: Shell volume of gelatin adsorbed onto Ni nanorods as a function of free gelatin in solution determined by the sequential depletion method.

As evident from Eq. 1, the relaxation frequency depends on the hydrodynamic size of the particles and the viscosity of the matrix. In the previous analysis, we used the viscosity of pure water which is virtually identical to the macroscopic viscosity of a gelatin sol at such low concentrations. However, if the changes in viscosity are not negligible, we can make use of the different scale dependence of the two contributions as function of the nanorod length. An increasing viscosity results in a constant ratio of $\omega_c^0/\omega_c^{H_2O} = \eta^{H_2O}/\eta^{\text{solvent}}$ independent of the nanorod length whereas the reduction ω_c^0 caused by an adsorbate layer with thickness λ is more pronounced at smaller nanorods, which is verified experimentally, Fig. 3.

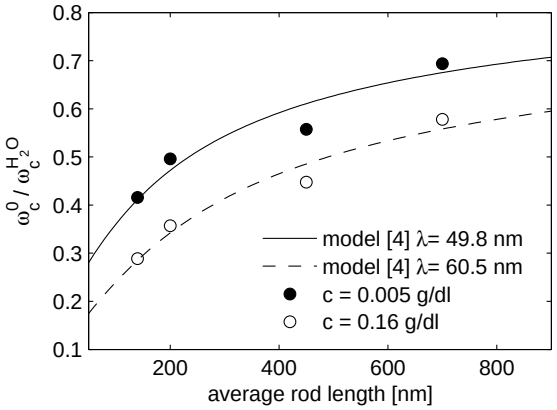

Figure 3: Normalized characteristic relaxation frequency of Ni nanorods in gelatin solutions as a function of the average rod length.

Acknowledgments

We acknowledge financial support by the DFG Priority Program 1681 (grant TS62/4-1).

References

[1] Masuda and Fukuda; Science 268 (1995), p. 1466.

[2] Bender P. et al.; J. Magn. Magn. Mater 323 (2011), p. 2055.

[3] Tschöpe A. et al.; J. Appl. Phys. 116 (2014), p. 184305.

[4] Aragon and Flamik; Macromolecules 42 (2009), p. 6290.

Orientational distribution functions of suspended spindle shaped hematite particles in external magnetic fields

C. Passow, A. Nack, J. Wagner

Universität Rostock, Dr.-Lorenz-Weg 1, 18059 Rostock

Colloidal hematite spindles are a well defined colloidal model system with tunable aspect ratio [1]. Due to the interaction with an external field, an isotropic-nematic phase transition can be induced in the presence of moderate magnetic fields, whereby spindle-shaped hematite particles align perpendicular to the direction of an external field [2]. To determine the magnetic properties of hematite spindles, their orientational distribution functions (odf) in dependence on the flux density of an external field are investigated by means of small angle X-ray scattering employing synchrotron radiation as a probe.

The energy of a hematite spindle in a magnetic field depends on a permanent magnetic moment $\boldsymbol{\mu}_P$ as well as on an induced magnetic moment which results from the anisotropy of its magnetic susceptibility $\Delta\chi = \chi_\parallel - \chi_\perp$, where $\chi_\parallel$ denotes the susceptibility parallel and $\chi_\perp$ perpendicular to the particle director. For the comparatively small magnetic anisotropy of hematite the energy in a field with the flux density B can be written as

$$V_P = -\mu_P B \cos\vartheta_\mu - \frac{\Delta\chi}{2\mu_0} B^2 \cos^2\vartheta_P$$

where ϑ_μ is the angle enclosed between the permanent magnetic moment and the field direction and ϑ_P the one between the particle director and the field direction. The magnetic moment of the particle is tilted by ϑ_{off} from the particle director. Due to the cylinder symmetry of the particles the cosine of ϑ_μ can be written as

$$\cos\vartheta_\mu = \cos\vartheta_P \cos\vartheta_{\text{off}} - \sin\vartheta_P \sin\vartheta_{\text{off}}.$$

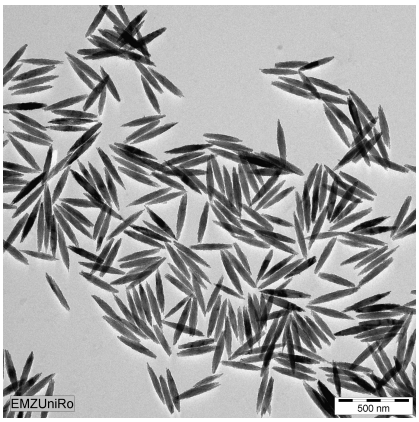

Since the Zeeman energy of the permanent dipole in an external field does not change under a rotation around the magnetic moment, a third Eulerian angle χ_P has to be considered. Opposite to the Zeemann energy, the energy of the induced dipole changes with χ_P if the permanent magnetic moment is not exactly parallel or perpendicular to the particle director. With the odf $p(\vartheta_P, \vartheta_{\text{off}}, \chi_P)$, in absence of particle-particle interactions, the scattered intensity can be written as

$$\begin{aligned} I(Q,\vartheta_Q) = &\int_0^\pi \int_0^{2\pi} \int_0^{2\pi} p(\vartheta_P, \vartheta_{\text{off}}, \chi_P) \\ &\times P(Q, \gamma(\vartheta_P, \varphi_P, \chi_P, \vartheta_Q)) \\ &\times \sin\vartheta_P \mathrm{d}\vartheta_\mathrm{P}\, \mathrm{d}\varphi_\mathrm{P}\, \mathrm{d}\chi_\mathrm{P}. \end{aligned}$$

Here, $P(Q,\gamma)$ is the form factor of the particle that depends on the modulus of the scattering vector and the angle γ between the particle director and the direction of the scattering vector. γ depends on the Eulerian angles $\vartheta_P, \varphi_P, \chi_P$ of the particle and the orientation ϑ_Q of the scattering vector with respect to the direction of the external field.

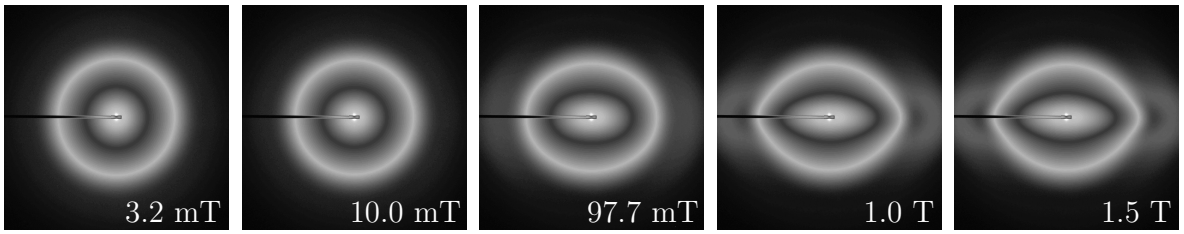

The magnetic parameters μ_P, ϑ_{offs} and $\Delta\chi$ are determined from a simultaneous fit of the small angle scattering in dependence on the modulus, the direction of the external field and the magnetic flux density. Herefore, the direction-dependent small angle scattering at 27 flux densities in the range $3 \times 10^{-3}\,\text{T} \leq B \leq 1.5\,\text{T}$ on a logarithmically equidistant scale is used. To reduce the two-dimensional scattering data, the intensity is sector averaged resulting in 72 sectors $\vartheta_Q = (0 \pm 2.5)°, (5 \pm 2.5)° \ldots (355 \pm 2.5)°$. The intensity of symmetrically equivalent sectors is averaged. After data reduction more than 2×10^5 symmetrically independent data points are used to determine three topological, three magnetic parameters and the number density of the particles.
With the form factor of polydisperse, spindle shaped particles, the field-dependent small angle scattering data can consistently be described. The topological parameters for the equatorial diameter, aspect ratio and polydispersity are in accordance to the results of electron microscopy.

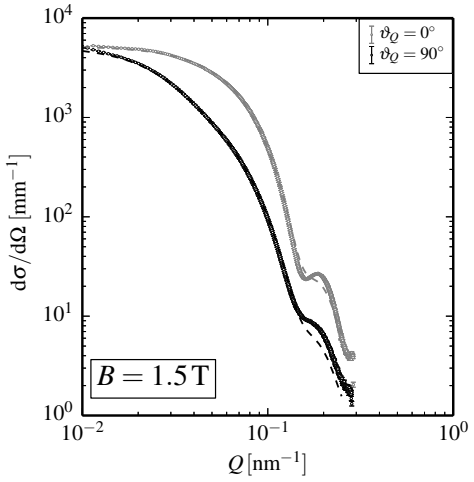

The aligning of hematite particles perpendicular to an external field results both from a negative magnetic anisotropy and a permanent magnetic field. The main contribution, however, results from a permanent magnetic field nearly orthogonal to the particle director. The tilt angle $\vartheta_{\text{offs}} = 78°$ is in accordance to the results of neutron diffraction experiments at spherical hematite nanoparticles [3]. This tilt angle results from the superposition of magnetic moments parallel and perpendicular to the trigonal axis which is the direction of the spindle axis. These moments originate from the coexistance of two magnetic phases which are stable below and above the Morin temperature at $T \approx 260\,\text{K}$, which, however, depends on the size and topology of the particles.

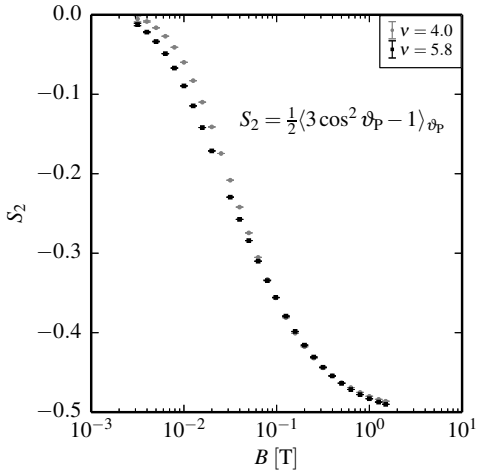

Financial support by the Deutsche Forschungsgemeinschaft in the framework of the priority program SPP 1681 is acknowledged.

[1] Ozaki et al. *Journal of Colloid and Interface Science*, 1984, 102, 146-151
[2] Märkert et al. *Journal of Applied Crystallography*, 2011, 44, 441-447
[3] Golosovsky et al. *Solid State Communications*, 2007, 141, 178 - 182

Effect of immobilisation of magnetic nanoparticles on its static and dynamic magnetisation behaviour

D. Eberbeck[1], A. P. Khandhar[2], K. M. Krishnan[3] and L. Trahms[1]

[1] Physikalisch-Technische Bundesanstalt, Berlin, Germany
[2] LodeSpin Labs, University of Washington – New Ventures Facility, Seattle WA 98195, USA
[3] Departments of Materials Science & Physics323, University of Washington, Seattle, WA9815, USA

Introduction

How immobilization of magnetic nanoparticles (MNP) changes their magnetic response to an external field? To address this question we immobilized structurally different MNP in different matrices. In order to catch effects of dipolar interaction between MNP, here we focus on large MNP which are preferable for e.g. hyperthermia, magnetic drug targeting and MPI (Magnetic Particle Imaging).

Materials and methods

We investigated the MNP systems MNP1, a high performing single core MNP-system with a narrow size distribution and two fractions of DDM128 (precursor of Resovist® with identical magnetic properties like Resovist®), E12 and E500, yielded by static magnetic separation at 12 mT and 500 mT. The MNP were immobilized by freeze drying in 10% mannitol resulting in a sugar matrix or by embedding the tracers in 12% gelatine. The sample's static and dynamic magnetisation behaviour was measured applying M(H) (MPMS, Quantum Design), Magnetorelaxometry (MRX), and MPS (MP-Spectrometer, Bruker BioSpin).

The distribution $f(d_m)$, assumed to be a lognormal one, of the effective magnetic diameters d_m referring to the diameter of a effective single domain sphere with the saturation magnetisation M_S was estimated analysing M(H) and Magnetorelaxometry (MRX) data [1]. From MRX-data also the anisotropy constant K is derived.

In order to compare M(H) and MPS-data quantitatively, the apparent 3rd harmonic of an MP-spectrum at 10 mT (applied excitation field in MPS) was derived from the measured M(H)-data as presented in [2], here denoted by $M_{3,s}$.

Results and discussion

The magnetic size distribution of the single core system MNP1 (mean diameter d_m=25 nm, σ=0.1) is nearly identical with the core size distribution obtained by TEM. The multicore MNP of DDM128 have fundamentally a bimodal size distribution, even after magnetic separation. Hence, the MNP contains large domains together with smaller ones. The mean magnetic moment of the fraction of larger MNP (E500, E12) are 1.5 aAm^2; 3.8 aAm^2 and 3.5 aAm^2 for E500; E12 and MNP1, respectively.

E500 and E12 were immobilised in sugar matrix and MNP1 in gelatine at low MNP concentrations (c(Fe)<1 mmol/L) in order to prevent dipolar interactions. This reduced the quasistatic magnetisation (Fig. 1a) by about 20%, 32% and 23%, respectively, here quantified by the $M_{3,s}$ (Table 1, marked rows). In case of E500 and E12 the dynamic magnetisation (MPS) drops additionally by 16%. In contrast, for MNP1 MPS-Signal drops by 20% in total, only, when fixing the MNP in gelatine. This low signal change may be attributed to the low anisotropy in connection with the high saturation magnetisation in MNP1, expressed by high H/H_K-ratio (Table 1). The fraction of magnetisation which may relax via Néel mechanism (relaxation in immobilised MNP), M_N/M, was calculated applying field dependent Néel relaxation time using the size distribution obtained from MRX-data. M_N/M, valid only for non-interacting moments, correlates quantitatively with mentioned signal of

immobilised MNP (Table 1). Slight deviations may be attributed to small interaction in these systems.

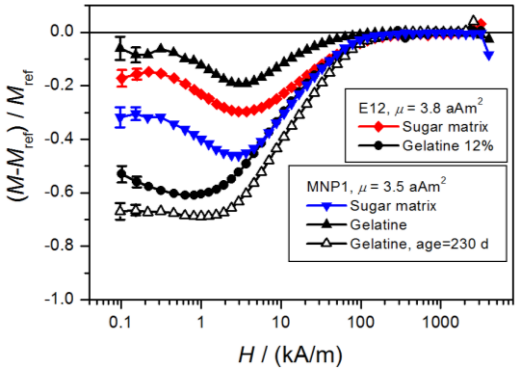

a)

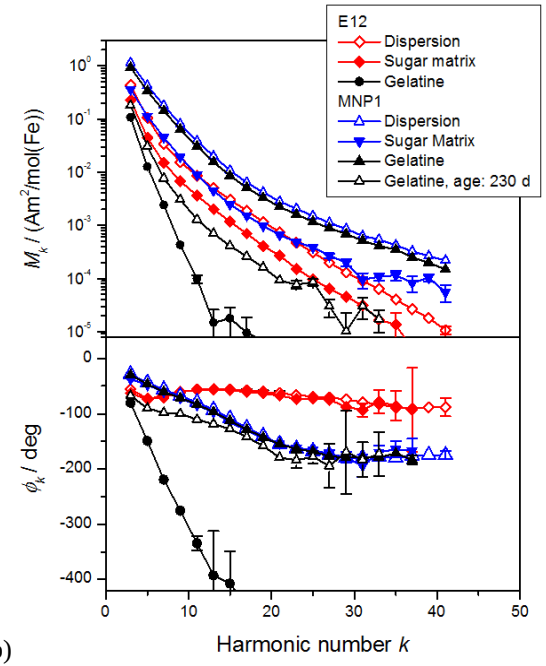

b)

Figure 1: Change of (a) the quasistatic magnetisation with respect to fluid reference sample (M_{ref}) and (b) MPS-signal (excitation field: 10 mT, 25 kHz) after immobilisation of MNP in indicated matrices.

However, the immobilisation in another matrix (E500 and E12 in gelatine, MNP1 in sugar matrix, c(Fe)<1 mmol/L) reduces the M_3 much stronger than in former matrices (Figure 1, Table 1). We attribute that to emerging dipolar interaction between MNP, despite of the low MNP concentration: Obviously, this interaction is evoked by aggregation, as shown by the development of the signals after partial drying of MNP1 in gelatine which naturally reduces the interparticle distances (Figure 1). Accordingly, we calculated the interaction of close packed MNP on the base of its structure yielding $E_{dd}/(k_BT)$=4±0.6, 11±1.5 and 11±1.5, for E500; E12 and MNP1, respectively, being in the same range like the anisotropy energy of $E_{dd}/(k_BT)$=8, 14 and 6. I.e. the smaller MNP of E500 with the lowest potential interaction also shows smaller effects. Interestingly, interaction may affect the whole spectrum qualitatively.

Table 1: Relations between third harmonics measured by MPS and calculated from quasistatic magnetisation (index s). Index f: fluid reference sample. anisotropy field: H_K=2 K/($\mu_0 M_s$), $\mu_0 H$=10 mT, M_N/M: fraction of magnetisation relaxing via Néel mechanism at 25 kHz

Sample	$\frac{M_{3,s}}{M_{3,sf}}$ %	$\frac{M_3}{M_{3,f}}$ %	$\frac{H}{H_K}$	$\frac{M_N}{M}$ %
E500				
sugar m.	80	63	0.20	70
gelatine	63	52	0.22	66
E12				
sugar m.	68	52	0.27	65
gelatine	33	25	0.34	27
MNP1				
sugar m.	46	32	0.38	90
gelatine	77	81	0.63	100
gelatine[1)]	23	16		

1) Sample aged by 230 days and dried partially reaching about 15% of its initial volume.

Conclusion

Immobilisation and dipolar interaction may alter static and dynamic magnetisation behaviour strongly. Accordingly, quantitative MPI may lead to substantial errors if reference sample is not adapted. Also the hyperthermia effect may change if large MNP aggregate.
In particular MPS reveals as a sensitive tool to quantify immobilisation and interaction effects with high specificity.

Acknowledgements

The research was supported by the DFG priority program SPP 1681.

References

[1] D. Eberbeck, F. Wiekhorst, U. Steinhoff, L. Trahms, J. Phys.: Condens. matter 18 (2006), S2829-S2846.
[2] D. Eberbeck, F. Wiekhorst, S. Wagner, L. Trahms, Appl. Phys. Lett. **98** (2011), 182502.

Microgels at the water/oil interface: In-situ observation of structural ageing and two-dimensional magnetic bead microrheology

Shilin Huang[1], Kornelia Gawlitza[2], Regine von Klitzing[2], Laurent Gilson[1], Johannes Nowak[3], Stefan Odenbach[3], Werner Steffen[1], Günter K. Auernhammer[1]

[1]*Max Planck Institute for Polymer Research, Ackermannweg 10, 55128 Mainz, Germany*
[2]*Stranski-Laboratorium für Physikalische und Theoretische Chemie, Technische Universität Berlin, Strasse des 17. Juni 124, 10623 Berlin, Germany*
[3] *Institute of Fluid Mechanics, Chair of Measuring and Automation Technology, Technische Universitt Dresden, 01062 Dresden, Germany*

Introduction

In the last decade microgel particles have been explored to be used as potential Pickering emulsion stablilizers. The most widely studied microgel particles are made of poly(N-isopropylacrylamide) (PNIPAM). PNIPAM microgels are cross-linked and swollen in water. PNIPAM microgel particles raised a lot of interest in basic research and applied science since they are responsive to outer stimuli. PNIPAM has a lower critical solution temperature (LCST) of 32°C in aqueous solution. At room temperature they are in the swollen state, and once heating above LCST they collapse. PNIPAM microgels are known to adsorb spontaneously and almost irreversibly at the oil/water interface. They can even stabilize emulsions similar to Pickering emulsions. However, the details of structure and the viscoelastic property of the microgel-laden interface are still not well known.

Results

We synthesized fluorescently-labled poly(N-isopropylacrylamide) microgels, and used confocal microscope to observe their arrangement at the water/oil interface. The microgel particles aggregated spontaneously at interface. The aggregated structure could reorganize, see Fig. 1. Their interaction is weak enough that they are also able to reorganise in already formed clusters. As the interaction between the microgel particles are long-ranged, we suggest that the capillary force is dominating the aggregation. The inter-particle distance is thus a balance of aggregation force and repulsive force (e.g., overlap of the coronas and electrostatic repulsion). The microgel particles can show different morphologies at the interface depending on the local particle concentration. At low concentration they form isolated domains, which can form percolating structures with increasing concentration. At higher concentration they form fractal-like structures.

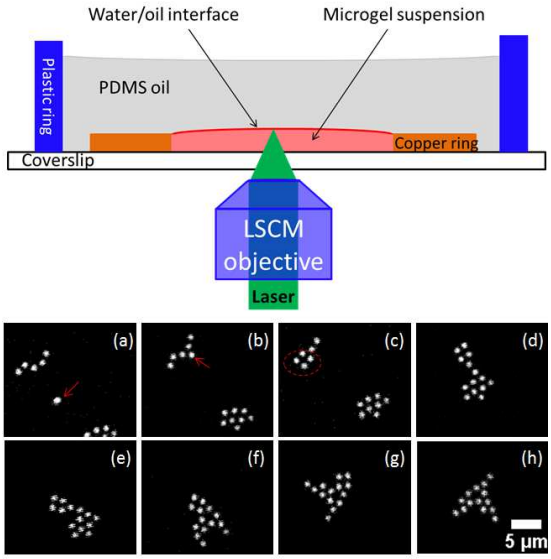

Figure 1 A sketch of the experimental setup and aggregation and assembly of microgel particles at the water/oil interface.

Different to the widely accepted picture that microgel particle tend to form hexagonal structure at an interface, our result pointed out the morphology of an interface is strongly dependent on the adsorption kinetics and history. Here, we used a system with high area/volume ratio, i.e. the adsorption was fast. The inter-particle distance, which is lower than assuming a hexagonal array, is dependent on the local particle concentration. We propose that there are two processes that set the inter-particle distances: aggregation by motion at the interface (at low concentration) and aggregation already during adsorption (at high concentration). The interfacial microgel structure did undergo ageing. Then the structure became denser and the voids in the structure became larger. The inter-particle distance also decreased during ageing (Fig. 2).

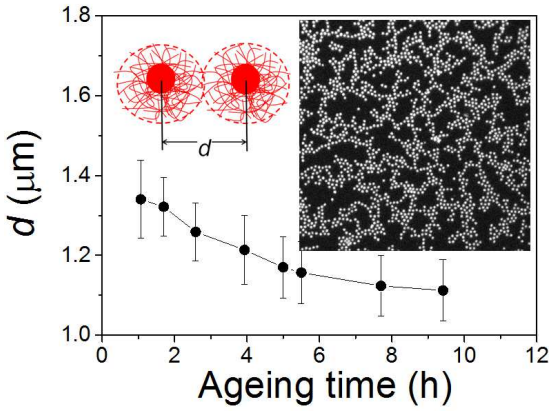

Figure 2 Aging of interface. The inter-particle distance also decreased during ageing

We used magnetic particle at the interface to apply a force to the microgel particles. We observed that on compression, the particles could be squeezed out on increasing the compression force (Fig. 3). A bridge formed by the microgel particles could resist compressional, extentional and bending force. Once deformed, the microgel particles at interface show cooperative rearrangements during deformation (Fig. 4).

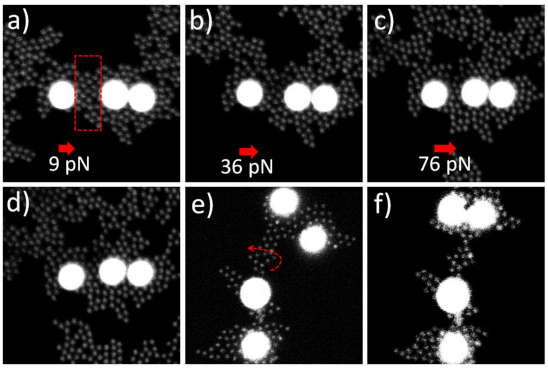

Figure 3 Using magnetic beads to compress the microgels at water/oil interface. The magnetic field was applied along the horizontal direction, and the field strength was increased from (a) 38.6 mT, (b) 60.2 mT to (c) 90.3 mT. Thus the corresponding magnetic force acting on the left particle was ~ 9 pN, ~ 36 pN and ~ 76 pN, respectively. (d) shows the morphology after removing the magnetic field. (e,f): A Lower magnetic field of 10.1 mT was applied horizontally. The toque acting on the bridge (arrow) is $\sim 4 \times 10^{-17}$ Nm. The structure in (e) changed into (f) after 3 min. Images size is 39 μm.

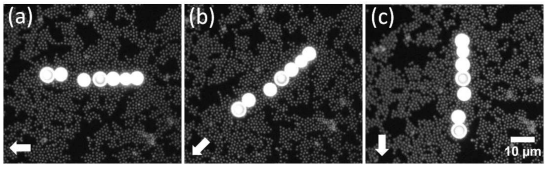

Figure 4 Shearing microgel-loaded interface by magnetic particle chain. A magnetic field of 216 mT is applied along the interface and quasi-staticly rotate counterclockwise, indicated by arrows. The scale bar is 10 μm.

Acknowledgments

We thank Dr. Peter Blümler for inspiring discussions on designing the Halbach magnetic arrays and acknowledge support by the DFG through the SPP 1681. GL acknowledges support by the DFG through the SPP 1486.

References

[1] S. Huang, K. Gawlitza, R. von Klitzing, L. Gilson, J. Nowak, S. Odenbach, W. Steffen, G. K. Auernhammer, Microgels at the water/oil interface: In-situ observation of structural ageing and two-dimensional magnetic bead microrheology, submitted.

Motion of soft magnetic particles in magnetorheological elastomers

T. Gundermann[1], S. Odenbach[1]

[1] TU Dresden, Chair of Magnetofluiddynamics, Measuring and Automation Technology, 01062 Dresden

Introduction

By combining magnetically controllable particles and a soft elastic matrix, a composite material with tunable physical properties can be developed. By applying a magnetic field, the particles inside the elastomeric matrix try to aggregate due to the interaction force of the particles influenced by the external magnetic field, the particle distance, their distribution and the elastic properties of the matrix itself.
The primary focus of this work was to develop a method to investigate this motion of the particles towards chain like aggregates in samples with isotropic particle distribution by using micro-computed-tomography (µ-CT) [1, 2] and a quantitative image evaluation method to separate the particles in the MRE. By using this algorithm, it was possible to compare different tomographic measurements of a MRE sample and obtain the 3D translation and rotation of the particles under magnetic field influence.

Samples

Cylindrical MRE Samples (d = h = 4 mm) with different particle weight contents of 0.5 to 15 wt.% have been produced. The sample itself was based on carbonyl iron powder with a mean diameter of d = 50 µm and a large size distribution. The particles have been dispersed in a soft polymeric matrix supplied by Wacker Corp. Germany. The basic matrix components were mixed with a high-viscosity softener. This leads to a reduction of the sedimentation rate during the polymerization process and to an isotropic particle distribution inside the elastomeric matrix.

Setup

The investigations were performed on a µ-CT system with an acceleration voltage of 160 kV. The µ-CT system has been combined with a sample holder coupled with two permanent magnets, enabling the investigation of the microstructure under influence of an external homogeneous magnetic flux density of approximately B = 270 mT [3, 4] After the characterization of the sample in its initial state, i.e. without external stimuli, it has been subjected to the magnetic field and its internal structure has been once more studied by µ-CT.

Results

It could be observed, that the particles try to aggregate to chain like structures parallel to the applied magnetic field (fig. 1a)
Also, the particles rotate by virtue of their shape anisotropy with their longest major axis in the direction of the field (fig. 1b).

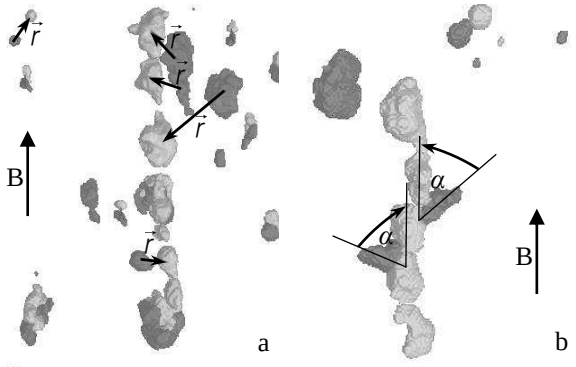

Fig. 1: Translation (a) and rotation (b) of particles under the influence of a magnetic field for a MRE sample with a content of 5 wt.%.

This results can be quantified by the norm of the displacement vector r (shown in fig. 1a) for the translation and the rotation angle α shown in fig. 1b.
Fig. 2 shows the motion of particles in the matrix under a magnetic field of B = 270 mT. It could be observed that the motion and the spread increases with increasing particle content. This can be explained by the fact that the polymerization and the elasticity of the matrix decreases with increasing particle content and the particles have a higher mobility, also the particle interaction force increases with increasing particle content.

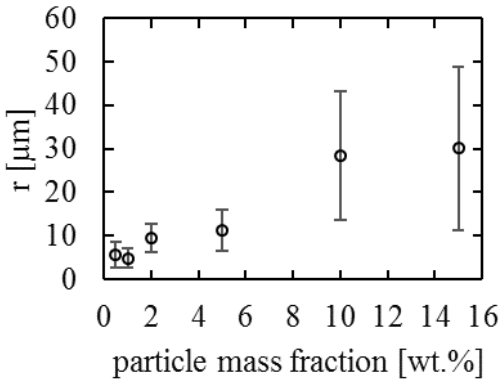

Fig. 2: The norm of the displacement vector r defines the translation of the particles inside the elastomeric matrix under the influence of a magnetic field of B = 270 mT for different particle mass fractions.

Considering the rotation of the particles, the shape anisotropy of the ferromagnetic particles shows an important role. Without magnetic field influence, the particles are isotropic dispersed in the matrix, therefore the distribution of α also is isotropic (fig. 3, black dots) By applying a magnetic field, the distribution of α shows a maximum at approximately 20° (fig. 3, grey dots). Reason for this is the interaction between magnetic forces, which tries to rotate the particles into the direction of the field and elastic restoring forces which counteract the magnetic forces.

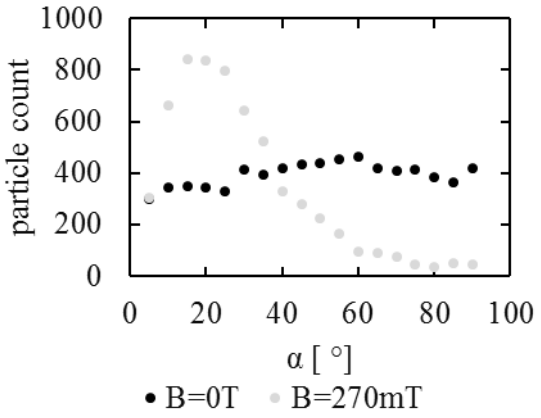

Fig. 3: The rotation angle α which describes the angle between the longest major axes and the magnetic field. The black dots shows the distribution if the magnetic field corresponds to B = 0 T and the grey dots show the distribution at B = 270 mT.

Summarized, we have found a method to analyze single particles in different kind of elastic matrices and to investigate their motion under the influence of a magnetic field which gives a new insight to microstructural effects in this kind of magnetic soft matter

Acknowledgments

DFG Zentralprojekt OD18/22 within SPP1681

References

[1] D. Günther, D. Yu Borin, S. Günther, and S. Odenbach, Smart Mater. Struct. **21** 015005 (2012)
[2] T. Borbath, S. Günther, D. Yu Borin, Th. Gundermann and S. Odenbach, Smart Mater. Struct. **21** 105018 (2012)
[3] Th. Gundermann, S. Günther, D. Yu Borin and S. Odenbach, J. Phys.: Conf. Ser. **412** 012027 (2013)
[4] Th. Gundermann and S. Odenbach, Smart Mater. Struct. **23** 105013 (2014)

Mössbauer spectroscopy for simultaneous in-situ disentanglement of Néel and Brown relaxation phenomena

J. Landers[1], S. Salamon[1], H. Remmer[2], F. Ludwig[2], H. Wende[1]

[1] Faculty of Physics and Center for Nanointegration Duisburg-Essen (CENIDE), University of Duisburg-Essen
[2] Institute of Electrical Measurement and Fundamental Electrical Engineering, TU Braunschweig

Introduction

Ferrofluids are promising materials for medical applications as well as mechanical engineering. For optimized utilization detailed knowledge of their fluidic and magnetic properties is essential, but often one has to make some efforts to obtain knowledge of both.
While, e.g., AC-susceptometry is a well proven technique to study the Néel relaxation behavior of magnetic nanoparticles and the Brownian motion of particles in fluids, it is limited by its ability to display the dominating, i.e. faster, relaxation process. Generally, other methods are also limited to obtain either Brownian OR Néel relaxation properties of a nanoparticular sample.
Mössbauer spectroscopy has been utilized to study Brownian motion before, since the fluids dynamic viscosity can be obtained from the broadening of the Mössbauer absorption lines, as shown in Fig. 1 [1-2]. Furthermore, it is one of the most prominent techniques to study Néel relaxation, because several regimes of relaxation frequencies can be identified studying the transition of the magnetically blocked sextet to the superparamagnetic doublet at higher temperatures [3-4].
Here we demonstrate the ability to simultaneously quantify relaxation parameters of Brownian motion and Néel relaxation by one series of spectra.

Methods

Commercial single-core iron oxide nanoparticles (IONPs, provided by Ocean NanoTech) with different diameter solved in glycerine-water solution were studied using Mössbauer spectroscopy in the temperature range from 220 K to ambient temperature to get insight in Néel and Brown relaxation phenomena.
Additional measurements of the magnetic AC-susceptibility were performed to obtain complementary information on the solutions dynamic viscosity and the particles superparamagnetic properties.

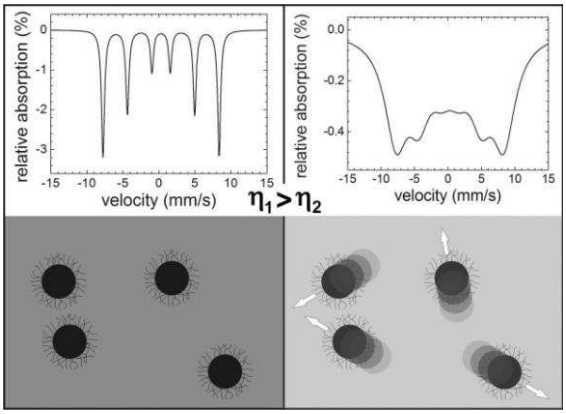

Fig. 1: Schematic line broadening and Brownian motion observable in ferrofluids of different dynamic viscosity.

Results

For nanoparticles larger than 15 nm, Mössbauer spectra near ambient temperature display a magnetically blocked sextet state, corresponding to the absence of fast Néel relaxation processes. For smaller particles, the transition of the magnetically blocked sextet to a superparamagnetic doublet was observed. Comparing the experimental spectra to theoretical calculations we are able to determine the particles magnetic anisotropy. Simultaneously, each subspectrum, sextets as well as doublets,

display a temperature dependent line broadening, providing information on the particles hydrodynamic diameter and the dynamic viscosity of the glycerine-water solution (Fig. 2).

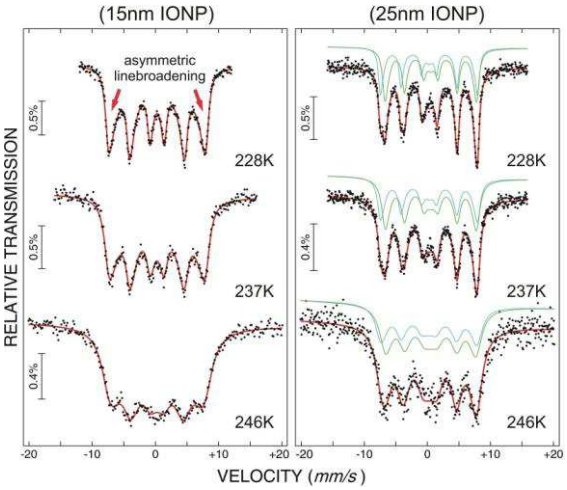

Fig. 2: Mössbauer spectra of 15 nm and 25 nm IONPs in glycerine-water solution measured at 228-246 K. Spectra display Brownian motion (line broadening) as well as beginning Néel relaxation (asymmetric, non-Lorentzian lines, left).

The temperature dependent decay in dynamic viscosity calculated from Mössbauer line broadening was crosschecked using rotation frequencies measured by AC-susceptometry, showing good agreement of both experimental methods (Fig. 3). Additionally, the domination of Néel relaxation indicated by AC-susceptometry in the high frequency regime for particles of 15 nm core diameter was verified by the Non-Lorentzian line shape in the Mössbauer spectra.
These results prove Mössbauer spectroscopy to be a versatile method for in-situ studies of Néel and Brown relaxation phenomena in ferrofluidic samples.

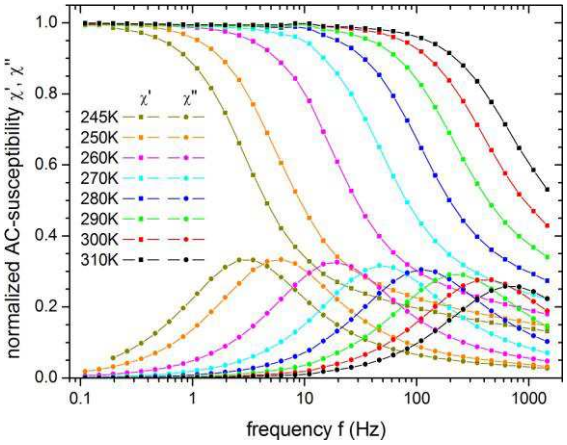

Fig. 3: Magnetic AC-susceptibility of 25 nm IONPs in glycerine-water solution measured at 245-310 K.

Acknowledgments

This work was supported by the DFG via Priority Program 1681 (WE2623/7-1 and LU-800/4-1). The authors are grateful to U. von Hörsten for his expert technical assistance.

References

[1] H. Keller and W. Kündig, Solid State Commun., **16**, 253-256 (1975)

[2] P. Fornal and J. Stanek, Acta Phys. Pol. A, **114**, 1667-1673 (2008)

[3] S. Mørup and E. Tronc, Phys. Rev. Lett., **72**, 3278-3281 (1994)

[4] J. Landers, F. Stromberg, M. Darbandi, C. Schöppner, W. Keune, and H. Wende, J. Phys.: Condens. Matter, **27**, 026002 (2015)

The anisotropy of the magnetoviscous effect in ferrofluids

J. M. Linke, S. Odenbach

Institute of Fluid Mechanics, Chair of Magnetofluiddynamics, Measuring and Automation Technology, 01062 Dresden, Germany

Introduction

If magnetic particles in a ferrofluid interact by dipole-dipole interaction, they form chain-like microstructures in the direction of an applied magnetic field [1]. This complex, magnetically controllable microstructure lies at the core of many interesting effects like viscoelasticity, shear-thinning and the magnetoviscous effect [2]. The latter describes the increase in the relative viscosity of a ferrofluid with interparticle interaction when a magnetic field is applied. The effect not only depends on the shearing of the fluid and the intensity of the applied magnetic field but also on the orientation of the magnetic field. In the present work this anisotropy of the magnetoviscous effect (MVE) has been studied in two ferrofluids - a cobalt ferrofluid with strong interparticle interaction and a magnetite ferrofluid with weak interaction.

Experimental method

The MVE has been measured in a slit die viscometer, in which the viscosity is proportional to the pressure loss along the die and the wall shear rate is variable by means of the flow rate [3]. The magnetic field has been applied by a four coil magnet system with a field homogeneity of 98% and three possible field orientations, illustrated in figure 1, parallel to: the fluid flow (1), the shear gradient (2), or the vorticity (3).

Ferrofluids

The ferrofluid with strong interparticle interaction has been supplied by the Strem Chemicals GmbH. It contained cobalt nanoparticles with a mean magnetic diameter

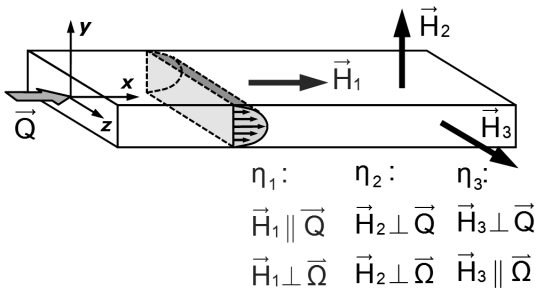

Fig. 1: Viscosity coefficients for different orientations of the magnetic field $\vec{H}$ with respect to the flow direction $\vec{Q}$ and the vorticity $\vec{\Omega}$.

of 15 nm and a coating of aluminum oxide and KorantinSH (N-oleyl sarcosine) dispersed in kerosene. The ferrofluid with weak interaction has been supplied by the FerroTec Ltd and contained magnetite particles with a mean magnetic diameter of 13 nm dispersed in a synthetic di-ester similar to the standard fluid APG513A. The average thickness of the surfactant coating s, the saturation magnetisation M_s, the initial susceptibility χ_{in}, the magnetic volume concentration ϕ calculated from M_s and the weighted interaction parameter λ_w of the fluids are summarised below.

Fluid	s (nm)	M_s (kA/m)	χ_{in} (-)	ϕ (vol%)	λ_w
Cobalt	3	10.6	2.53	0.7	10.6
Magnetite	2	28.1	1.76	6.3	2.5

Results

In both fluids the strongest MVE and also the strongest shear thinning have been observed for the magnetic field orientation parallel to the shear gradient ($\Delta\eta_2$). The longer the microstructures in the fluid become, the stronger is the viscous force they experience when oriented parallel to the shear gradient, up to a point where the

structures cannot grow any further and rupture. In the cobalt fluid this leads to a shear stabilizing in strong magnetic fields, compared to a continuously increasing shear thinning of the magnetite fluid. To gain an insight into the sphericity of the particles and structures in the fluid, the change in the viscosity for the field orientation parallel to the shear gradient, $\Delta\eta_2$, has been compared to the orientation parallel to the flow, $\Delta\eta_1$. For spherical, non-interacting particles the ratio $\Delta\eta_2/\Delta\eta_1$ is expected to be 1. Since both fluids contain elongated structures $\Delta\eta_2/\Delta\eta_1$ is larger than 1 but decreases with increasing shear rate and disintegration of the structures as seen in figure 2 (top). Further, $\Delta\eta_2/\Delta\eta_1$ decreases with increasing field intensity because the growth of microstructures oriented perpendicular to the flow is less significant than the growth of structures oriented in the direction of the flow.

At high shear rates and low field intensities, i.e. for short microstructures, the weakest MVE was found in both fluids in a field oriented parallel to the vorticity ($\Delta\eta_3$). In the magnetite ferrofluid $\Delta\eta_3$ even became zero in agreement with Shliomis' theory of non-interacting spherical particles. At low shear rates and strong fields, however, the weakest MVE was observed in a magnetic field parallel to the flow ($\Delta\eta_1$) because elongated microstructures oriented in the direction of the flow offer less hindrance to the flow than structures oriented perpendicular to the flow. Furthermore, the friction at the side walls of the slit die introduces an additional shear gradient, which turns the structures oriented parallel to the vorticity away from their neutral orientation. This effect becomes stronger for longer structures and enhances $\Delta\eta_3$, consequently the MVE ratio $\Delta\eta_3/\Delta\eta_1$, shown in figure 2 (bottom), rises beyond 1 with increasing field intensity and decreasing shear rates.

While the magnetoviscous behaviour of the magnetite fluid with weak interparticle interaction can be explained coherently by the field-driven formation and shear-induced disintegration of chain-like microstructures, the cobalt ferrofluid shows a different behaviour of $\Delta\eta_2/\Delta\eta_1$ and $\Delta\eta_3/\Delta\eta_1$ at weak magnetic fields < 10kA/m which still needs to be understood. Thus, future experiments will have to be complemented by molecular dynamics simulations to relate the rheological behaviour to microstructural changes.

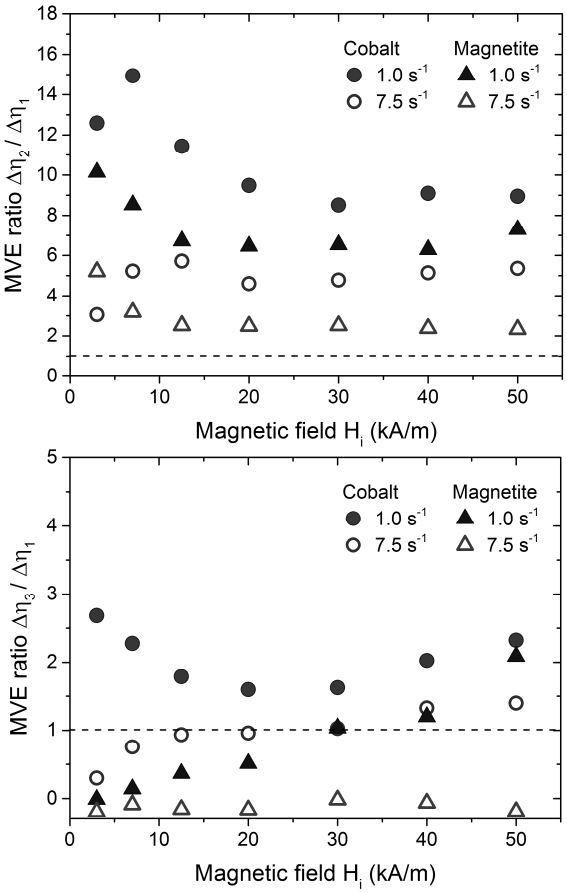

Fig. 2: Field and shear dependent ratios of the magnetoviscous effects $\Delta\eta_2/\Delta\eta_1$ (top) and $\Delta\eta_3/\Delta\eta_1$ (bottom) of a cobalt and a magnetite ferrofluid. The dashed line marks a ratio of 1.

Acknowledgments

We gratefully acknowledge the funding by the DFG grant Od18/18.

References

[1] L. M. Pop et al., *J. Magn. Magn. Mater.* **289** 303-306, 2005.

[2] S. Odenbach, *Magnetoviscous Effects in Ferrofluids*, Springer, Berlin, 2002.

[3] J. M. Linke, S. Odenbach, *J. Phys.: Condens. Matter* **27** 176001-7, 2015.

Characterization of ferrogels for biomedical applications

N. Löwa[1*], M. Seidel[1], F. Wiekhorst[1]

[1] *Physikalisch-Technische Bundesanstalt, Berlin, Germany;* [*]*norbert.loewa@ptb.de*

Magnetic nanoparticles (MNP) are of great interest in bio- and nanomedicine. Their magnetic properties make them ideally suitable for a broad spectrum of diagnostic and therapeutic applications, e.g. cancer-targeted drug delivery, Magnetic Resonance Imaging (MRI) and Magnetic Particle Imaging (MPI). MPI offers a means of direct measurement of MNP with zero background signal of diamagnetic tissue [1]. Unlike MNP tracer used in MPI, MRI contrast agents are not directly visualized since they merely affect surrounding protons and consequently the MR signal. Nevertheless, MPI strongly depends on the structure of the MNP such as magnetic moment and magnetic anisotropy. To this end, the embedding of MNP into matrices (e.g. tissue or gel) may attenuate the MPI signal performance due to complete or partial elimination of Brownian relaxation or (in case of larger MNP) strong magnetic dipole-dipole interaction. The latter also affects the MNP-modulated signal in MRI [2].

Materials & Methods

In this study we investigated how the matrix and the MNP size define the magnetic properties of the studied systems and therefore relevant MRI/MPI imaging parameter. For this purpose small and large-sized MNP were embedded in various matrizes. We prepared water-based agarose gels, hydrogels, gelatine gels, silica gels as well as gellan gum (a novel tissue engineering biomaterial) of different gel strength. Subsequently the water dispersed MNP were mixed with the gels to a final iron concentration of 1 mmol/L. Additionally one MNP sample was freeze dried after adding mannitol solution.

From quasistatic $M(H)$ measurements (i.e. DC magnetometry) we determined the mean effective magnetic core size of each MNP sample according to [3] and the dipolar interaction according to [4] using the liquid MNP sample and the MNP-gels, respectively. The dynamic magnetic behaviour was investigated by Magneto-relaxometry (MRX), as MRX measures the temporal decay of the magnetisation after a polarising field pulse and depends crucially on the local MNP mobility.

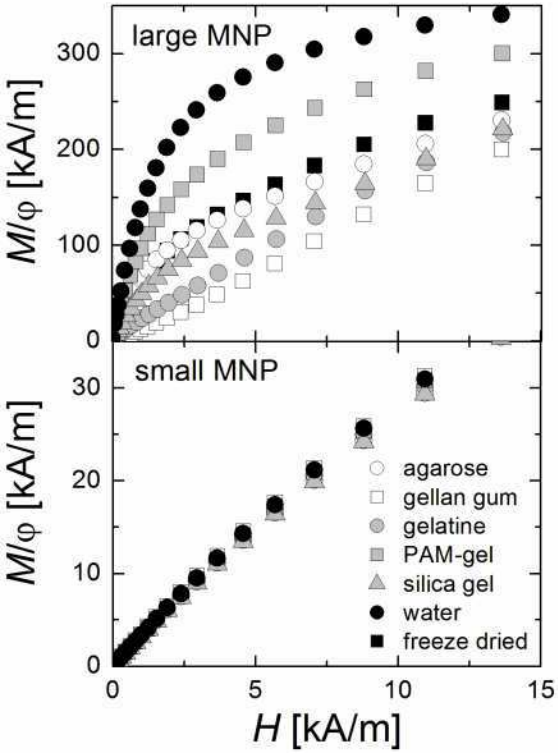

Figure 1 | Magnetization measurements: The magnetization of the gel samples containing small (lower graph) and large (upper graph) MNP as a function of applied field strength.

A Magnetic Particle Spectrometer (MPS), which can be considered as a zero-dimensional MPI scanner, was used to measure the spectral response to an oscillating magnetic field (B_{excit}=25 mT, f_0=25 kHz, T=37°C) of the samples. The most relevant MRI parameter (relaxation times

T_1 and T_2) of each sample were determined at 60 MHz (1.5 T) and 37°C with a Bruker mq60 minispec using a saturation recovery pulse sequence and a CPMG sequence, respectively**.**

Results

From $M(H)$ measurements we found that the dipolar interaction of small MNP embedded in gels was significantly lower as for large MNP indicated by analyzing changes of the initial susceptibility. For large MNP the initial susceptibility strongly decreased up to 100% (gellan gum) while for small MNP it was not affected significantly compared to the liquid state. The dynamic magnetic behaviour as measured by MRX varied strongly and indicated the presence of different binding states. The highest mobility was measured for MNP embedded in hydrogel.
Interestingly, the MPS signals did not change for small MNP (<10%) whereas NMR relaxivity strongly decreased up to 300%. Large MNP showed smaller differences for NMR relaxivity but stronger discrepancies in MPS signals (up to 80%) compared to small sized MNP.

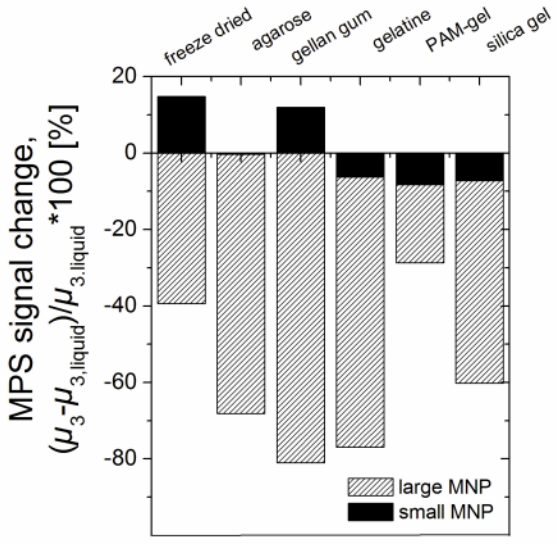

Figure 2 | MPS measurements: The percentage difference of MPS signal (third harmonic amplitude μ_3) of small (black bars) and large (striped bars) MNP embedded in gel matrizes compared to MNP in water.

Conclusion

We found that matrices may change the relevant imaging parameters for MRI and MPI strongly. Whereas MPI signals were merely altered only for larger MNP which may exhibit strong dipole-dipole interactions, MRI signals were significantly reduced in both cases (small and large MNP). The investigations of several MNP-matrix combinations demonstrate the range of MRI and MPI signal variations and show that MPI signal is sensitive to both MNP properties and environment as it is for contrast agent based MRI. These results give an indication of expected MPI and MRI signal variations in tissue- or cell-targeted applications.

Acknowledgements

The research was supported by the German Research Foundation, through DFG Research Units FOR917 and KFO 213.

References

[1] B. Gleich, J. Weizenecker. “Tomographic imaging using the nonlinear response of magnetic particles,” *Nature*, vol. 435, no. 7046, pp. 1214–1217 (2005).

[2] H. Arami, M.R. Ferguson, A.P. Khandhar, K.M. Krishnan. “Size-dependent ferrohydrodynamic relaxometry of magnetic particle imaging tracers in different environments,” *Med. Phys.*, 40: 071904 (2013).

[3] D. Eberbeck, F. Wiekhorst, S. Wagner, L. Trahms. “How the size distribution of magnetic nanoparticles determines their magnetic particle imaging performance,” *Appl. Phys. Lett.*, 98: 182502 (2011).

[4] P. Allia, M. Coisson, P. Tiberto, F. Vinai, M. Knobel, M.A. Novak, W.C. Nunes. "Granular Cu-Co alloys as interacting superparamagnets," *Phys. Rev.* B 64: 144420 (2001).

Development and characterization of hypericin-loaded iron oxide nanoparticles

H. Unterweger[1], D. Subatzus[1], C. Janko[1], R. Tietze[1], M. Schuster[2], A. R. Boccaccini[3] and C. Alexiou[1]

[1]ENT-Clinic, Section for Experimental Oncology and Nanomedicine, Else Kröner-Fresenius-Stiftung Professorship, Universitätsklinikum Erlangen, Glückstr. 10a, 91054 Erlangen,Germany.
[2]Materials for Electronics and Energy Technology, Department of Materials Science and Engineering, University Erlangen-Nürnberg, Martensstr. 7, Erlangen, Germany
[3]Institute of Biomaterials, Department of Materials Science and Engineering, University Erlangen-Nürnberg, Cauerstr. 6, Erlangen, Germany.

Introduction

Hypericin is a photosensitizer, which can be used for Photodynamic Therapy (PDT). Upon activation with a specific wavelength, reactive oxygen species (ROS) are generated, which can oxidize cellular components, which in the end is leading to cell death. The distinct advantages of PDT (e.g. strictly local cytotoxic effects, non or minimally invasive, fast recovery of patients, no development of resistance, and biocompatibility with other therapies) have already been proven to be beneficial for the treatment of different types of cancer, especially in surface tumors. Among others, the limitation of this treatment is due to low pharmacological doses within the region of interest and suboptimal local efficacy. A possible solution for these problems is the linking of the photosensitizer to superparamagnetic iron oxide nanoparticles (SPION). In this work we describe a novel approach, where such a drug delivery vehicle is designed based on the combination of Magnetic Drug Targeting (MDT) and PDT.

Methods

Dextran coated SPIONs were synthesized in a cold gelation process, as described previously [1]. The surface of the particles was functionalized in order to achieve a platform to link the photosensitizer hypericin to the particle surface.
The physicochemical characterization of the particles was performed via dynamic light scattering, Transmission electron microscopy (TEM), X-ray diffraction (XRD), UV-Vis spectroscopy and Fourier transform infrared spectroscopy (FTIR). The hypericin loading efficacy was determined via high-performance liquid chromatography (HPLC-MS). Furthermore, biological characterization was performed in a flow cytometer with the non-adherent Jurkat cell line by investigation of the viability after treatment with and without illumination.

Results & Discussion

Particle sizes obtained by dynamic light scattering were in the range of 55 to 70 nm, whereas investigation of single magnetite or maghemite particle diameter was performed by TEM and XRD and results in about 4.5 - 5.0 nm. The particles are colloidally stable and FTIR indicated the successful functionalization. Hypericin was linked to functionalized particles via reaction with glutaraldehyd. The obtained drug loaded particles were stable over weeks. The biological activity of our formulation was tested in vitro with the non-adherent Jurkat cell line. The cells were treated with free and particle-bound hypericin, with and without illumination for different time intervals. The experiments revealed no toxicity of pure nanoparticles as well as hypericin without exposure to light, whereas the combination of drug and light induced cell death in a concentration and exposure time dependent manner. Finally, the origin of

the phototoxic behavior could be attributed to the generation of ROS, as determined by a DCFH-DA assay.

Conclusion

The combination of SPIONs´ targeting abilities with hypericin´s phototoxic properties represents a promising approach for merging MDT with PDT for the treatment of cancer.

Figures

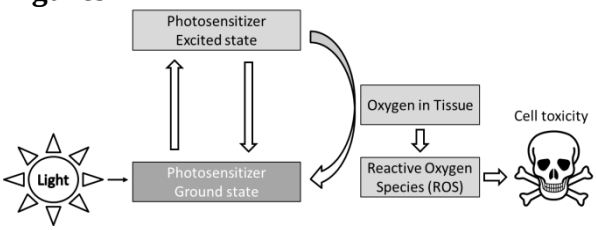

Figure 1: Basic Principle of Photodynamic Therapy.

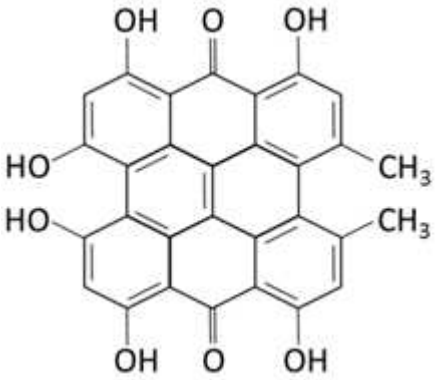

Figure 2: Molecular Structure of hypericin.

Acknowledgments

DFG Excellence Cluster EAM

References

[1] Unterweger H, Tietze R, Janko C, et al. International Journal of Nanomedicine. 2014, 9 (1), 3659-3676.

Multicellular spheroids: A model for nanoparticle-cell interaction studies

J. Demut[1], C. Gräfe[1], C. Bergemann[2], A. Hochhaus[1], J. H. Clement[1]

[1] *Klinik für Innere Medizin II, Abteilung Hämatologie und Internistische Onkologie, Universitätsklinikum Jena, Jena, Germany; johanna.demut@med.uni-jena.de; joachim.clement@med.uni-jena.de*
[2] *chemicell GmbH, Berlin, Germany*

Introduction

Nanoparticles are increasingly used for clinical and biomedical applications as for contrast agents in magnetic resonance imaging. Especially superparamagnetic iron oxide nanoparticles (SPIONs) are developed for this purpose [1]. Despite the fact that several nanoparticles are already approved and commercially available, the precise action on cellular level and on the human body is poorly understood. In that regard, the penetration into tissue and the interaction with cells are of particular interest. Multicellular spheroids represent a model to investigate such effects on tissue-like cell structures [2].

Methods

Multicellular spheroids composed of human breast tumor cells (BT-20) and human brain microvascular endothelial cells (HBMEC) were prepared with the hanging-drop method using 30,000 cells per drop. They were incubated with SPIONs coated with different polymers (positive polyethylenimine, neutral starch and negative carboxymethyldextran) with various concentrations for 3 hours.

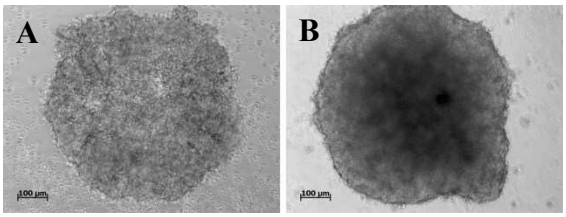

Figure 1: Light microscopic imaging of multicellular spheroids composed of HBMEC (A) and BT-20 cells (B). scale bar 100 µm.

The interaction of SPIONs with multicellular spheroids was studied by laser scanning microscopy (LSM). Serial trypsination was used to dissociate the spheroids layer by layer [3]. To investigate the penetration of SPIONs into the multicellular spheroids they were embedded in 1% agarose, formalin-fixed, dehydrated and then embedded into paraffin. 4 µm FFPE-sections were prepared which were stained with Prussian blue and counterstained with haematoxylin.

Results and Discussion

Microscopic analysis revealed that vital and stable 3D cell culture systems could be established.

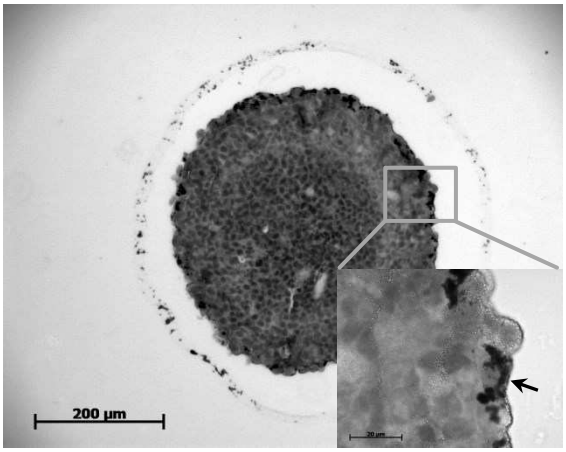

Figure 2: Multicellular BT-20 spheroids were incubated for 3 h with 25 µg/cm² fluidMAG-PEI/750/O, embedded in 1% agarose, formalin-fixed and paraffin-embedded. 4 µm sections were prepared. Iron was stained with Prussian blue which shows internalized nanoparticles (arrow). Cell nuclei were counterstained with haematoxylin. Scale bar 200 µm (insert 20 µm).

The breast cancer derived BT-20 cells formed denser spheroids than HBMEC cells (Figure 1). LSM analysis showed that the application of differentially coated SPIONs resulted in characteristic charge-dependent patterning on the spheroids. Positively charged SPIONs exhibited intense interaction with spheroid surfaces, whereas neutral charged showed moderate and negatively charged only weak interaction. In order to get an impression of the distribution of the nanoparticles within the spheroids, the serial trypsination method was used. In our hands the procedure was not suitable for accurate and reproducible preparation of cell layers. This issue could be overcome by applying embedding and sectioning of the spheroids (Figure 2). After 3 hours of incubation the positively charged fluidMAG-PEI/750/O are located within the first cell layer of the BT-20 spheroids and were predominately aggregated. In case of the HBMEC spheroids nanoparticles were found in deeper layers attributed to the loose package of the cells.

Conclusion

Multicellular spheroids show a tissue-like phenotype with pronounced cell-cell interactions. Therefore they are a suitable model system to investigate the interaction and penetration of SPIONs with/into tissue. Thus spheroids embody a valuable tool to create a bridge between *in vitro* and *in vivo* test systems.

Acknowledgments

We highly acknowledge the professional help of Brigitte Specht by preparing the tissue sections. This work was supported by the DFG high priority program 1681 (Grant CL202/3-1).

References

[1] Hofmann-Amtenbrink, M., Hofmann, H., Montet, X. (2010). "Superparamagnetic nanoparticles - a tool for early diagnostics." Swiss Med Wkly 140: w13081.

[2] Lee, J., Lilly, G.D., Doty, R.C., Podsiadlo, P., Kotov, N.A. (2009). "In vitro toxicity testing of nanoparticles in 3D cell culture." Small 5: 1213-1221.

[3] Keithley, R.B., Weaver, E.M., Rosado, A.M., Metzinger, M.P., Hummon, A.B., Dovichi, N.J. (2013) "Single cell metabolic profiling of tumor mimics," Anal Chem 85: 8910-8918.

Circulating SPIONs: Magnetic targeting and *in vitro* effect on monocytic cell recruitment by primary human endothelial cells.

J. Matuszak [1], P. Dörfler [1], J. Zaloga [1], H. Unterweger [1], C. Alexiou [1] and I. Cicha [1*]

[1]*ENT-Clinic, Section of Experimental Oncology und Nanomedicine (SEON), Else Kröner-Fresenius-Stiftungsprofessur, University Hospital Erlangen, Glückstraße 10a, 91054 Erlangen, Germany*

Magnetic targeting is considered a promising method to accumulate the diagnostic or therapeutic nanoparticles at the sites of atherosclerotic lesions, but little is known about the effects of magnetic nanoparticles on the vascular cells.

Here, we analysed the biological effects and the endothelial accumulation of circulating SPIONs (superparamagnetic iron oxide nanoparticles) in an *in vitro* model of arterial bifurcations. Two types of SPIONs were used: Lauric acid-BSA-coated SPIONs (78.7 nm hydrodynamic diameter, ζ-potential -37.3 mV) and dextran-coated SPIONs (82.5 nm hydrodynamic diameter, ζ-potential +5.5 mV).

Under flow conditions, human umbilical vein endothelial cell (ECs) grown in the bifurcating slides were perfused at 10 dyne/cm^2 for 18 h with medium containing SPIONs. Without magnetic force, circulating SPIONs were well-tolerated up to 400 µg/mL. Applying the external magnet allowed accumulation of lauric acid-BSA-coated SPIONs in non-uniform shear stress regions, even at concentrations as low as 3 µg/mL.
Increased uptake of SPIONs at non-uniform shear stress region did not affect EC viability or resistance to shear stress exposure.
Importantly, no significant differences in TNF-α-induced THP-1 monocytic cell recruitment were detected between controls and SPION-treated ECs.

Taken together, magnetic targeting allows localized accumulation of increased amounts of SPION at the region of interest under physiologic-like flow conditions, thus enabling a substantial reduction of the applied dose. *In vitro* no severe toxic or biological effects were observed. These findings indicate that magnetic targeting can constitute a suitable technique for the delivery of imaging and therapeutic nanoparticles to atherosclerotic plaques.

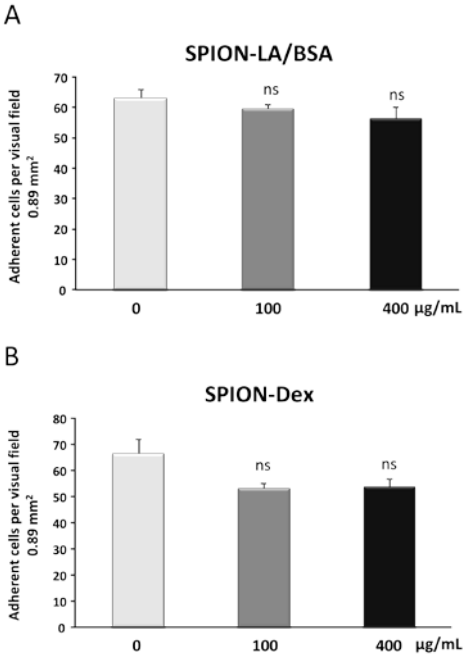

Fig.1: Adherent THP-1 monocytes at the non-uniform shear stress region after 18h of SPION exposure under flow. ECs were stimulated with TNF-α for 2h before dynamic adhesion assay. Shown is the mean value ± SEM (one-way ANOVA).

Funding:
DFG CI 162/2-1, EU project FP7-NMP-2012-LARGE-6-309820 "NanoAthero".

Magnetic Fluids Composed of Modified Co-Ferrite Nanoparticles – A new Approach for Tunable Coercivity and Relative Magnetization?

N. Buske[1] and S. Dutz[2]

[1] *MagneticFluids, Köpenicker Landstr. 203, 12437 Berlin: n.buske@magneticfluids.de*
[2] *Institute of Biomedical Engineering and Informatics (BMTI), Technische Universität Ilmenau, Gustav-Kirchhoff-Straße 2, 98693 Ilmenau: silvio.dutz@tu-ilmenau.de*

Introduction

Magnetite ($FeOxFe_2O_3$) particles with diameter around 10 nm have a very low coercivity (H_c) and relative remanent magnetization $M_{rel} = M_r/M_s$. In comparison to this, Co-ferrite ($CoO \times Fe_2O_3$) particles have a very high H_c and M_{rel}, which is very favorable for magnetic recording [1].
Unfortunately, these particles are magnetically too hard to obtain suitable specific heating power (SHP) in magnetic hyperthermia [2] or good tracer performance in magnetic particle imaging (MPI) [3].
For optimization/tuning the magnetic properties, the Fe^{2+} ions of magnetite were substituted by Co^{2+} step by step (Scheme 1) in our study which results in a Co doped inverse spinel lattice with adjustable Fe^{2+} substitution degree (Figure 1).

$$(Co^{2+})_a + (Fe^{2+})_{1-a} + (Fe^{3+})_2 + (OH^-)_8 \Rightarrow$$
$$Co_a^{2+}Fe_{1-a}^{2+}Fe_2^{3+}O_4 + 4H_2O \qquad a = 0 \ldots 1$$

Scheme 1: Reaction equations for preparation of Co doped inverse spinels.

A Co concentration of 0% (a = 0) leads to formation of pure magnetite particles and at a Co concentration of 25% (a=1) pure $CoFe_2O_4$results.

Methods

The particles were prepared from Co^{2+}, Fe^{2+}, and Fe^{3+} chloride mixtures (0.02 molar) at different "a"-values by co-precipitation with sodium hydroxide under stirring at 100°C for 90 minutes reaction time. The obtained particles were washed with distilled water using magnetic separation technique and stabilized in water with hydrochloric acid (intermediate, with positively charged particles) and with citric acid (final MF, pH = 7, negatively charged particles). All samples were filtrated through a 0.8µm filter.

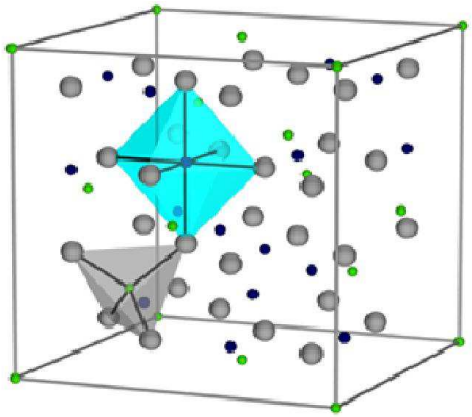

Figure 1: Inverse spinel lattice of Fe_3O_4 or $CoFe_2O_4$. A constant amount of Fe^{3+}, but variable Co^{2+}/Fe^{2+} ion mixture, are located in the octahedral gaps (blue spheres in upper cell). The tetrahedral gaps (yellow spheres in bottom cell) contain a constant amount of Fe^{3+}only.

The structural properties of prepared particles were determined by means of transmission electron microscopy (TEM) and X-ray diffraction (XRD). For the magnetic characterization of the samples (M_s, M_{rel}, and H_c) a vibrating sample magnetometer (VSM) was used. Magnetic heating performance for hyperthermia was investigated in calorimetrical measurements in alternating magnetic fields of different field strength and frequency.

Results

For the ferrofluids containing the prepared particles, only a limited dependence of H_c

and M_{rel} on the Co content in the particles was found (Figure 2). This confirms a proper and stable dispersion of the particles within the ferrofluid and magnetic properties are determined mainly by hydrodynamic particle size and a possible (but vanishingly low) particle agglomeration.
For dry particle samples, a strong correlation between Co content and resulting H_c and M_{rel} was found. For increasing Co concentrations from 0 to 8.6% (substitution rate "a" from 0 to 0.33) only a slight increase of H_c was found, but from 12 to 25% ("a" from 0.5 to 1) a strong linear increase of H_c results (Figure 2). Within this linear range of dependency, the magnetic properties of the particles, especially H_c, can be tuned easily by changing Co content of the particles.

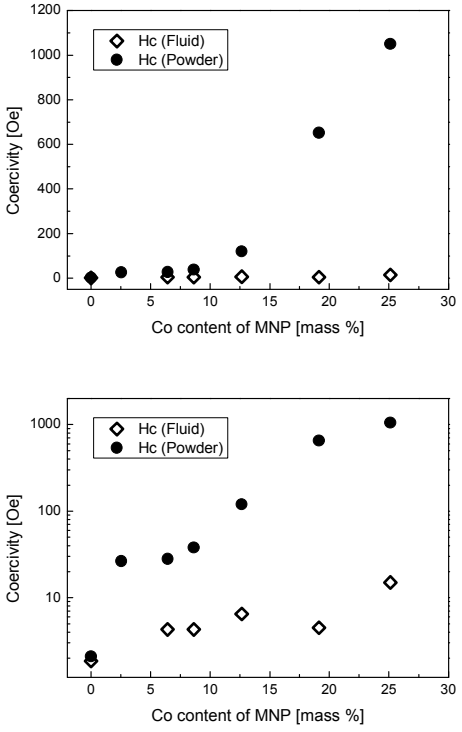

Figure 2: Coercivity of fluid and powder samples (linear and logarithmical scale) of prepared particles as function of the Co concentration of the crystal.

Discussion

Here prepared particles have an inverse spinel lattice of oxygen atoms with iron (and/or cobalt) in the gaps of the lattice. In the tetrahedral gaps only Fe^{3+} can be located. The octahedral gaps of the lattice (Figure 1) contain Fe^{3+} and Fe^{2+}, whereby the Fe^{2+} was substituted step by step by Co^{2+} in our experiments. To verify this hypothesis, the Fe/Co ratio of the ferrites was checked.
Iron and cobalt are chemically very similar elements. Therefore, a strong magnetic interaction at higher ion concentrations and at closest ion contact in the octahedral gaps seems to be possible and caused the strong increase of the coercivity with increasing Co concentration. Similar results were found for the combination of different metal-ferrites using the layer by layer technology [4].
In ongoing studies, gels containing the here prepared ferrite particles (immobilized) will be tested in magnetic hyperthermia and for MPI.

Acknowledgments

We thanks Therakine GmbH, Berlin for generous support of this work.

References

[1] C. Gansau and N. Buske, DE Patent 10205332B4 (2002).
[2] S. Dutz and R. Hergt. *Magnetic Particle Hyperthermia – A promising tumor therapy?* Nanotechnology 25: 452001 (2014).
[3] S. Dutz, D. Eberbeck, R. Müller, M. Zeisberger. *Fractionated magnetic multicore nanoparticles for magnetic particle imaging*. Springer Proceedings in Physics 140: 79–83 (2012).
[4] J.H. Lee et al. *Exchange-coupled magnetic nanoparticles for efficient heat induction*. Nature Nanotechnology 6: 418–422 (2011).

Synthesis of magnetic hydrogels with tunable morphologies

S. Hinrichs[1], D. Peters[1], M. Junk[1], Q. Xiong[1], B. Fischer[1]

[1] Physical Chemistry, University of Hamburg

Stimuli responsive hydrogels offers a broad variety of useful application in medical as well as technical fields [1,2]. Most of the hydrogels react to an external stimulus like temperature, pH or light [3,4,5]. Hydrogels who can also respond to a magnetic (or electric) field broaden the possibility for further applications [6, 7]. These, so called ferrogels, combine the stimuli-responsive properties of the matrix with the magnetic properties of a ferrofluid.

In ferrogels not only spherical magnetic particles are from interest, but also anisotropic particles, because the particle shapes influence the magnetic properties strongly. Especially the coactivity force is higher for anisotropic particles than for spherical particles [11]. Therefore anisotropic particles are even stronger influenced by an external magnetic field and can be used as sensitive particles for magnetic resonance tomography [8].

Here we present a simple method to tune the particle shape by a hydrothermal approach. Therefore Akaganeit precursor were synthesized (Fig. 1A) out of $FeCl_3$ solution. The Akaganeit precursor is cylindrical and has a broad polydispersity, so the length of the cylinders range between 20 and 50 nm and the width is about 5 nm. This precursor structure is also present during the synthesis process of the hematite spindles [9-12].

In a second step, the Akaganeit precursors are hydrothermally treated. The particle shape is in this step influenced via the pressure, Temperature, pH and concentration (Fig. 1 B-D). The formation of the hematite cubes have been recently discussed by Malik et al. [13].

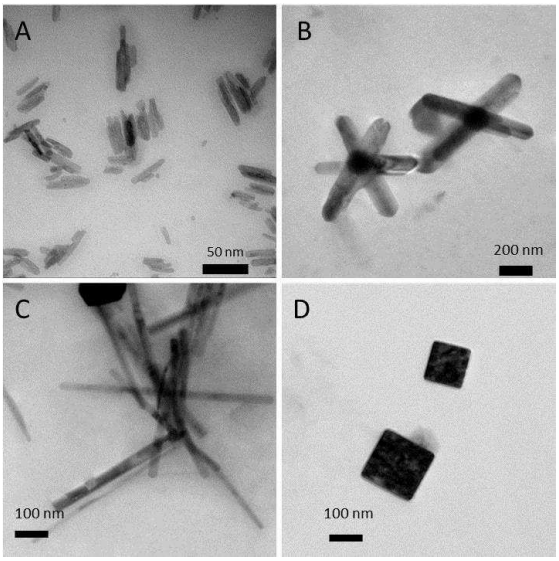

Figure 1: Different morphologies of hematite particles (B-D) prepared out of Akaganeit (A).

The silica-covered particle will be then embedded in a thermoresponsive hydrogel based out of poly-N-isopropylacrylamid (pNiPAAm) and Methylenbisacrylamid (BIS) and Allylamin. Afterwards the micro gelparticles will be crosslinked with glutaraldehyd to get a macrogel [14].

pNiPAAm has a volume phase transition (VPT) around 34°C. By changing the content of crosslinker BIS the VPT can be slightly shifted. In addition the distribution of the crosslinker is of importance, because this also influences he temperature behavior. Varga et al showed that a homogenous distribution compared to a heterogeneous distribution leads to a stronger swelling behavior at lower temperature [15]. For core-shell particle the temperature behavior differs. It also depends on the thickness of

the shell as well if the particles are completely covered.
The temperature dependence is investigated by means of dynamic light scattering. Here we will demonstrate how the temperature behavior of the microgel particles already depends on the preparation method.

Acknowledgments

The authors thank the DFG priority program SPP 1681 „Field controlled particle matrix interactions: synthesis multiscale modelling and application of magnetic hybrid materials" for financial support.
The authors thank U. Koenig for TEM measurements.

References

[1] A. E. Smith, X. Xu, and C. L. McCormick, Progress in Polymer Science 35, 45 (2010).
[2] C. de Las Heras Alarcon, S. Pennadam, and C. Alexander, Chemical Society reviews 34, 276 (2005).
[3] A. M. Menzel, Physics Reports 554, 1 (2015).
[4] A. Kumar, A. Srivastava, I. Y. Galaev, and B. Mattiasson, Progress in Polymer Science 32, 1205 (2007).
[5] E. S. Gil and S. M. Hudson, Progress in Polymer Science 29, 1173 (2004).
[6] R. Messing and A. M. Schmidt, Polymer Chemistry 2, 18 (2011).
[7] P. Calvert, Advanced Materials 21, 743 (2009).
[8] N. Lee et al., Proceedings of the National Academy of Sciences of the United States of America 108, 2662 (2011).
[9] M. Ozaki, T. Egami, N. Sugiyama, and E. Matijević, Journal of colloid and interface science 126, 212 (1988).;
[10] M. Ozaki, H. Suzuki, K. Takahashi, and E. Matijević, Journal of colloid and interface science 113, 76 (1986).
[11] C. Märkert, B. Fischer, and J. Wagner, Journal of Applied Crystallography 44, 441 (2011).
[12] J. Wagner, C. Märkert, B. Fischer, and L. Müller, Physical Review Letters 110 (2013).
[13] V. Malik, B. Grobety, V. Trappe, H. Dietsch, P. Schurtenberger; Col-loids and Surfaces A 445: 21-29 (2014).
[14] Z. Hu and G. Huang, Angew. Chem. Int. Ed. Engl. 42, 4799 (2003).
[15] R. Acciaro, T. Gilanyi, and I. Varga, Langmuir 27 (2011).

Aspects of a standardized characterization and description of nanomagnetic suspensions for biomedical applications

U. Steinhoff, O. Posth, D. Schmidt

Physikalisch-Technische Bundesanstalt, Abbestr. 2-12, 10587 Berlin, Germany

Magnetic nanoparticles (MNPs) suspended in fluids are of great interest for biomedical and clinical applications. Manufacturers, distributors, end-users and researchers require different information on MNP properties depending on their perspective in the application scenario. A standardized description of MNP properties will improve the quality and reliability of MNP based products, widen their application range and foster acceptance of nanotechnology in society. A comprehensive summary of physicochemical methods characterizing the main structural and magnetic parameters is a prerequisite for a standardized description of these materials.

Introduction

Although MNP suspensions have been researched and applied already for a considerable number of years, there exists no standardized way of characterizing and expressing their main physicochemical properties. This represents a considerable obstacle for introducing new MNP based biomedical and clinical applications like for example Magnetic Particle Imaging (MPI). A possible way of improving this situation is the preliminary formulation of a tentative normative document for a standardized MNP description. This document can then iteratively be discussed and updated together with MNP suspension manufacturers, appliers, end-users and other socioeconomic groups interested in MNPs. Eventually, the document can enter a normative process as it is performed by national (DIN), European (CEN/CENELEC) or international (ISO) standardization organizations.

Methods and results

Measurements on dried MNP powder provide important information on structural and magnetic properties of the metal oxide MNP cores. The interpretation of the measurement data can be based on well established models. However, the ensemble behavior in powder does in most cases not represent the suspension behavior, firstly because the interaction of the particles and the suspension medium is missing and secondly, because average distances and thus the dipolar interaction energy between the particles has changed. MNP suspensions make up realistic samples for the ensemble behavior but the model based interpretation might become extremely complicated due to field dependent changes in MNP formation and interaction (e.g. chain formation) which have to be included in the interpretation. All these effects can be further modulated by the actual dilution of the MNP, which should also be taken into account.

In the description of the structural composition of a typical iron oxide based MNP suspension, there should be a clear distinction between the different compartments of the suspension: metal oxide cores, organic coating and suspension medium.

The chemical characterization of MNP suspensions should be performed separately for the three compartments and the results should be presented using a standardized nomenclature and a nanomaterial vocabulary (ISO/TR 11360). It remains questionable whether the exact chemical and structural composition of the MNP ensemble can be measured and expressed with

reasonable effort. Furthermore, the term "polycrystalline iron oxide" for superparamagnetic iron oxide nanoparticles (SPIONs) seems to be sufficient in many application scenarios [1].

Static or dynamic M(H) measurements are widely used for the determination of the magnetic behavior of MNP suspensions. An important issue in the interpretation of M(H)-curves is the treatment of the dia- or paramagnetic background signal generated by the suspension medium and other parts of the measurement equipment. So far there is no established method how to treat this background signal, especially at low MNP concentrations or high external fields.

In the description of the magnetic behavior of MNP suspensions, it is important to distinguish between properties of single particles and the ensemble behavior. Single MNP cores exhibit a constant magnetic moment that is oriented depending on the anisotropic crystal structure and on the external magnetic field. In addition, the orientation of the constant magnetic moment of the MNP is continuously varied by thermal agitation. In contrast, an ensemble of suspended MNP exhibits superparamagnetic behavior with a non-zero field-dependent macroscopic magnetic moment only in the presence of an external magnetic field. Here, thermal agitation will influence the amplitude, but not the direction of the macroscopic net magnetic moment. In most MNP applications, the ensemble behavior is the relevant level of description. For those applications, the energy absorption of the MNP suspension under the influence of an external magnetic field is one of the most relevant parameters. It is given as the product of the sample's magnetic moment and the respective external magnetic induction. The SI-unit of the differential expression per field and mass compartment is $JT^{-1}kg^{-1}$, which equals emu/g in the obsolete but still used CGS-system.

In Small Angle X-ray Scattering (SAXS) and Dynamic Light Scattering (DLS), measurements can be performed and results can be expressed according to the standards ISO 17867 and ISO 22412, respectively. For all measurement methods providing a size distribution, be it a core size or a hydrodynamic size, the regulations of ISO 9276/1-6 (Representation of results of particle size analysis) should be obeyed. It might even be possible to present the distribution of particle moments or anisotropy energy according to the schemes in ISO 9276/1-6.

Conclusion

Applying existing harmonized vocabulary and normative documents, a considerable improvement in the description of MNP suspensions can be reached. A clear distinction between magnetic core, organic coating and suspension medium properties is important. The magnetic behavior can be described from a particle based or from an ensemble based perspective, leading to completely different expressions. In the interpretation of magnetic measurements on MNP suspension, it should always be clear whether focus is on single magnetic nanoparticles or on the suspension as a uniform object. Expression of measurement results in SI units is indispensible for the comparison of analysis results. SI units should be used in all describing documents for MNP suspensions.

Acknowledgments

This work was supported by the German Federal Ministry of Economics and Technology grant No. KF2303711UW2 and by the EU FP7 research program "Nanomag" FP7-NMP-2013-LARGE-7

References

[1] Jun YW, Jang JT, Cheon J, Magnetic nanoparticle assisted molecular MR imaging, Adv. Exp. Med. Biol. 2007, 620:85-106.

SANS, Mössbauer and magnetic characterization of interacting iron oxide nanoparticles

Philipp Bender[1], Diego Alba Venero[1], Luis Fernández Barquín[1], Rocio Costo[2], Jeppe Fock[3], Catherine Frandsen[3], Mikkel Fougt Hansen[3], Sarah Rogers[4], Peter Svedlindh[5], Erik Wetterskog[5], Christer Johansson[6]

[1]*CITIMAC, Universidad de Cantabria, Spain*
[2]*Instituto de Ciencia de Materiales de Madrid, CSIC, Spain* [3]*Department of Physics, Technical University of Denmark* [4]*ISIS-STFC, Rutherford Appleton Laboratory, United Kingdom* [5]*Faculty of Technology, Uppsala University, Sweden* [6]*Acreo Swedish ICT AB, Göteborg, Sweden*

Introduction

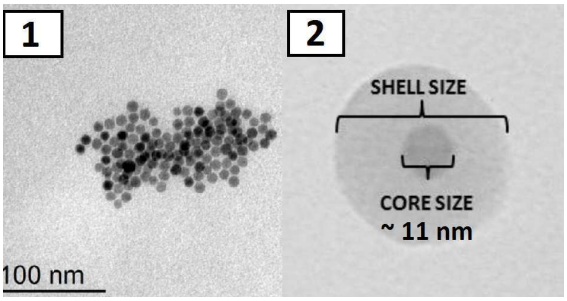

Figure 1: TEM micrographs of sample 1 (iron oxide cores surrounded by DMSA) and sample 2 (iron oxide cores coated with a $\sim$ 30 nm thick silica shell). From the analysis of $>$ 100 particles from both samples an average iron oxide core size of $\sim$ 11 nm with low polydispersity (σ $<$6%) was obtained.

The magnetic properties of an ensemble of iron oxide nanoparticles primarily depend on the structural properties of the individual particles, but also on interparticle interactions. The presence of dipolar interactions has significant implications e.g. in biomedical applications such as hyperthermia [1]. The standardization of the determination of the magnetic parameters driving those applications (e.g. magnetic moment, relaxation frequency, interparticle interactions) is a need for the near future.
The present study focuses on the analysis of two samples (Figure 1) of iron oxide nanoparticles with nearly identical average core diameters ($\sim$ 11 nm) and low polydispersity ($\sigma \leq 6\%$) according to TEM analysis, but with varying amount of dipolar interactions due to different coating routines. In the first sample (**sample 1**), the particles were coated with an organic surfactant (DMSA) and aggregated to clusters consisting of several dozens individual particles. In contrast, the particles of the second sample (**sample 2**) were surrounded by a $\sim$ 30 nm rigid silica shell increasing the interparticle distance, which should significantly decrease the amount of dipolar interactions. To investigate the influence of dipolar interactions on the magnetization behavior of the iron oxide particles a detailed analysis of combined Small Angle Neutron Scattering (SANS), Mössbauer and magnetization experiments was performed.

Results

The core-shell morphology of the nanoparticles from sample 2 observed in TEM could be veryfied by the SANS measurement in the freeze-dried state (powder), shown in Figure 2. The SANS intensity in the intermediate q-range could be fitted very well with a core-shell model [2] including the structure factor of hard spheres. The obtained structural parameters of the particles (iron oxide core diameter $\sim$ 11 nm, polydispersity of cores $\leq$ 6%, silica shell size $\sim$ 30 nm) were in very good agreement with TEM analysis.

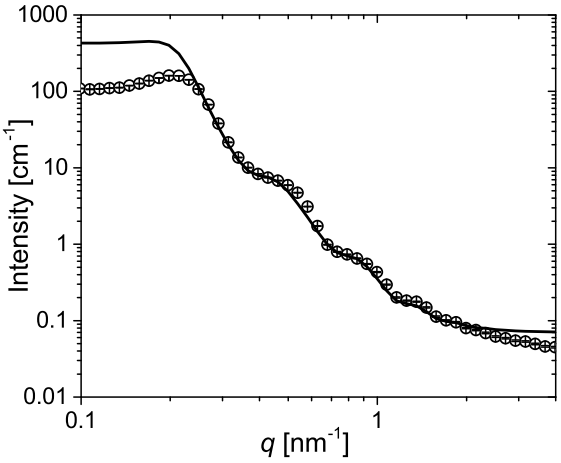

Figure 2: SANS intensity of sample 2 in the freeze-dried state (powder). The measurement was fitted (straight line) with a core-shell model including the structure factor of hard spheres, verifying the structural parameters (core diameter distribution, shell thickness) obtained from TEM. The discrepancies in the low and high q-range can be attributed to a small number of large particles.

According to Mössbauer measurements the chemical composition of the iron oxide nanoparticles in both samples were virtually identical and predominately maghemite.
Hence, the two particle systems can be regarded as model systems to investigate the influence of dipolar interactions on the magnetization behavior of the nearly monodisperse iron oxide cores.
Whereas the room-temperature magnetization curves of the two samples were nearly identical, the ZFC/FC-curves differed significantly (Figure 3). This difference can exclusively attributed to the significantly higher dipolar interactions in sample 2. By applying global fitting routines [3] to analyze the magnetization (Langevin), ZFC and FC measurements [4], values for the saturation magnetization, core diamater distribution and anisotropy constant could be extracted. Comparison between the obtained values for both samples as well as with literature values hence enabled to evaluate the influence of dipolar interactions on these parameters.

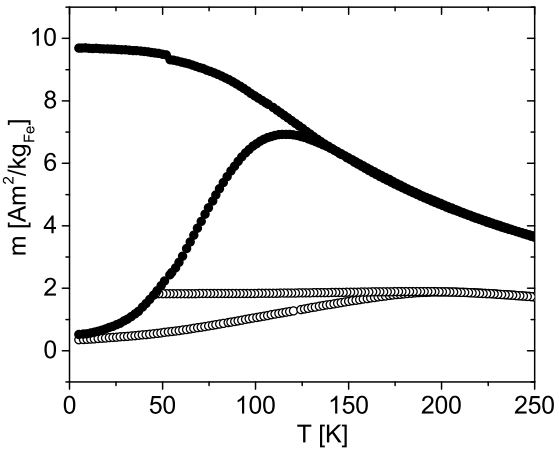

Figure 3: Zero field cooled (ZFC) and field cooled measurements of sample 1 (black spheres) and sample 2 (open spheres) in colloidal dispersion (iron concentration $\approx$ 2 mg/mL) at a field amplitude of 1 mT normalized to the iron content.

Acknowledgments

This work is part within a 18-institution consortium to standardize the characterization of iron oxide nanoparticles and is supported by EC FP7 NMP project NanoMag Project (grant no. 604448).

References

[1] I. Andreu, E. Natividad, L. Solozábal, O. Roubeau, JMMM 380 341-346 (2015).

[2] J. Pedersen, Adv. Colloid Interface Sci. 70 171-210 (1997).

[3] A. Tamion, M. Hillenkamp, F. Tournus, E. Bonet, V. Dupuis, APL 95 062503 (2009).

[4] F. Tournus, E. Bonet, JMMM 323 1109-1117 (2011).

Magnetic susceptibility of magnetorheological composites

Dmitry Yu. Borin, Stefan Odenbach
TU Dresden, Institute of Fluid Mechanics, Dresden 01062

Magnetorheological (MR) materials are composites of magnetically soft microparticles dispersed in a carrier medium, which typically is a liquid (MR fluid) or a solid elastic matrix (MR elastomer). Upon an external magnetic stimulus, the particles of a MR composite become magnetized and can form aggregates elongated in the direction of the applied field. The aggregation of particles results in a change of the rheological properties of the material. This change is referred as the MR effect. The aggregation process of the particles is reversible and can be easily dynamically controlled. Due to these properties the MR composites are widely used in various technical applications from brakes, clutches and actuators to dampers of vehicles, bridges or skyscrapers. A central advantage of MR elastomers is the preventing of sedimentation of the micron-sized magnetic particles, which occurs in the carrier liquid of MR fluids. Moreover, it is possible to tune an anisotropy of MR elastomers orienting the particles with an external magnetic field applied during the matrix cross-linking process. There are many publications regarding various aspects of MR materials synthesis and modification, as well as works presenting MR devices and technologies. Reviews on these topics are given in [1, 2].

The field controlled rheology of a MR composite is governed by the magnetic behaviour of the powder particles. Magnetic properties for the powdered materials are usually determined in situ, i.e. measuring magnetization curves of the prepared composite.

The powder suspended in the matrix of a conventional MR material is, as a rule, carbonyl iron which is a material without magnetic hysteresis. Nevertheless, the measured composite magnetization M at the decreasing field H will be higher than the magnetization at the increasing field. The same is expected for the differential susceptibility $\chi = dM/dH$. This behaviour is associated with a formation of structures or motion of particles due to magnetic interactions when the field is first applied. When the particles are fixed inside a hard matrix or fixed inside aggregates already oriented parallel to the external field, this effect is vanishing.

However, there is a lack of knowledge about a correlation between a microstructure and macroscopic steady state magnetic properties of MR composites. In our work we have considered MR composites with different kinds of matrices and initial structural anisotropy. Furthermore, the concentration of the magnetic powder ϕ has been varied. In figure 1 an initial susceptibility for various kinds of MR composites as a function of the powder concentration is given. As a reference the Maxwell-Garnett approximation is provided:

$$\chi = \frac{3\phi}{1-\phi}. \qquad (1)$$

This equation gives χ/ϕ close to 3 for low concentrated composites. Our results have shown that this works well only for diluted samples containing randomly distributed magnetic particles fixed on their positions, i.e. composites without any interparticular interactions and structuring effects.

Experimental data on magnetic properties of low concentrated elastic samples are fol-

lowed by microstructural observations performed using X-Ray tomography [3, 4] (figures 2 and 3). Herewith a realistic discussion of the obtained results is ensured.

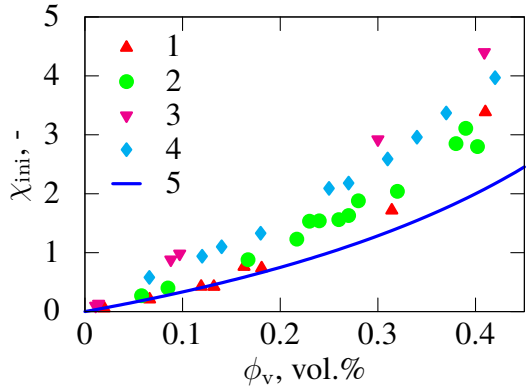

Figure 1: *Initial susceptibility of various MR composites: 1 - solid matrix; 2 - soft elastic matrix; 3 - structured particles in an elastic matrix; 4 - liquid matrix; 5 - Maxwell-Garnet prediction.*

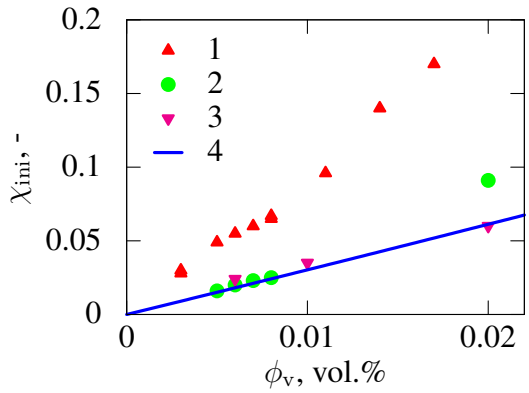

Figure 2: *Initial susceptibility of low concentrated MR composites: 1 - with structures oriented $\parallel$ to an applied field; 2 - with structures oriented $\perp$ to an applied field; 3 - non-structured samples; 4 - Maxwell-Garnet prediction.*

A susceptibility of low concentrated (up to 1 vol.%) non-structured composites as well as structured samples with chains oriented perpendicular to an externally applied field can be sufficiently well predicted using the Maxwell-Garnet equation. Structured samples oriented parallel to the field obviously have a higher susceptibility (χ/ϕ ~9,5), which apparently does not depend on the number of chains and their thickness, as can be seen comparing the tomographic data and χ values for samples manufactured under different field strength applied during curing (figure 3). A possible reason of this is a chain demagnetization factor which remains equal for different samples when the ratio of the chains length and thickness $L/d >> 1$. Obtained results provide basics for further discussions of the field depended properties of MR composites and should serve for correct theoretical predictions of their physical behaviour.

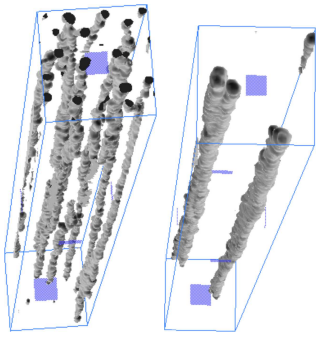

Figure 3: *Microstructure of the low concentrated elastic MR composite structured in a low ($< 10kA/m$) (left) and in a high ($> 200kA/m$) (right) magnetic field. Initial magnetic susceptibility for both samples is ~0.07. The capture boxes have cuboid shape with 15mm x 1 mm x 1 mm dimensions*

References

[1] Yancheng Li, Jianchun Li, Weihua Li, and Haiping Du. A state-of-the-art review on magnetorheological elastomer devices. *Smart Materials and Structures*, 23(12):123001, 2014.

[2] Norman M Wereley, editor. *Magnetorheology*. RSC Smart Materials. The Royal Society of Chemistry, 2014.

[3] D Günther, D Yu Borin, S Günther, and S Odenbach. X-ray micro-tomographic characterization of field-structured magnetorheological elastomers. *Smart Materials and Structures*, 21(1):015005, 2012.

[4] T Borbáth, S Günther, D Yu Borin, Th Gundermann, and S Odenbach. Xct analysis of magnetic field-induced phase transitions in magnetorheological elastomers. *Smart Materials and Structures*, 21(10):105018, 2012.

Experimental investigations towards the effects of small particles on the structure formation of interacting particles

E. Siebert[1], V. Dupius[2], S. Neveu[2], S. Odenbach[1]

[1] Chair of Magnetofluiddynamics, Measuring and Automation Technology, Technische Universität Dresden
[2] Sorbonne Universit´es, UPMC Univ Paris 06, UMR 8234, PHENIX, F-75005 Paris, France
CNRS, UMR 8234, PHENIX, F-75005 Paris, France

Introduction

Ferrofluids have numerous applications, like the sealing of rotating shafts or cooling of high-tech loudspeakers. As well, they have a high potential to be an effective tool for cancer treatment. For all those applications the interparticle interaction in presence of a magnetic field is a crucial parameter, since it determines the structure formation processes and thereby the change of physical properties of the entire fluid system. The change of viscosity under the influence of a magnetic field is one of those effects, which is denoted as the magnetoviscous effect (MVE) R [1] and calculated by

$$R = (\eta_H - \eta_{H=0}) / \eta_{H=0} \quad . \qquad (1)$$

How the different composition of a ferrofluid influences the interaction among the particles and therefore the particles' aggregation behaviour is the scope of the presented study.

Especially the effect of small particles, which are not interacting among themselves, on the interacting large particles' structure formation processes, was topic of numerous theoretical studies and simulations [2] as well as of experimental investigation [3]. The possible interactions of small and large particles are shown in Fig. 1 according to Wang and Holm [4].

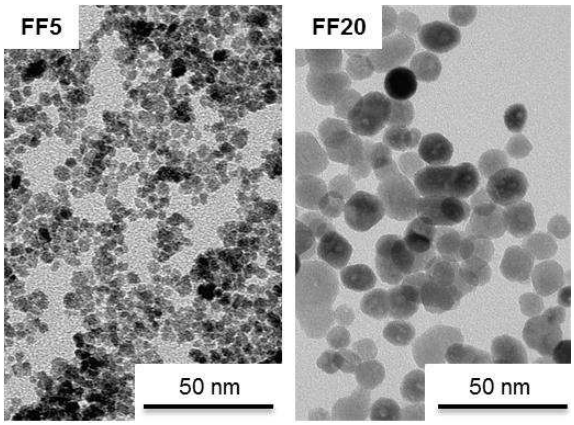

Figure 2. Basic fluids FF5 and FF20 for the presented investigation. Images by TEM.

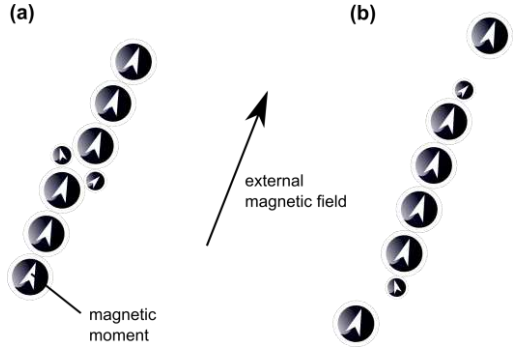

Figure 1. (a) shows the chain-destabilization and (b) the "Poisoning" effect of the chain shortening due to presence of small particles according to [4].

Here the "Poisoning" effect describes the decrease of the MVE in the presence of small particles in a bidisperse model fluid, when the volume concentration of the small particles exceeds a value of $\phi_S \sim 0.01$, while the volume fraction of the large particles is assumed to be constant. Accordingly, this predicted "Poisoning" effect has been experimentally examined by a systematic variation of the relative quantity of small and large particles in a fluid.

Experimental setup

An especially designed rheometer has been used, which allows to measure the viscous properties of a fluid under influence of a magnetic field. In this study a constant magnetic field strength of H_{ex} = 35kA/m has been applied.

Two basic ferrofluids with a narrow size distribution were synthesized using a modified Massart process. The fluids FF5 and FF20 contain only small (S) or large (L) ionically stabilized cobalt ferrite particles in deionized water as a carrier liquid respectively (see TEM images in Fig. 2). These fluids were mixed in three different ratios i:

$$i = \phi_S / \phi_m , \qquad (2)$$

where m denotes the volume fraction of all particles.

Results and discussion

No change of viscosity was measurable in the small particle fluid (FF5) under an applied magnetic field and thus one can assume that the respective particles generate no microstructures. With the ferrofluid sample A0 containing only large particles (ϕ_L = 0.23 vol%) diluted in deionized water, a distinct MVE was obtained under the influence of a magnetic field. The theory of the "Poisoning" effect predicts these values to decrease in the presence of small particles. In Fig. 3 it can be seen, that in contrast to that, the MVE is approximately one order of magnitude higher, when adding small particles to a constant volume portion of large particles (fluid sample A0.75 – $i_{A0.75}$= 0.75). Consequently, the "Poisoning" effect was not measurable.

To understand how the ratio of small and large particles influences the interaction behaviour in a ferrofluid in respect to its rheological properties the **S**mall **P**article **I**nfluence **P**arameter (SPIP) had been firstly introduced by Siebert et al. [3] and is calculated by

$$SPIP = (R_i - R_{i=0}) / R_{i=0} \qquad (3)$$

Here R_i and $R_{i=0}$ represent the MVE with and without small particles respectively. Fig. 4 shows the SPIP as a function of the shear rate for the fluid sample Sets A, B and C. The values of MVE of the ferrofluid samples B0.9 ($i_{B0.9}$= 0.9) and C0.97 ($i_{0.97}$= 0.97) prove the general increased structure formation. It is obvious that the presence of small particles strongly stimulates the chain growth and additionally has an intense stabilizing effect on the generated microstructures. This is documented by the increment of SPIP with increasing shear rate, which indicates a suppressed shear thinning behaviour.

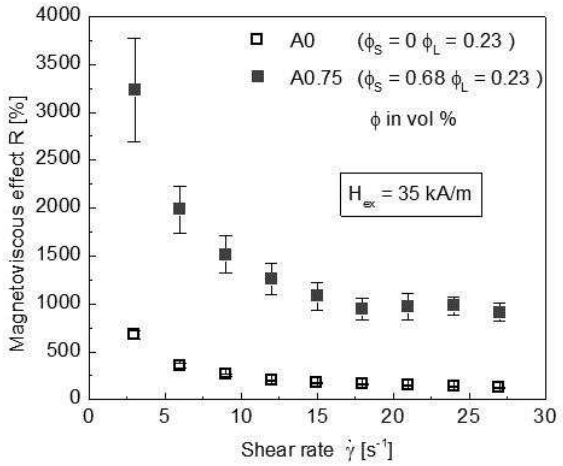

Figure 3. MVE vs. shear rate under an applied magnetic field. Presented are the fluid samples A0 containing only large particles and A0.75 where small particles are added (mixing ratio i = 0.75)

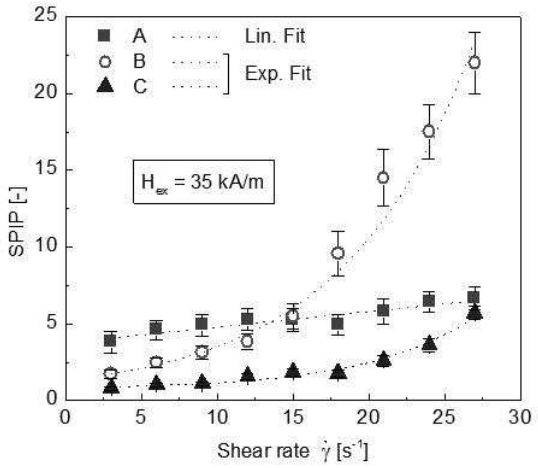

Figure 5. The Small Particle Influence Parameter (SPIP) plotted against shear rate under influence of an applied magnetic field.

Conclusion

The presented investigation shows that the appearance of small particles moderates the aggregation process of the large ones and stabilizes the formed structures as well.

References

[1] S. Odenbach (2002), L. N. in Phys. 71
[2] S. S. Kantorovich (2003), JMMM 258
[3] E. Siebert, V. Dupuis, S. Neveu, S. Odenbach (2015), JMMM 374
[4] Z. Wang, C. Holm (2003) Ph. Rev. E 68

Buckling of paramagnetic chains in soft gels

Shilin Huang[1], Giorgio Pessot[2], Peet Cremer[2], Rudolf Weeber[3], Christian Holm[3], Johannes Nowak[4], Stefan Odenbach[4], Andreas M. Menzel[2], Günter K. Auernhammer[1]

[1]*Max Planck Institute for Polymer Research, 55128 Mainz, Germany*
[2]*Institut für Theoretische Physik II: Weiche Materie, Heinrich-Heine-Universität Düsseldorf, 40225 Düsseldorf, Germany*
[3]*Institute for Computational Physics, Universität Stuttgart, 70569 Stuttgart, Germany*
[4] *Institute of Fluid Mechanics, Chair of Measuring and Automation Technology, Technische Universität Dresden, 01062 Dresden, Germany*

Introduction

Magneto-responsive hybrid gels (MRGs) have been attracting great attention due to their tunable elasticity, swelling properties and shape that can be remotely controlled by a magnetic field. They have potential applications as soft actuators, artificial muscles, as well as sensors and can serve as model systems to study the heat transfer in hyperthermal cancer treatment. Compared to other stimuli-responsive gels, MRGs have the advantage of fast response, controlled mechanical properties and reversible deformabilities. A typical MRG consists of a chemically cross-linked polymer network swollen in a good solvent and embedded magnetic particles.

The origin of the magnetic-responsive behavior of MRGs is the magnetic interaction between the magnetic filler particles as well as their interaction with external magnetic fields. Different theoretical routes have been pursued to investigate the magneto-elastic effects of MRGs: macroscopic continuum mechanics approaches, mesoscopic modeling, and more microscopic approaches that resolve individual polymer chains. An experimental model system showing a well-defined particle distribution and a measurable magneto-elastic effect can help to understand the magneto-elastic behavior of MRGs at different length scales [1].

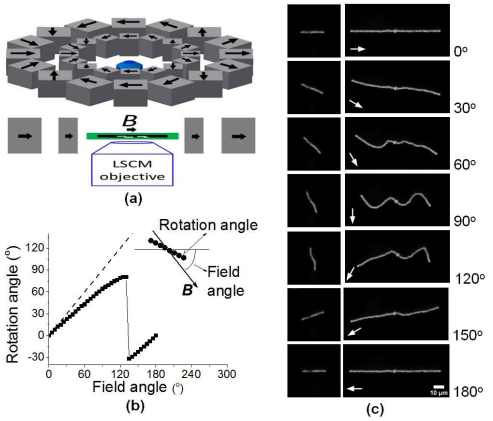

Figure 1 (a) Laser scanning confocal microscopy (LSCM) was used to observe the morphologies of the paramagnetic chains in the soft gels. The Halbach magnetic array provided a homogeneous magnetic field (here $B = 216.4 \pm 1.1$mT). This array could be rotated to change the orientation of the magnetic field. (b) The orientation of the magnetic field B was successively increased from 0° to 180° in 36 steps (square points). A magnetic chain of 15 particles rotated to follow the magnetic field, but the rotation angle was smaller than the orientation angle of B (dashed line). (c) Morphologies of magnetic chains in a soft gel change when the orientation angle of B increased. The scale bar is 10 μm. The gel in (b) and (c) had a storage modulus G' of 0.25 ± 0.06 Pa.

Results

We study the magneto-elastic coupling behavior of paramagnetic chains in soft polymer gels exposed to external magnetic fields. A laser scanning confocal microscope is used to observe the morphology of the paramagnetic chains and the deformation field of the surrounding gel network. The paramagnetic chains in soft polymer gels show rich morphologies under oblique magnetic fields, in particular a pronounced buckling deformation (Fig. 1-2).

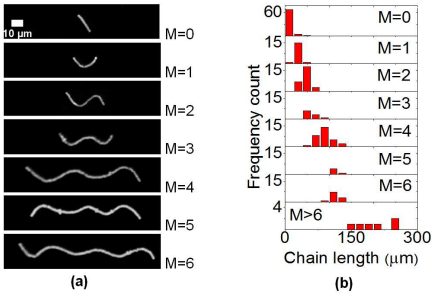

Figure 2 (a) Different morphologies of paramagnetic chains in a soft gel ($G' = 0.25 \pm 0.06$ Pa) under a perpendicular magnetic field (100.8 ± 0.5 mT). The original chain direction was horizontal, and the applied magnetic field was vertical. The scale bar is 10 μm. (b) Frequency count of different buckling morphologies in the same sample. M is the number of half waves.

The buckling morphology depends on the length of the chain, the strength of the magnetic field and the modulus of the gel (Fig. 3). Longer chains form buckling structures with a higher number of half waves. Higher strengths of the magnetic field and a lower modulus of the gel matrix can lead to higher deformation amplitudes. The deformation field in the surrounding gel matrix confirms that the embedding polymer network is strongly coupled to the paramagnetic chain (Fig. 4a). A minimal magneto-elastic coupling model is developed to describe the morphological behavior of the paramagnetic chains in the soft gel under a perpendicular magnetic field. The total energy functional can be expressed as followed:

$$E_{tot} = E_{magn} + E_{bend} + E_{displ} + E_{contr}$$

The chains deform in order to decrease the magnetic energy (E_{magn}) (Fig. 4). This is hindered by the simultaneous deformation of the gel matrix, which increases the elastic energy of the gel (E_{displ}, E_{contr} and E_{bend}). Furthermore, we found indication that the embedded magnetic chains themselves feature a certain bending rigidity (also contributing to E_{bend}), possibly due to polymer chains adsorbed on the particle surfaces.

Acknowledgments

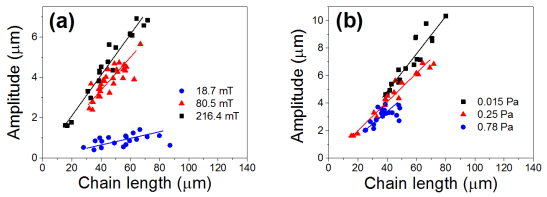

Figure 3 Influence of chain length, strength of magnetic field and elastic modulus of the gel matrix on the amplitude of the S-shaped chains, observed when the magnetic field is applied perpendicularly to the initial chain orientation. (a) The elastic modulus of the gel was 0.25 ± 0.06 Pa, and the magnetic field strengths were 216.4 ± 1.1 mT (squares), 80.5 ± 0.4 mT (triangles) and 18.7 ± 0.1 mT (circles), respectively. (b) The magnetic field strength was 216.4 ± 1.1 mT and the elastic moduli of the gel were 0.015 ± 0.005 Pa (squares), 0.25 ± 0.06 Pa (triangles) and 0.78 ± 0.22 Pa (circles), respectively.

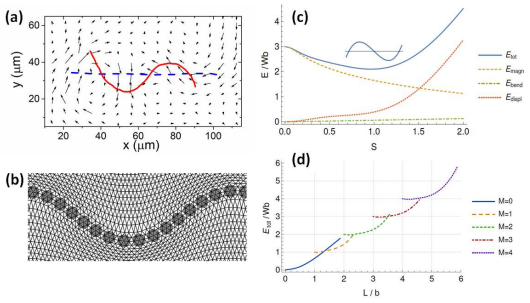

Figure 4 (a) Tracer particles were inserted into the gel matrix of the sample. Tracking these embedded tracer particles, the deformation field in the gel matrix was determined. The solid line represents the skeleton of the magnetic chain and the dashed line indicates the original chain shape. (b) Simulation result. When the boundary layer is assumed to be stiffer than the bulk, the buckling effect occurs. (c) Contributions to the total energy as a function of the strength S of deformation. We always observed the global minimum for symmetric shapes. (d) Energies E_{tot} of chain deformations as a function of chain length L and number of half-oscillations M. Each curve describes a shape of M half-waves with a minimum total length of $(M-1)b$. The resulting curves show crossing points from where the total energy for an increasing L can be lowered by bending one extra time (jumping to a higher M) rather than conserving the same shape.

We thank Dr. Peter Blümler for inspiring discussions on designing the Halbach magnetic arrays and acknowledge support by the DFG through the SPP 1681.

References

[1] S. Huang, G. Pessot, P. Cremer, R. Weeber, C. Holm, J. Nowak, S. Odenbach, A. M. Menzel, G. K. Auernhammer, *Buckling of paramagnetic chains in soft gels*, arXiv:1504.03884, 2015.

Magnetic-Field Dependence of Brownian and Néel Time Constants in AC Magnetic Fields

J. Dieckhoff, M. Schilling, and F. Ludwig*

Institut für Elektrische Messtechnik und Grundlagen der Elektrotechnik, Technische Universität Braunschweig

** Corresponding author: f.ludwig@tu-bs.de*

Introduction

The dynamics of magnetic nanoparticles (MNPs) is generally described via an effective time constant which is related to the Brownian τ_B and Néel time constant τ_N by

$$\tau_{eff} = \frac{\tau_B \tau_N}{\tau_B + \tau_N} .$$

In zero or small ($\xi = mB/(k_B T) << 1$) magnetic fields, the well-known expressions for the Brownian and Néel time constants are generally used relating them to hydrodynamic size and viscosity as well as anisotropy energy. For a number of applications, however, the knowledge of the time constants in larger magnetic fields ($\xi \geq 1$) is of vital importance. For example in magnetic particle imaging (MPI), the magnetic markers are simultaneously exposed to ac and dc fields of up to 25 mT amplitude. For a model-based reconstruction, appropriate expressions for the field-dependence of the time constants are important. In magnetic hyperthermia, the SAR (specific absorption rate) is often discussed with ac susceptibility (ACS) measurements, however, the nanoparticles are exposed to rather large ac fields. Also for nanorheological investigations in the presence of background fields, the effect of the field on the time constant must be separated from its effect on the rheological parameters such as viscosity and shear modulus.

Here we investigate the effect of the amplitude of an ac magnetic field as well as of superimposed static fields – both parallel and perpendicular to the ac field – on Brownian and Néel time constants applying ac susceptometry.

Methods

All ACS measurements were performed with a fluxgate-based measurement setup described in detail in Dieckhoff et al. [1]. It allows one to record ACS spectra in the frequency range from 2 Hz to 9 kHz at ac field amplitudes of up to 9 mT and superimposed dc fields of up to 9 mT (for small ac excitation fields).

The effective time constants were determined by fitting the measured imaginary part χ'' of the complex susceptibility with the Navriliak-Negami formula [2].

As samples, single-core iron oxide nanoparticles SHP-25 from Ocean Nanotech having a mean core diameter of 25 nm were used. Standard, low-field ACS measurements indicated that the majority of nanoparticles suspended in DI water follow the sinusoidal excitation field via the Brownian mechanism. Since the Brownian peak in χ'' of aqueous SHP-25 suspensions lies in the low-field limit at around 10 kHz, the 25 nm particles were suspended in a water-glycerol mixture (volume ratio 30:70) resulting in a viscosity of around 25 mPs·s, thus shifting the maximum in χ'' to below 1 kHz. In order to study the effect of the field amplitude on the Néel time constant, the nanoparticles were immobilized by freeze-drying in mannitol.

Results and discussion

Fig. 1 depicts the imaginary part χ'' as a function of frequency measured on a SHP-25 suspension for different ac field amplitudes. As can be seen, the maximum shifts with increasing ac field amplitude towards larger frequencies caused by a decrease of

the Brownian time constant. In Fig. 2, the imaginary part measured on the freeze-dried reference sample is shown. Unfortunately, the maximum for low field amplitude lies below 2 Hz but it shifts with increasing field amplitude into the measurement window.

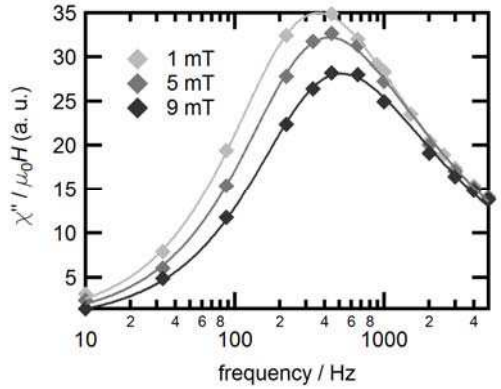

Fig. 1: Measured imaginary part as a function of frequency and field magnitude for SHP-25 suspension.

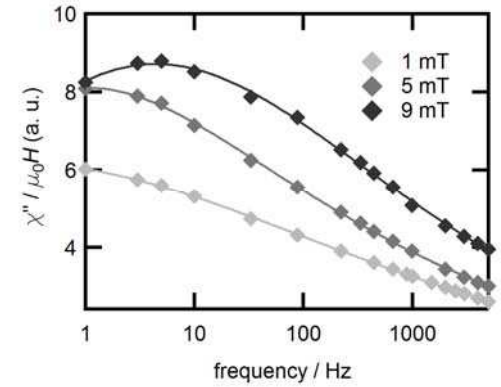

Fig. 2: Measured imaginary part as a function of frequency and field magnitude for freeze-dried SHP-25 sample.

Fig. 3 depicts the extracted time constants as a function of ac field amplitude. Apparently, the field dependence of the Néel time constant is much stronger than that of the Brownian one. The dependence of the Brownian time constant on ac field amplitude was fitted with an equation derived by Yoshida and Enpuku from solving the Fokker-Planck equation [3]:

$$\tau_{B,H} = \frac{\tau_{B,0}}{\sqrt{1 + 0.126\xi^{1.72}}} \qquad (1)$$

The best fit was obtained for a mean magnetic moment of $1.6\,\mathrm{aA \cdot m^2}$ which is in agreement with the value from magnetization curve measurements.

Unfortunately, there is no appropriate model for the dependence of the Néel time constant on ac field amplitude (there are expressions for $\tau_{N,H}$ which are applied for the analysis of MRX curves; they hold, however, only in the limit $\xi < 1$ [4]). Thus, equation (1) is modified to fit the field dependence of τ_N based on the determined magnetic moment. Similar measurements were also performed for small ac field amplitudes superimposed by static fields parallel or perpendicular to the ac field. The obtained dependencies of the time constant on the dc field magnitude were fitted with expressions derived by Raikher and Shliomis [5], providing *m* values comparable to the one quoted before.

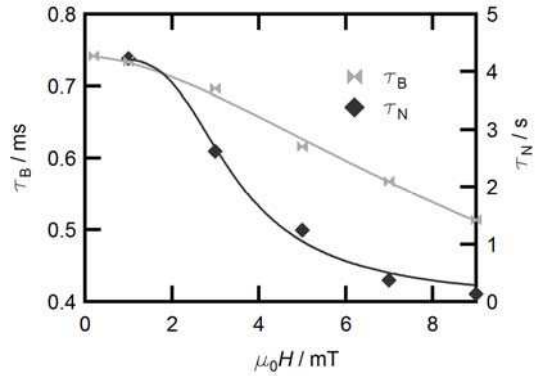

Fig. 3: Brownian and Néel time constant as a function of AC magnetic field magnitude for liquid and freeze-dried 25 nm single-core iron oxide particle samples. Note the different ordinate axes.

Acknowledgements

Financial support by the European Commission Framework Programme 7 under NANOMAG Project (NMP-LA-2013-604448) is acknowledged.

References

[1] J. Dieckhoff, M. Schilling, F. Ludwig, Appl. Phys. Lett. **99**, 112501 (2011).

[2] S. Havriliak, S. Negami, Polymer **8**, pp. 161-210 (1967).

[3] T. Yoshida, K. Enpuku, Springer Proc Phys **140**, pp. 9-13 (2012).

[4] F. Ludwig et al., J. Appl. Phys. **101**, pp. 113909 (2007).

[5] Y. L. Raikher, M. I. Shliomis, *Advances in Chemical Physics*, vol. 87, W. Coffey, Eds. New York: Wiley, 1994, pp. 595-751.

A Capillary Viscometer for biocompatible Ferrofluids.

Johannes Nowak[1], Stefan Odenbach[1]

[1] *Chair of Magnetofluiddynamics, Measuring and Automation Technology, Technische Universität Dresden, Dresden 01062, Germany*

In the research of biomedical applications ferrofluids receive a growing importance. The suspended magnetic particles can be used e.g. as carriers for chemotherapeutic agents or for hyperthermia – an artificial heating of diseased areas [1].
Regarding those potential applications it is important to have a good understanding of the fluids' behavior if an external magnetic field is applied to guarantee a safe and effective application. Therefore the Magnetoviscous Effect (MVE) has to be taken into account – an increasing viscosity of the fluid if a magnetic field is applied [2], caused by the structure formation of the nanoparticles. It was shown before that a rather strong effect can be measured for magnetic fluids used in the biomedical context [3]. Those measurements could only be realized under conditions not reflecting those of an actual application regarding the geometry, the shear rate ranges and the magnetic field strengths.
Therefore a capillary viscometer was developed to fit those requirements. The capillary reflects an artery model and the shear rates as well as the magnetic field strengths were adapted to requirements fitting the biomedical application.

Experimental

The principle of the capillary viscometer is presented in fig. 1. It is based on an exchangeable capillary allowing different inner diameters. For the present investigation three capillaries with inner diameters of 0,46 mm (A), 1,02mm (B) and 1,36 mm (C) were used and previously characterized using computer tomography (fig. 2).
The pressure drop over the capillary, which can be used to calculate the viscosity, is measured using the hydraulic principle. Therefore a membrane separates the measurement fluid and a silicone oil. The actual measurement involves the differential pressure transmitted by the silicone oil (fig. 1). The advantage of this setup is that the measured signal is not affected by the applied magnetic field.

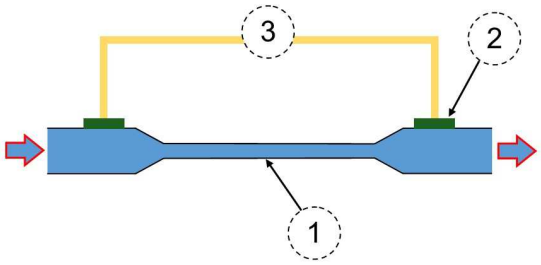

Figure 1: Principle of the capillary viscometer. (1) is the capillary, (2) the membrane separating the two fluids and (3) the position of the pressure sensor.

This magnetic field can be applied by different coil setups as the measurement setup is movable. For this work two systems were used: a Helmoltz setup enabling precise magnetic field strengths up to 45 kA/m and a setup with a B-E25 magnet (Bruker, USA) enabling magnetic field strengths up to 500 kA/m. Both have a field homogeneity of ≥98%.
For the experiments the ferrofluid fluidMAG-DX (Chemicell, Germany) was used. It consists of multicore iron oxide particles, a dextran polymer to enable stable agglomerates and water as carrier liquid. The fluid shows superparamagnetic behavior and a strong MVE was found using rotational rheometry.

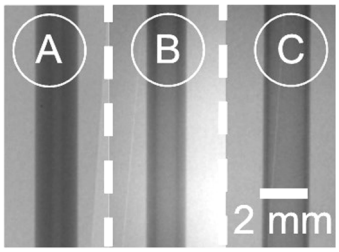

Figure 2: Capillaries used for the measurements.

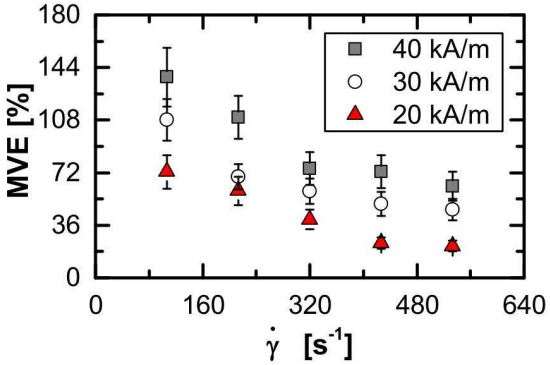

Figure 3: The MVE measured with the capillary B for different magnetic field strengths.

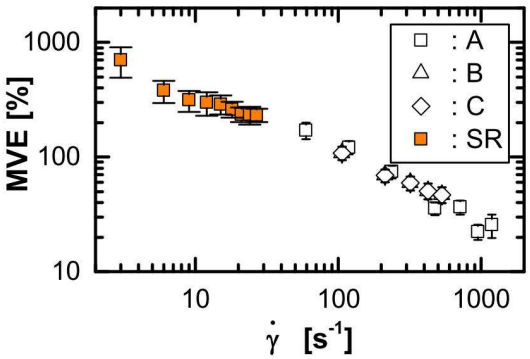

Figure 4: The MVE for all three capillaries (A,B,C) and rotational rheometry (SR) [3] for 30 kA/m.

Results

The experimental investigations revealed a strong MVE for the ferrofluid for all three capillaries. Exemplary the effect is depicted in fig. 3 for capillary B for several magnetic field strengths. The MVE is denoted as R and calculated with the viscosity when a magnetic field is applied $\eta_{(H)}$ and the zero-field viscosity $\eta_{(H=0)}$ [2]:

$$R = \frac{\eta_H - \eta_{H=0}}{\eta_{H=0}}. \qquad (1)$$

It is readily visible that still a strong effect is present despite the high shear rates, and that this effect slightly decreases with increasing shear rate and decreasing magnetic field. In fig. 4 the effect is presented for all three capillaries in comparison to data measured with rotational rheometry. It can be concluded that the effect is independent of the capillary diameter and that it is comparable to results measured with the rotational rheometry.

For strong magnetic field strengths up to 500 kA/m a saturation of the effect up to 250 kA/m was found while above this field strength the effect increased again (fig. 5). This behavior might be depending on the capillary diameter but requires further experimental investigations.

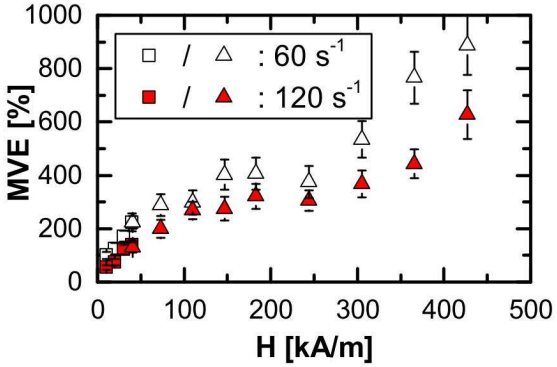

Figure 5: The MVE depending on the magnetic field strength for capillary A and two shear rates.

It can be concluded that despite the high shear rates a rather strong MVE was measured which has the potential to influence the biomedical application of ferrofluids and should be taken into account for further research.

Following investigations will include detailed studies of the MVE at strong magnetic fields and will take care of the question if a particle interaction of the magnetic particles and blood cells occurs if blood is used as diluting agent.

Acknowledgments

Financial support by the Deutsche Forschungsgesellschaft under Grant no. OD18/23-1 is gratefully acknowledged.

References

[1] S. Dürr, C. Jano, S. Lyer, P. Tripal, M. Schwarz, J. Zaloga, R. Tietze, C. Alexiou (2013): Magnetic nanoparticles for cancer therapy; Nanotech Rev 2(4), 395-409

[2] S. Odenbach; (2002) The Magneto-viscous Effect in Ferrofluids; Berlin: Springer

[3] J. Nowak, F. Wiekhorst, L. Thrams, S. Odenbach; (2014) The influence of hydrodynamic diameter and core composition on the magnetoviscous effect of biocompatible ferrofluids; J. Phys.: Condes. Matter 26, 17600

Homoclinic snaking near the surface instability of a ferrofluid

David J.B. Lloyd[1], Christian Gollwitzer[2], Ingo Rehberg[2], and Reinhard Richter[2]

[1] *Department of Mathematics, University of Surrey, Guildford, GU2 7XH, UK*
[2] *Experimentalphysik V, Universität Bayreuth, D-95440 Bayreuth, Germany*

Introduction

Spatially localised patterns are observed in such different systems like semiconductor lasers, gas discharges, vibrated granular media, intermittent coquette flow [1] or the normal field instability in ferrofluids [2]. The Homoclinic Snaking scenario has proven to be an important mechanism for localisation [1]. Here each alternating turn of a "snake" in control parameter-phase space is correlated with the emergence of a further interior cell of the localized pattern. This scenario has been unveiled in more than hundred theoretical studies, however, experimental evidence in two dimensional systems is sparse so far.

Figure 1 Photo of a localized patch of seven spikes on a layer of ferrofluid.

Experimental results

We report on localised patches of cellular hexagons observed on the surface of a magnetic fluid in a vertical magnetic field (cf. Figure 1). These patches are spontaneously generated by jumping into the neighborhood of the unstable branch of the domain covering hexagons of the Rosensweig instability upon which the patches equilibrate and stabilise. They are found to coexist in intervals of some control parameter around this branch. By means of a pulse technique we unveil sequences of stable patches comprising intervals with one, three, seven … up to 21 spikes. These sequences may be a signature of Homoclinic Snaking.

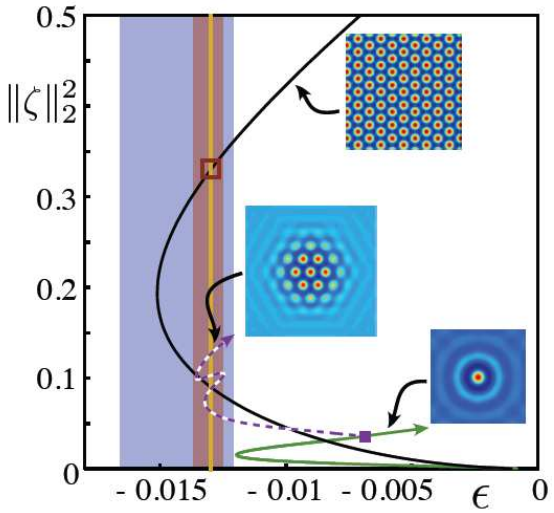

Figure 2 Normalised hydrostatic energy vs. the control parameter ϵ computed for the Rosensweig instability in a ferrofluid of permeability μ_r = 2. The bifurcation diagram shows the domain covering hexagons and the emergence of a fully localised hexagon patch (dashed) bifurcating from a solitary spike (green).

Numerical results

We formulate a general energy functional for the system and a corresponding Hamiltonian that provides a pattern selection principle allowing us to compute Maxwell points for general magnetic permeabilities. At these Maxwell points the energy of a single hexagon cell that lies in the same

Hamiltonian level set as the flat state, has the same energy. Using numerical continuation techniques we investigate the existence of localized hexagons in the Young-Laplace equation coupled to the Maxwell equations. We find cellular hexagons possess a Maxwell point providing an energetic explanation for the multitude of measured hexagon patches. Furthermore, it is found that planar hexagon fronts and hexagon patches undergo homoclinic snaking as indicated in figure 2. Thus we are corroborating the experimentally detected intervals.

Besides making a contribution to the specific area of ferrofluids, our work paves the ground for a deeper understanding of homoclinic snaking of two-dimensional localised patches of cellular patterns in many physical systems.

Acknowledgments

The authors thank R. Maretzki and A. Beetz for recording the HDR picture of figure 1.

References

[1] E. Knobloch, *Annu. Rev. Condens. Matter Phys.* **6**, 325 (2015).

[2] R. Richter and I. V. Barashenkov, *Phys. Rev. Lett.* **94**, 184503 (2005).

[3] D. B. Lloyd, B. Sandstede, D. Avitabile, & A. R. Champneys, *SIAM J. Appl. Dynam. Syst.* **7**, 1049 (2008).

[4] D. B. Lloyd, C. Gollwitzer, I. Rehberg, R. Richter, submitted to *J. Fluid. Mech.* (2015)

Can a magnetic snail creep uphill?

Anita Freundorfer[1], Ingo Rehberg[1], and Reinhard Richter[1]

[1] *Experimentalphysik 5, Universität Bayreuth, 95440 Bayreuth, Germany*

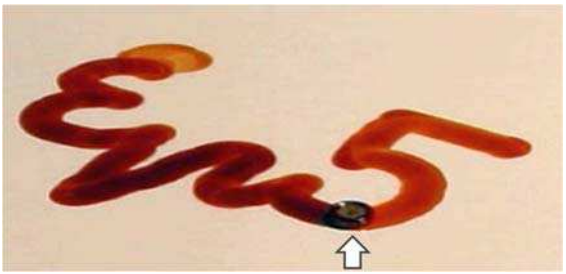

Figure 1 The magnetic snail (see arrow) is traveling on a trace forming the text “Ep5”.

We investigate how a magnet can autonomously travel on a ferrofluidic film. The photo in Fig. 1 displays a trace of ferrofluid (the text “Ep5”) together with the magnet. The latter moves on this trace, up to the end, like an inverse snail absorbing its own slime. In this way it is an autonomous mobile robot.

For a quantitative investigation we use the setup sketched in Fig. 2. An inclined plane made from perspex® is positioned in-between an electro luminescent film and a camera. The angle of inclination α is measured by means of an electronic goniometer connected to a computer. On top of the ramp a magnet with a mass of 2g and a diameter of 8 mm is positioned on a volume of 32 ± 3 µl ferrofluid and kept in place by a trigger. Activating the trigger, the magnet slides down the plane with the velocity v leaving a straight trace of ferrofluid. Reaching the end of the plane the inclination is switched to 0°. Now the magnet is traveling back on its own trace, as displayed in Fig. 3a. Figure 3b indicates that the ferrofluidic film ahead of the magnet is thicker than the one behind it. Apparently this asymmetry results in an effective Kelvin force, which is driving the magnet.

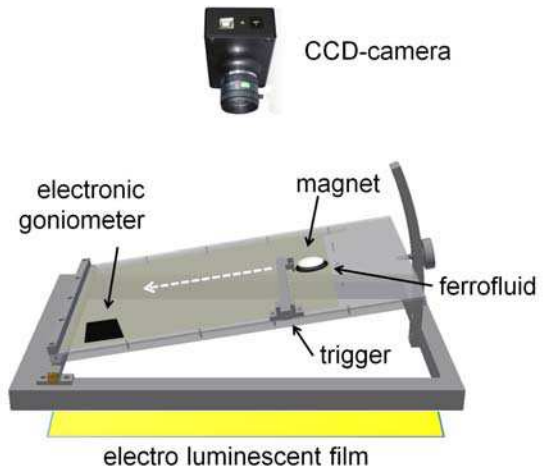

Figure 2 Scheme of the experimental setup.

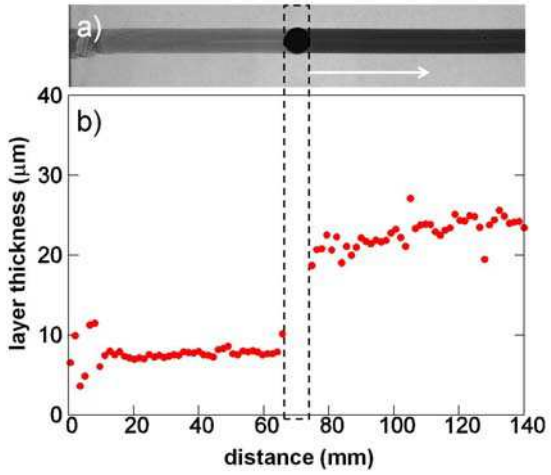

Figure 3 The trace of the snail (a) and its measured thickness (b).

The thickness h of the film in Fig.3b is measured by means of light absorption. For calibration we use a ferrofluidic ramp as shown in Fig. 4. The solid line stems from the multi-exponential fit of Eq.(1), which is taking into account the polychromatic nature of the radiation emitted by the light source [1]

$$\frac{I}{I_0}(x) = f_1 \exp(\mu_1 x) + f_2 \exp(\mu_2 x) + (1 - f_1 - f_2)\exp(\mu_3 x) \qquad (1)$$

where μ is the extinction coefficient.

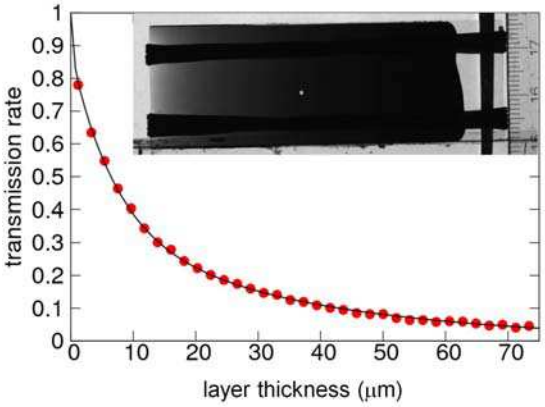

Figure 4 Absorption curve for a ferrofluidic ramp, enclosed by two microscope slides (see inset) with a distance of 0μm at the l.h.s and a distance of 100μm at the r.h.s.

For different angles of inclination α of the plane we record the time dependent position $x_\alpha(t)$ of the magnet and determine its velocity $v_\alpha(t) = dx_\alpha(t)/dt$. The latter depends on the thickness $h_\alpha(t)$ of the ferrofluidic film. For a specific time t_0 we plot in Fig. 5 the layer thickness versus the capillary number $Ca = \eta \cdot v(t_0)/\sigma$ where η denotes the viscosity and σ the surface tension. The experimental data are well described by the equation

$$h = a \cdot Ca^{1/2}, \qquad (2)$$

independent of t_0. This scaling law is known from the dip coating of a vertical plate pulled out of a liquid [2].

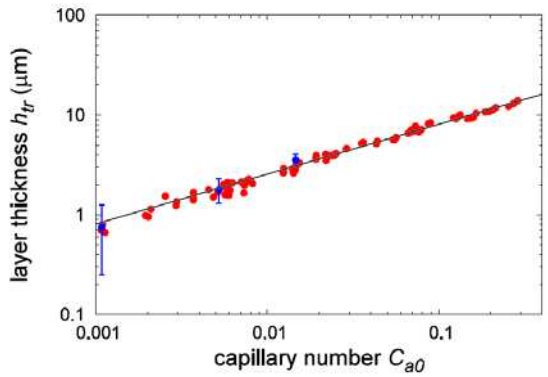

Figure 5 Thickness of the ferrofluidic trace vs. capillary number and fit by Eq.(2).

After the magnet arrives at the bottom of the plane the latter is switched to an angle β. For $\beta = 0$ it travels back on its trace in the plane. We gradually increase β. Indeed the magnetic snail can creep uphill for $\beta \le 1.2^0$, as shown in Fig.6.

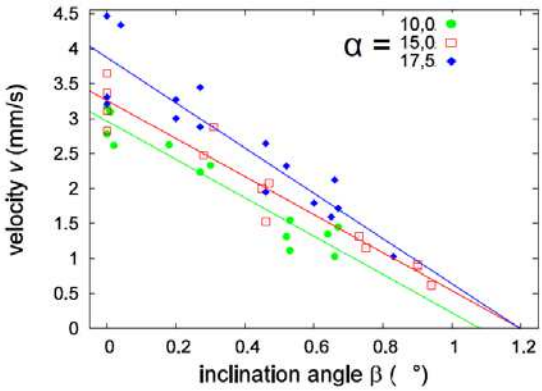

Figure 6 The snail creeps with v uphill on an inclined plane of angle β. The trace thickness varies with α.

To conclude, a permanent magnet is sliding on a previously well prepared homogeneous film of ferrofluid. Its apparently autonomous motion is guided by the trace and driven by a reduction of the over-all magnetic field energy: the ferrofluid is collected at the magnet. Our magnetic snail may be used to transport small cargo, like drugs, on complex path ways. It can easily be miniaturized and may also be useful for microfluidic applications.

Acknowledgments

The authors thank S. Hartung for first measurements, V. Frette, U. Thiele for discussions, K. Oetter for help with the setup and S. Messlinger for creating an USB-driver for the commercial goniometer-chip.

References

[1] Ch. Gollwitzer, R. Richter, I. Rehberg, G. Mathies and L. Tobiska, *The Surface Topography of the Rosensweig Instability — a Quantitative Comparison between Experiment and Numerical Simulation*, J. Fluid Mech. 571, 455-474 (2007).

[2] S. Weistein, K. Ruschak, *Coating flows*, Annu. Rev. Fluid. Mech. 76 066301 (2004).

Effects of the magnetization on the particle structure of magnetorheological elastomers

M. Schümann, S. Odenbach

Chair of Magnetofluiddynamics, Measuring and Automation Technology, Technische Universität Dresden, Dresden 01062, Germany

Introduction

Magnetorheological elastomers are a special kind of magnetic field-responsive smart materials developed in the last years, where magnetic micro particles are embedded in a soft elastomer matrix. As a result the magnetoactive effects on the mechanical properties are combined with a stable, soft elastic material. The investigation of the interaction of the particles with the external magnetic fields and the matrix is a subject of ongoing research. Computed X-ray micro tomography proved to be a reliable method to investigate the particle structure of such composite materials [1, 2].
With the new kind of samples investigated in this work, an effect of an external magnetic field on the orientation of NdFeB microparticles was observed.

Material

Wacker silicone components and silicone oil were used to produce the elastomer, in which 35 wt% of highly anisotropic shaped NdFeB particles MQA by Magnequench were embedded. The median of the particle size distribution is 92 µm.

Methods

The polymerized samples were tested with a DYNA-MESS universal testing machine with and without the presence of an external magnetic field with a flux density of 220 mT in direction of the cylinder axis. Subsequently, the sample was tomographed with the TomoTU cone beam tomography setup. Figure 1 shows a slice of the reconstructed tomography data. 15,000 particles were separated and evaluated. The major axes were calculated for each particle. The sample was then magnetized using a Lake Shore VSM, providing a magnetic field up to 2 T, leading to a remanent magnetization of the sample in direction of the cylinder axis. The described measuring procedure was then repeated. At this point the tomography was conducted in presence of an external magnetic field with a flux density of 220 mT in direction of the cylinder axis as well.

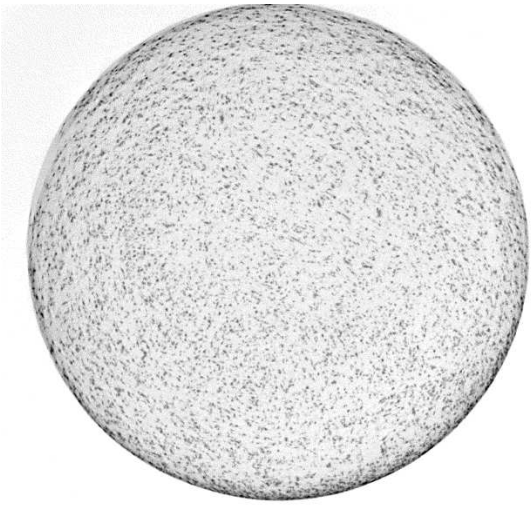

Figure 1: Slice of the reconstructed tomography before magnetization showing the highly anisotropic particles randomly oriented in the sample.

Magnetorheological effect

The unmagnetized sample shows a significant increase of the elastic modulus in presence of the magnetic field, proving the soft magnetic behavior of the unmagnetized particles.
After magnetization the sample shows an overall increase in stiffness and a significant increase of the effect of the external magnetic field on the elastic modulus. The results are visualized in figure 2.

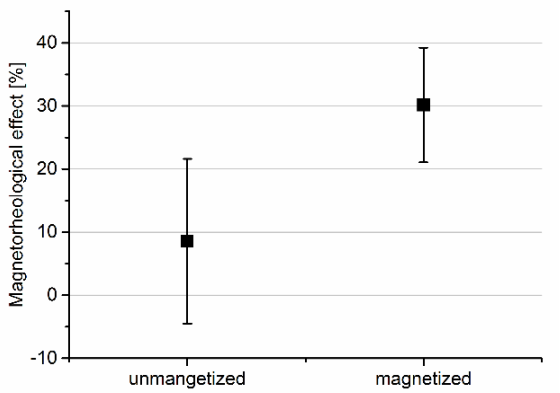

Figure 2: The magnetorheological effect, induced by a 220 mT magnetic field, was calculated as a change of the elastic modulus of the sample. Here the effect before and after magnetization with a 2T magnetic field is shown.

Particle structure

The angle between the longest major axis of the highly anisotropic particles and the direction of magnetization was calculated from the evaluated geometry data for every particle. It was shown, that the angle decreased due to the magnetization as a result of particles rotating towards the direction of magnetization to align themselves within the magnetic field. As a result of the elastic linkage between the particles and the matrix no complete alignment was observed. In figure 3 the rotation of the particles is visualized schematically.

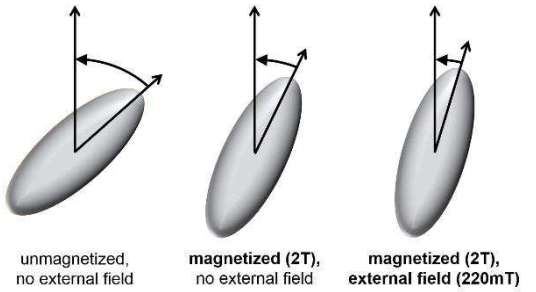

Figure 3: Rotation of a particle after permanent magnetization (2 T) and in presence of an external magnetic field (220 mT). Both magnetic fields pointing in the same direction aligned with the sample cylinder axis.

Figure 4 shows the frequency distribution of the calculated angles. Before magnetization the frequency of the angles is homogeneously distributed, indicating a random orientation of the particles. After magnetization this distribution shows a largely increased number of particles with small angles. This effect is enforced by the further application of an external field.

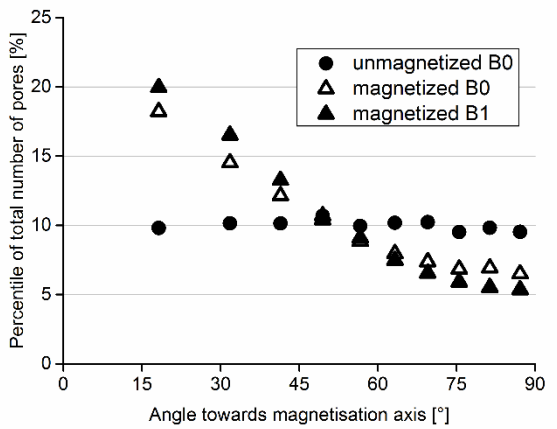

Figure 4: Frequency distribution of the calculated angle between the particle main axis and the magnetization direction.

Conclusion and outlook

A rotation of magnetized NdFeB-microparticles embedded in a silicone matrix was observed by means of computed X-ray micro tomography. This change in particle structure may be linked to the change in elastic properties of the sample after magnetization.

So far this work shows the applicability of the utilized methods to evaluate changes in particle structures induced by magnetic fields, observed with magnetorheological elastomers.

Future work will include a more detailed examination of the particle arrangement, as well as an evaluation of the motion and rotation on a single particle basis [3].

A fine tuning of the matrix material may lead to a higher effect of particle structure change.

Acknowledgments

Financial support by DFG (Grant. No. OD18/21) within SPP1681 is gratefully acknowledged.

References

[1] Borbáth T, Günther S, Borin D Y, Gundermann T, Odenbach S. (2012). Smart Mater. Struct. 21(10), 105018

[2] Günther D, Borin D Y, Günther S, Odenbach S (2012). Smart Mater. Struct. 21(1), 015005

[3] Gundermann T, Odenbach S (2014) Smart Mater. Struct. 23(10), 1050

Experimental determination of the critical Rayleigh number for the thermomagnetic convection with focus on the fluid composition

M. Heckert, L. Sprenger, A. Lange, S. Odenbach

TU Dresden, Chair of Magnetofluiddynamics, Measuring and Automation Technology, 01062 Dresden

Introduction

Thermomagnetic convection denotes a transport phenomenon in magnetic fluids driven by a thermal gradient resulting in a gradient in the magnetic field [1]. It is characterized by the thermal and magnetic Rayleigh numbers. Convection sets in if the destabilizing magnetic force exceeds the stabilizing effects of the fluid's viscosity η and thermal conductivity κ. Finlayson [1] theoretically predicts an onset of convection if the condition of

$$\frac{Ra}{Ra_{\mathrm{c}}} + \frac{Ra_{\mathrm{m}}}{Ra_{\mathrm{m,c}}} \geq 1 \qquad (1)$$

is met. The phenomenon was first investigated experimentally by Schwab [2, 3], and later by Engler [4, 5]. The present investigations aim at the experimental determination of the critical magnetic Rayleigh number in dependence from the fluid's composition.

Experimental Setup

Three differently composed fluids are chosen for the experimental investigations. Particles are always made from magnetite, the NF4000C's and EMG905's carrier liquid is kerosene, while APG513A is an ester-based fluid with significantly higher viscosity. All ferrofluids are provided by Ferrotec, USA, and their properties are listed in Table 1, i.e. the particle's concentration ϕ and diameter $\bar{d}$, the fluid's saturation magnetization M_{S}, density ρ, and viscosity η. The particle size distribution for the fluids according to Chantrell et al. [6] is presented in Fig. 1.
The onset of convection is determined by the heat flux transported across a layer of magnetic fluid placed in a homogeneous magnetic field while the temperature difference is risen step by step. Convection intensifies the heat flux in comparison with the conductive one, and the critical temperature difference marking the transition is obtained. This leads to combinations of thermal and magnetic Rayleigh numbers for each setup of temperature difference and magnetic field.

Table 1: Properties of the fluids at 313 K.

Property	EMG905	NF4000C	APG513A [5]
ϕ, %	7.6 ±1%	5.3 ±2%	6.6
$\bar{d}$, nm	12.7 ±1%	8.6 ±2%	12.9
M_{S}, kA/m at 289 K	34.2 ±1%	23.9 ±2%	28.5
ρ, kg/m^3	1323 ±0.1%	1158 ±0.1%	1345
η, mPa·s	10.01 ±1%	6.55 ±0.5%	84

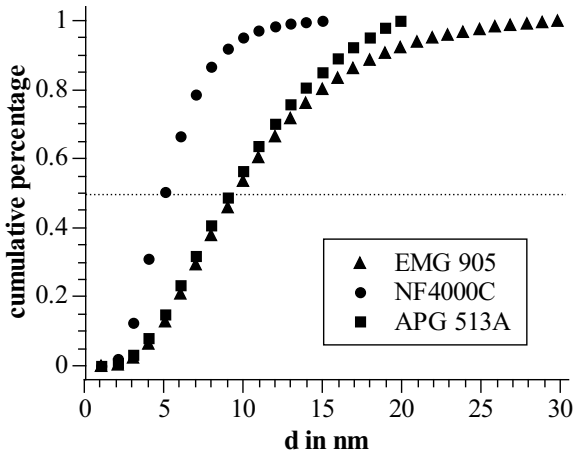

Figure 1: The particle size distribution according to Chantrell [6] is plotted for the three fluids under investigation.

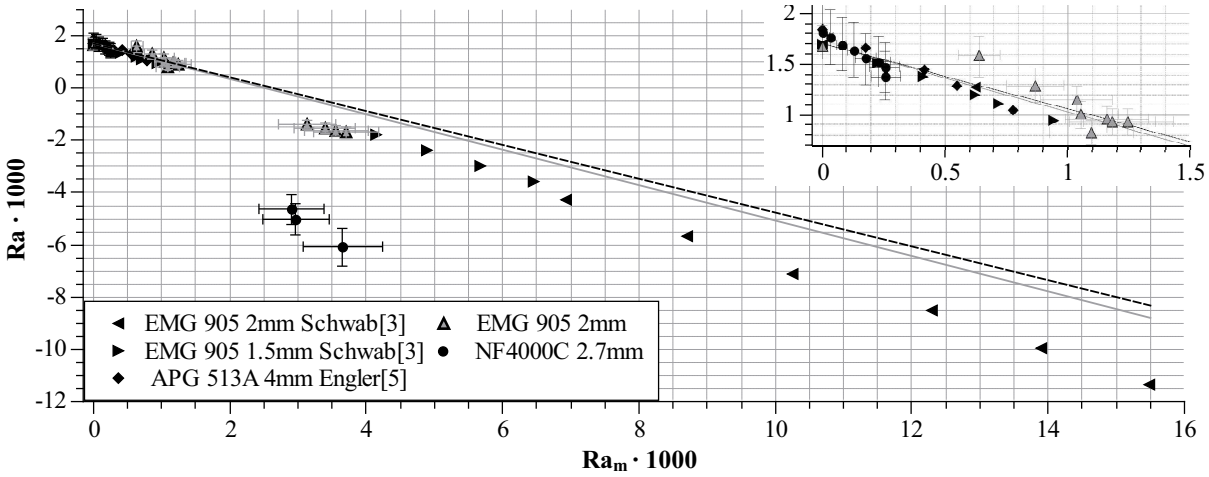

Figure 2: Thermal and magnetic Rayleigh number of the experiments, and of literature are presented, critical thermal and magnetic Rayleigh number are depicted as intercepts [7].

Table 2: Critical thermal and magnetic Rayleigh numbers calculated on basis of Eq. 1.

Fluid	Ra_{c}	$Ra_{\mathrm{m,c}}$
EMG 905	2082	1998
NF4000C	1925	856

Results and Discussion

The Rayleigh numbers of each experimental run and their corresponding point of transition are plotted in Fig. 2. The critical thermal Rayleigh number, denoting the onset of convection in absence of a magnetic force is gained by the intercept of the y-axis. The critical magnetic Rayleigh number describes the onset of convection if buoyancy-driven forces are absent, and can be obtained by the intercept on the x-axis. The critical values are listed in Table 2. The solid line in Fig. 2 depicts the theoretical prediction of the interdependence of the Rayleigh numbers considering the fluidic composition of EMG905, while the dashed line stands for the fluidic properties of NF4000C. While the experimental data for the EMG905 and the former APG513A seem reasonably close to the theoretical critical magnetic Rayleigh number of ≈2500 [7], the NF4000C's critical value is significantly smaller. The NF-fluid's narrower particle size distribution and smaller particle size are assumed being responsible for the change in the convective behavior.

Acknowledgements
The authors especially thank Kuldip Raj from Ferrotec for the support with the fluid samples. The financial support by the Deutsche Forschungsgemeinschaft in project LA1182/3 is gratefully acknowledged.

References

[1] B. A. Finlayson, J. Fluid Mech. 40 (1970) 753767.

[2] L. Schwab et al., J. Mag. Mag. Mater. 39 (1983) 113114.

[3] L. Schwab, LMU München, Diss, 1989.

[4] H. Engler et al., J.Phys.: Condens. Matter 20 (2008) 204135.

[5] H. Engler, TU Dresden, Diss, 2010.

[6] R. W. Chantrell et al., IEEE Trans. Mag. MAG-14 (5) (1978) 975977.

[7] M. Heckert et al., J. Mag. Mag. Mater. (381) (2015) 337343.

Development and experimental evaluation of gel phantoms for Magnetic Particle Imaging

R. Sandig[1], D. Baumgarten[1], F. Wiekhorst[2], A. Weidner[1], S. Dutz[1*]

[1] *Institute of Biomedical Engineering and Informatics (BMTI), Technische Universität Ilmenau, Gustav-Kirchhoff-Straße 2, 98693 Ilmenau, Germany; silvio.dutz@tu-ilmenau.de*
[2] *Physikalisch-Technische Bundesanstalt, Abbestraße 2-12, 10587 Berlin, Germany*

Introduction

Magnetic nanoparticles (MNP) experience increasing interest for a variety of medical and pharmaceutical applications, e.g. for magnetic drug targeting or magnetic hyperthermia. For all of these applications it is necessary, or at least advantageous, to obtain a homogeneous MNP distribution within the tissue. At the moment, no commercially available method exists to image the MNP distribution. Standard medical imaging methods like Magnetic Resonance Imaging (MRI) or X-ray Computed Tomography (CT) provide no satisfying results regarding spatial resolution of obtained images.

A promising approach to determine spatial MNP distribution within tissue is Magnetic Particle Imaging (MPI). In MPI, the local nonlinear magnetic response of MNP in the tissue exposed to an external sinusoidal magnetic field is used to reconstruct a 3-dimensional image of the magnetic particle distribution which can be related to structural features of the tissue [1]. In the past 10 years there was a rapid progress in development of MPI scanners and nowadays the very first preclinical devices are commercially available from Bruker BioSpin (Ettlingen, Germany). To evaluate performance of commercial as well as various custom-made scanners in several laboratories, defined test phantoms are needed. Measurement phantoms for MRI have limited suitability for this purpose and thus the aim of the here presented study is to develop and evaluate test phantoms for MPI which enable the assessment of present MPI scanners.

Methods

Pre-requirement for development of test phantoms is the establishment of a suitable MNP-matrix combination, which enables a homogeneous MNP distribution, combined with a strong immobilization of the MNP within the matrix as well a high mechanical stability of the matrix material. For this, magnetic multicore nanoparticles of about 50 nm were prepared as described before [2], coated with different shells (Dextran, CM-Dextran, and DEAE-Dextran) and embedded in 6 various matrix materials (gelatin, agarose, agar-agar, ballistic gel, and two different gelatin-oil mixtures).

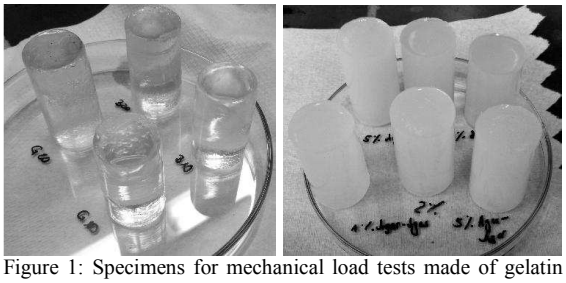

Figure 1: Specimens for mechanical load tests made of gelatin and ballistic gel (a) as well as agar-agar and agarose (b).

The obtained MNP-matrix combinations were tested for their mechanical stability by means of mechanical load tests (Figure 1). The degree of MNP distribution and immobilization within the matrix was determined by optical investigation of the samples with a microscope and by investigation of the magnetic particle properties measured by vibrating sample magnetometry (VSM).

The most promising MNP-matrix combination was used to manufacture measurement objects of different shape (spheres, cubes) and different size (5, 10, 20 mm) embedded in a phantom matrix with an overall

geometry of a cylinder with D = 50 mm and H = 60 mm. The resulting test phantoms were evaluated for their suitability to simulate MNP loaded areas within a non-magnetic matrix by means of MRI (Bruker Icon) and MPI (Bruker BioSpin preclinical MPI-scanner).

Results

As a measure for the agglomeration of the MNP within the matrix served the coercivity. Here we assume, that an increasing coercivity is caused by unwanted agglomeration of the particles. In case of low coercivity of embedded MNP, the absence of agglomerates in the matrix was checked by microscopy. In summary, microscopic and magnetic investigations revealed, that bare and CM-Dextran coated MNP show the best results regarding homogeneous distribution of the MNP within the matrix (Figure 2).

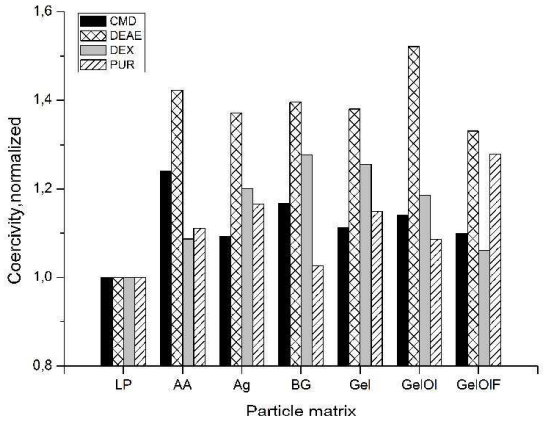

Figure 2: Coercivity of different MNP-matrix combinations, normalized to the coercivity of dried MNP (LP).

Resulting from these investigations, the combination of CM-Dextran coated MNP within ballistic gel was chosen as the most suitable material of our tested combinations for test phantom building.
Several strategies for preparation of measurement objects and their embedding in the phantom matrix were tested and will be discussed together with the results of the test measurements in our presentation.

Acknowledgments

The authors thank M.Sc. Mathias Fritz (TU Ilmenau) for assistance during microscopy.

References

[1] **Gleich** B, Weizenecker J. Tomographic imaging using the nonlinear response of magnetic particles. nature **2005**; 435: 1214–1217.

[2] **Dutz** S, Clement JH, Eberbeck D, Gelbrich Th, Hergt R, Müller R, Wotschadlo J, Zeisberger M. Ferrofluids of magnetic multicore nanoparticles for biomedical applications. J Magn Magn Mater **2009**; 321/10: 1501–1504.

Remote-controlled Magnetic Activation of the Self-healing Effect in Elastomeric Composites

A. Shaaban, N. Hohlbein, A. M. Schmidt

Department Chemie, Institut für Physikalische Chemie, Universität zu Köln, Luxemburger Str. 116, D-50939 Köln, email: annette.schmidt@uni-koeln.de

Introduction

The research interest on remote-controlled multiple responsive materials has increased over the last few decades. In this respect, the combination of magnetic nanoparticles with soft materials offers several perspectives towards smart adaptive materials that can be manipulated by external magnetic fields. In particular, the local heat dissipation by magnetic nanostructures in oscillating electromagnetic fields (OEMF) provides the option to increase the temperature locally and thus stimulate dynamic processes, e. g. for temperature-triggered shape changes.

In this work we show that temperature-induced mechanisms for self-healing in polymers [1], [2] can effectively be activated by magnetic heating of tailored magnetic fillers. We systematically investigate the influence of the size, shape, composition and magnetocrystalline anisotropy of nanoscopic magnetic filler particles in an acrylate-based ionomeric elastomer on their heating and healing characteristics. The thermal energy that is dissipated locally in the particles' environment under field influence triggers the dynamic rebonding within the matrix, thus activating the self-healing process.

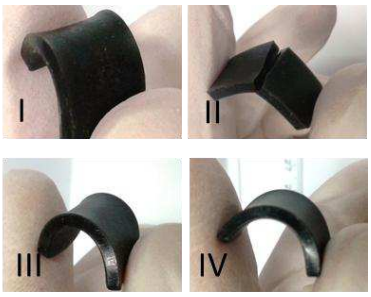

Figure 1. Illustration of cut`n`heal experiments.

The magnetic trigger is shown to result in a fast response and allows the contactless, remote-controlled restoration of the mechanical properties of a sample after damage. Under optimized conditions, a particle volume fraction as low as 0.05 vol% is sufficient to reach a healing efficiency of > 90 % after 15 min of irradiation.

Results and Discussion

Magnetic nanoparticles of different composition, size, and shape, are incorporated into a model elastomer matrix that recently was shown to show an effective, temperature-induced self-healing behavior. The matrix is based on a Zn-neutralized ionomer (M_w ~ 60.000 g·mol^{-1}, PDI ~ 1.3) with n-butyl acrylate as the main component, which lead to flexible backbone with low T_g = -41, and 5% neutralized acrylic acid groups.[3] By using appropriate field parameters (250 kHz and 31.5 kA·m^{-1}), we investigate the heating and healing profiles of pristine and damaged elastomer samples. The healing efficiency is quantified in tensile experiments of macroscopically cut samples. In addition, the impact of the fillers on the rheological properties of the matrix is examined.

The magnetic nanofillers increase the mechanical strength of the elastomers and act as "nano-hotspots" in the electromagnetic energy dissipation under field influence. By heating the material intrinsically across the transition temperature, the self-healing process is activated.[3]

A comparative investigation concerning Fe_3O_4, $CoFe_2O_4$, and Co-based particles in the size range of 10 nm – 200 nm and with spherical, cubic of rod-like shape was employed with the ultimate goal to result in a tailored design for an effective energy har-

vesting (Figure 1a). The resulting composites were analyzed on their magnetic, thermal and mechanical properties.

In dynamic rheology, the materials show an overall viscoelastic behavior. Figure 1b shows the thermograms for a series of P@FC composites. A Langevin-like temperature increase with time is noticed due to the remaining heat loss to the environment. The steady-state temperature at long times, T_s, as well as the initial heating rate $(dT/dt)_{t\to 0}$ increase with increasing particle fraction, and already at volume fractions as low as 0.1 vol%, the heating is fast enough to reach 150 °C in 10 minutes. At ν_{NP} = 0.05 vol%, the ionic transition temperature T_i is reached within a few minutes.

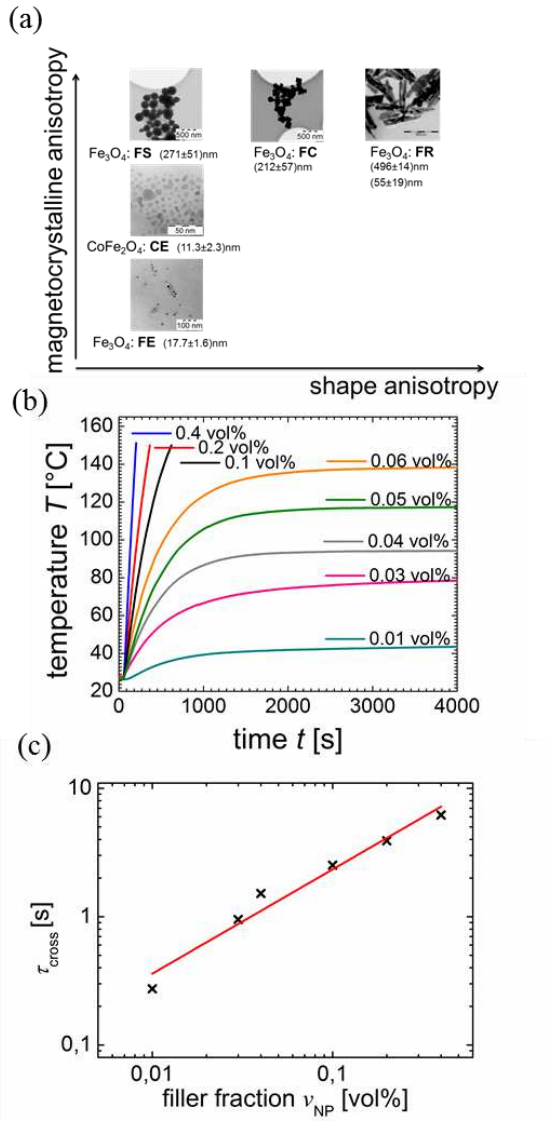

Figure 2. a) Overview of the magnetic nanoparticles of different magnetocrystalline and shape anisotropy; b) HF measurements of P@FC with increasing filler fraction and c) relaxationtime at τ_{cross} with increasing FC filler fraction.

When comparing the dependence of the steady-state temperature T_s and heating rate $(dT/dt)_{t\to 0}$ on the filler fraction for different particle types, the cubic (**FC**) particles show the best heating efficiency among the particles, followed by single-domain particle (**FE**) and (**CE**) then the spherical (**FS**) and the rod-like (**FR**) particles.

All composites show a qualitative similar dynamic mechanical behavior in oscillatory rheology. At low frequencies, the shear loss (G'') modulus is dominant, indicating a prevailing viscous behavior. With increasing frequency, the shear storage (*G'*) modulus increases, and a *G''/G'* cross-over to a dominating elastic behavior is observed at a frequency that depends on the ion content and the nature of the counter ion. Figure 1c show a nearly linear scaling of the respective characteristic times $\tau = 2\pi/\omega_{cross}$ for composites based on (**FC)** particles, as these are shown to be the most suitable for the heating efficiency. The impact of the particulate filler fraction can be attributed to a slow-down of the sticky reptation process and can be interpreted as an involvement of the filler particles in the phase behavior of the materials.[3]

Acknowledgments

This work was financially supported within the DFG-SPP 1568 "Generic principles of self-healing materials" (SCHM1747/7-1).

References

[1] J. a. Syrett, C. R. Becer, and D. M. Haddleton, Polym. Chem., vol. 1, no. 7, pp. 978–987, 2010.

[2] N. Hohlbein, M. von Tapavicza, A. Nellesen, and A. Schmidt, W. H. Binder, Ed. Wiley-VCH, 2013, pp. 323–342.

[3] N. Hohlbein, A. Shaaban, and A. M. Schmidt, Polymer, 2015, doi:10.1016/j.polymer.2015.04.024.

Long-term phantom for MRI and X Ray imaging of body tissues enriched with magnetic nanocomposites

H. Rahn[1,2], R. Woodward, M. House[2], S. Dutz[3] , D. Engineer[4] , K. Feindel[4] , T. StPierre[2], and S. Odenbach[1]

[1] *Technische Universität Dresden, Institute of Fluid Mechanics, Chair of Magnetofluiddynamics, 01062 Dresden, Germany*
[2] *The University of Western Australia, School of Physics, Crawley, Perth WA 6009, Australia*
[3] *Technische Universität Illmenau, Institut für Biomedizinische Technik und Informatik,Illmenau, Germany*
[4] *The University of Western Australia, Centre for Microscopy and Characterisation Analysis, Crawley, Perth WA 6009, Australia*

We have made a preliminary study of a long-term phantom for MRI and X-Ray imaging of body tissues enriched with magnetic nanocomposites suitable for 3-dimensional and quantitative imaging of tissues after, for example, magnetically assisted cancer treatments.

The approach was to perform a cross-calibration of XµCT and MRI. For this a long-term phantom system suitable for MRI and XCT has been developed, applied and tested. The result is the specification of a sensitivity range for standard imaging techniques as XµCT and MRI.

For the calibration phantoms the following requirements have been defined:

- The body material shall represent biological tissue for MRI and X-Ray imaging;
- The body material has to be homogeneous e.g. without air bubbles;
- The magnetic nanoparticles have to be suspended homogeneously and immobilised the body material;
- The developed phantom system hast to be long-term stable over minimum several months.

The developed phantoms consist of an elastomer with different concentrations of multi-core magnetic nanocomposites (MNC)[1]. The matrix material is a synthetic thermoplastic gel, PermaGel (PG) [2]. It consists of white petroleum oil and styrenic copolymers, thus it is classified as a “physically associated gel”. Because PG is primarily made of white oil any measurable weight loss or evaporation rate is expected. Consequently, it is stable at room temperature over several months [3].

We prepared 12 different magnetic component concentrations in a range of 0 mg/ml to 6.91 mg/ml, as shown in Figure 1a). These cylinders have been layered to stack of three PG-MNC-cylinders which are separated by blank PG as shown in Figure 1b).

a) b)

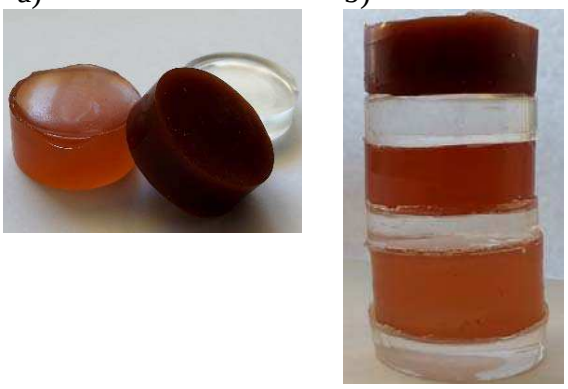

Figure 1a): cylinders of three different nanoparticle concentrations and a pure gel cylinder; b): one of four stacks of cylinders with three nanoparticle concentrations separated by blank gel cylinders

The developed phantoms have been analysed with NMR Relaxometry (Bruker minispec mq 60) at 1.4 T to obtain R2 transverse relaxation rates, with SQUID (Superconducting QUan¬tum Interference Device) magnetometry and ICP-MS (Inductively Coupled Plasma Mass Spectrometry) to verify the magnetite concentration, and with XµCT and 9.4 T MRI to visualise the phantoms 3-dimensionally and also to obtain R2 rates.

MRI is also one of the mainstays in clinical imaging techniques and diagnostics. MRI is powerful for imaging soft tissues, as internal organs and brain. MRI is based on

the principles of Nuclear Magnetic Resonance (NMR). Different to CT based on X-Rays, MRI uses a strong magnetic field and radio frequency excitation for imaging. The MRI data is generated by manipulation and measurement of changes in the small magnetic moments linked to hydrogen atoms in the visualised object.
The MRI measurements have been performed at the "Harry Perkins Institute". The used MRI-apparatus "Bruker BioSpin MRI" is a small animal and molecular MRI for pre-clinical research. It provides a magnetic field of 9.4 T [4].
The phantom stacks were placed inside the coil separated by an acrylic glass cross (as shown in Figure 2 a).

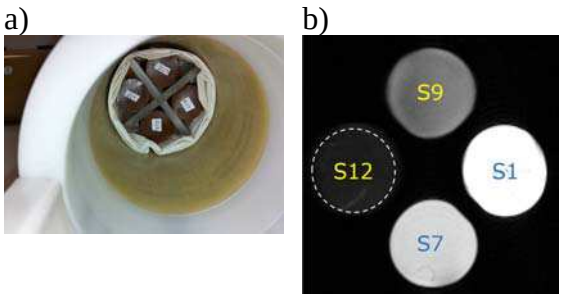

Figure 2a): Arrangement of the four sample stacks within the MRI coil. b) MRI-signal of different PG or PG-MNC samples. S1 is a blank gel and gives a strong bright signal and S12 is the highly nanocomposites enriched gel. Here, almost no signal is detectable.

The result is a 3-dimensional volume composed of 2 dimensional grey scale images. One image is shown in Figure 2b). There an axial section of all four samples can be seen. Thereby the most least concentrated sample S1 (blank PG) gives the brightest signal (bright grey to white) while the highly concentrated sample S12 is almost not visible (black).
R2 values from NMR-Relaxometry had a strong linear correlation (R = 0.994) with magnetite concentration between 0 mg/ml up to 4.5 mg/ml. For the XµCT-apparatus, we defined a sensitivity range from 0.723 mg/ml to 6.91 mg/ml. For MRI, the MSME data produced strong linear correlations (R = 0.990 and 0.991, respectively) over magnetite concentrations between 0mg/ml and 1.435 mg/ml. As expected, high-field MRI has better sensitivity for nanoparticles with low to moderate magnetite concentrations, while XµCT performs best with moderate to high magnetite concentrations. The common detection range of 9.4T MRI and XµCT for magnetite in this PG-MNC phantom lies between 0.723 mg/ml and 1.435 mg/ml.

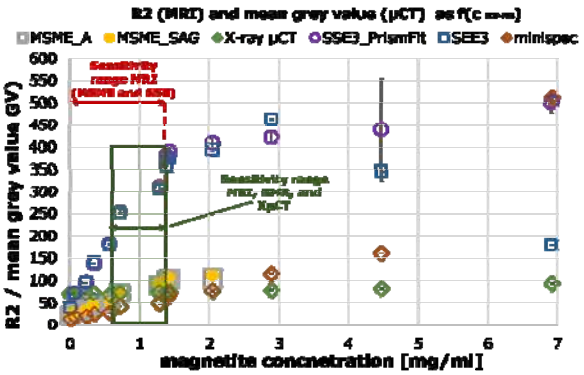

Figure 3: Summary of compared measuring techniques NMR, XµCT, and MRI.

Acknowledgments

These studies are supported by the Deutsche Forschungsgemeinschaft (DFG-RA 2633/1-1).

References

[1] Dutz S., et al. Ferrofluids of magnetic multicore nanoparticles for biomedical applications; J. of Magn. and Magn. Mat. 321 (2009) 1501 – 1504
[2] Perma Gel Safety Data Sheet according to 1907/2006/EC (REACH), 1272/2008/EC (CLP), and GHS
[3] Private communication with Darryl D. Amick, PhD, President of the company
[4] http://www.bruker.com

Magnetic filament brushes

P. A. Sánchez[1], E. S. Pyanzina[2], E. V. Novak[2], J. J. Cerdà[3], T. Sintes[3] and S. S. Kantorovich[1, 2]

[1] *University of Vienna, Sensengasse 8, 1090, Vienna, Austria.*
[2] *Ural Federal University, Lenin av. 51, 620000, Ekaterinburg, Russia.*
[3] *Instituto de Física Interdisciplinar y Sistemas Complejos (CSIC-UIB), E-07122 Palma de Mallorca, Spain.*

We present a theoretical study on the equilibrium behaviour of a supramolecular magnetoresponsive surface with potential for different applications, such as enhanced magnetorehological systems and filtering devices. This surface consists of a relatively dense array of magnetic filaments, *i.e.*, colloidal magnetic particles crosslinked with polymers to form permanent linear chains.[1] Recently, we have shown that such filaments may have a considerably stronger magnetic response than purely self-assembled chains of magnetic colloids.[2] In this case, every filament in the array is grafted to a flat substrate, forming a polymer brush-like structure that is expected to be highly controllable by means of external magnetic fields.

We study and optimise the properties of the magnetic filament brush by performing extensive computer simulations with a coarse-grained model that takes into account the correlations between the magnetic moments of the particles and the backbone crosslinks.[2,3] We highlight the differences between the magnetic filament brush and conventional non-magnetic polymer brushes, and determine the dependence of the magnetic brush properties on the main experimental synthesis parameters, such as the magnetic moment of the particles, the chain length and the grafting density.

Acknowledgments

This research has been partially supported by the Austrian Research Fund (FWF): START Projekt Y 627-N27. Authors are grateful to the Ural Federal University stimulating programme. S.S.K, E.S.P. and E.V.N. are supported by RFBR mol-a-ved 15-32-20549. S.S.K. is also supported by the EU-Project 642774 ETN-Colldense and the Ministry of Education and Science of the Russian Federation (Contract 02.A03.21.000, Project 3.12.2014/K).

References

[1] R. Dreyfus *et al*. Nature 2005, 437, 862; J. J. Benkoski *et al*. J. Polym. Sci., Part B: Polym. Phys. 2008, 46, 2267; K. Erglis *et al*. J. Phys.-Condens. Mat. 2008, 20, 204107; Z. Zhou *et al*. ACS Nano 2009, 3, 165; J. Byrom *et al*. Langmuir 2014, 30, 9045; H. Singh *et al*. Nano Lett. 2005, 5, 2149; A. Cēbers. Curr. Opin. Colloid. Interface Sci. 2005, 10, 167; M. Belovs *et al*. Phys. Rev. E 2009, 79, 051503; F. Fahrni *et al*. Lab Chip 2009, 9, 3413; M. Babataheri *et al*. J. Fluid Mech. 2011, 678, 5; I. Javaitis. Adv. Mat. Res. 2011, 222, 221.

[2] P. A. Sánchez *et al*. Soft Matter 2015, 11, 2963.

[3] J. J. Cerdà *et al*. Soft Matter 2013, 9, 7185.

Vinamax: a simulation tool for nanoparticle magnetization dynamics

J. Leliaert[1,2], A. Coene[2], A. Vansteenkiste[1], G. Crevecoeur[2], B. Van Waeyenberge[1], L. Dupré[2]

[1]*Dept. of Solid State Sciences, Ghent University, 9000 Gent, Belgium*
[2]*Dept. of Electrical Energy, Systems and Automation, Ghent University, 9000 Gent, Belgium*

Introduction

We present Vinamax [1], a simulation tool for the magnetization dynamics of nanoparticles. Vinamax numerically solves the Landau-Lifshitz equation and can be used in biomedical research where nanoparticle imaging techniques, such as magnetorelaxometry [2] and Electron Paramagnetic Resonance [3] are developed. In these applications, it can help to gain insight in the underlying physics, validate higher level models and study their limitations.

Methods

In the micromagnetic framework [4] the magnetization is described by a space and time dependent continuum vector field $\mathbf{m}$, normalized to the saturation magnetization M_{sat}. Each nanoparticle is assumed to be uniformly magnetized and is approximated by a single macrospin. The magnetic dynamics of each nanoparticle are described by the Landau-Lifshitz equation [5]:

$$\frac{d\mathbf{m}}{dt} = -\frac{\gamma_0}{1+\alpha^2}\left(\mathbf{m}\times\mathbf{B}_{\text{eff}} + \alpha\mathbf{m}\times\mathbf{m}\times\mathbf{B}_{\text{eff}}\right). \quad (1)$$

Where γ_0 denotes the gyromagnetic ratio and α is the dimensionless Gilbert damping constant. The effective field $\mathbf{B}_{\text{eff}}$ is derived from the energy terms and is the sum of the different effective field terms that influence the magnetization:

$$\mathbf{B}_{\text{eff}} = \mathbf{B}_{\text{ext}} + \mathbf{B}_{\text{anis}} + \mathbf{B}_{\text{demag}} + \mathbf{B}_{\text{therm}} \quad (2)$$

For a detailed description of the implementation of the different terms in eq. (2) and the possibilities of Vinamax, we refer to Ref. [1], where Vinamax was also extensively tested against the micromagnetic software package MuMax3 [6].
$\mathbf{B}_{\text{ext}}$ is an externally applied field that can be both space and time-dependent. This field gives rise to the Zeeman energy density:

$$E_{\text{Zeeman}} = -M_{\text{sat}}\mathbf{B}_{\text{ext}}\cdot\mathbf{m} \quad (3)$$

Most iron oxide nanoparticles used in biomedical applications have uniaxial anisotropy [7], for which the energy density reads

$$E_{\text{Anisotropy}} = K_{u1}\left[1-(\mathbf{m}\cdot\mathbf{u})^2\right]. \quad (4)$$

In Vinamax, both the size and direction of the anisotropy can be chosen freely. Furthermore, it is also possible to simulate nanoparticles with a cubic anisotropy with Vinamax.
The third term in eq. (2) is the demagnetizing field. This field originates from the dipolar interactions between all particles [1]. The strength of Vinamax lies in the fact that this long range interaction can micromagnetically be taken into account for large amounts of particles in virtually any configuration due to an efficient calculation using a fast multipole method.
Finally, $\mathbf{B}_{\text{eff}}$ contains a stochastic term $\mathbf{B}_{\text{therm}}$ to take thermal fluctuations into account [8]. The size and properties of $\mathbf{B}_{\text{therm}}$ are determined by Brown [9] with the fluctuation-dissipation theorem. In this contribution we focus on the correct implementation and influence of this field.

Results

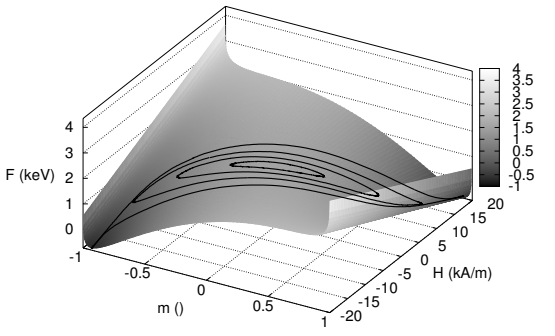

Figure 1: The free energy landscape and magnetization of an ensemble of particles with radius 8 nm, $M_{sat} = 400$kA/m and $K_{u1} = 1000$ J/m^3 at $T = 300K$. The loops (from inner to outer) correspond with external fields with amplitude 2, 5, 10 and 20 kA/m with a frequency of 100 kHz.

To investigate effects of finite temperatures on nanoparticle magnetization reversal, we simulated the magnetization of non-interacting nanoparticles in a time-varying external field applied along their anisotropy axis. In a large-scale study we vary the particle size, the amplitude and sweep rate of the external field. As an example, Fig. 1 shows the magnetization as function of external field on top of the free energy landscape for which we derived an analytical expression. The time-dependent external field is responsible for the shift of the global minimum from $m \approx 1$ to $m \approx -1$. The presence of a local minimum is responsible for the observed hysteresis. Note the divergence of the free energy for m close to -1 and 1, due to the high entropy is these configurations. We emphasize that the implementation of the thermal field in Vinamax results in the correct magnetization for high fields, i.e. the magnetization lies in the local minimum close but not equal to -1 or 1.

Conclusion

In conclusion, we presented Vinamax. This simulation tool is able to micromagnetically simulate magnetic nanoparticles and can be used to gain insight in the underlying physics of biomedical applications, or to validate and study the limitations of higher-level models. Here, we focused on the correct implemtation of temperature effects in simulations of nanoparticles in a time-dependent field, and visualised the results on top of the free energy landscape for which we derived an analytical equation.

References

[1] Jonathan Leliaert *et. al. Medical & biological engineering & computing*, pages 1–9, 2015.

[2] F Wiekhorst *et. al. Pharmaceutical Research*, 29:1189–1202, 2012.

[3] A Coene *et. al. Journal of Physics D: Applied Physics*, 46(24):245002, 2013.

[4] William Fuller Brown. Number 18. Interscience Publishers New York, 1963.

[5] L.D. Landau and E.M. Lifshitz. *Phys. Z. Sowietunion*, 8:153, 1935.

[6] Arne Vansteenkiste *et. al. AIP Advances*, 4(10):–, 2014.

[7] Quentin A Pankhurst *et. al. Journal of physics D: Applied physics*, 36(13):R167, 2003.

[8] William T. Coffey and Yuri P. Kalmykov. *Journal of Applied Physics*, 112(12):–, 2012.

[9] William Fuller Brown. *Phys. Rev.*, 130:1677–1686, Jun 1963.

Tailoring superelasticity of soft magnetic materials

Peet Cremer, Hartmut Löwen, Andreas M. Menzel

Institut für Theoretische Physik II: Weiche Materie, Heinrich-Heine-Universität Düsseldorf, D-40225 Düsseldorf, Germany

Introduction

Magnetic gels are hybrid materials composed of colloidal magnetic particles embedded in an elastic polymer matrix [1]. Due to the coupling of elastic and magnetic interactions, the material properties can be dynamically [2] and reversibly [3] tuned by applying an external magnetic field. Such soft magnetoresponsive materials have a wide range of applications as tunable dampers, vibration absorbers, sensors, and soft actuators.
Here we analyze the nonlinear stress-strain behavior of anisotropic uniaxial magnetic gels using computer simulation. Experimentally, these systems are synthesized by applying a homogeneous external field while cross-linking the polymer matrix, which leads to the formation of chains of magnetic particles along the field direction.

Simulation

We consider spherical magnetic particles which are translationally coupled to the elastic matrix. Their magnetic dipolar moments can freely reorient so that there is no rotational coupling to the matrix [4]. The elastic matrix between the particles is represented by a mesh of tetrahedra that can affinely deform according to the Neo-Hookean hyperelastic model. Although the deformation within each tetrahedron is affine, the combined distortion of many tetrahedra can represent globally inhomogeneous deformations.
Our numerical samples consist of magnetic particles arranged in parallel chain-like aggregates, spanning the system in one direction. In the plane perpendicular to the chain axes, the chains are randomly distributed. We stretch the samples parallel to the chain axes and analyze their nonlinear stress-strain behavior, also in reaction to additional external magnetic fields.

Results

The obtained stress-strain curves show a pronounced nonlinear regime, where the material exhibits superelastic behavior. In this nonlinear superelastic regime, the sample can be extended without further increasing the applied stress. There are two effects leading to this nonlinearity: A structural transition and a reorientation transition. As we demonstrate, both transitions are susceptible to external fields, which enables tuning of the stress-strain behavior. Thus, we can show that the stress-strain behavior of magnetic gels shows remarkable similarities to that of superelastic shape-memory alloys and can be tailored to suit a specific application.

Acknowledgments

Support from the DFG through the SPP 1681 and from the ERC Advanced Grant INTERCOCOS (Grant No. 267499) is gratefully acknowledged.

References

[1] M. Zrínyi, L. Barsi, and A. Büki, *Ferrogel: a new magneto-controlled elas-*

tic medium, Polym. Gels Netw. **5**, 415 (1997).

[2] M. Tarama, P. Cremer, D. Y. Borin, S. Odenbach, H. Löwen, and A. M. Menzel, *Tunable dynamic response of magnetic gels: Impact of structural properties and magnetic fields*, Phys. Rev. E **90**, 042311 (2014).

[3] G. Pessot, P. Cremer, D. Y. Borin, S. Odenbach, H. Löwen, and A. M. Menzel, *Structural control of elastic moduli in ferrogels and the importance of non-affine deformations*, J. Chem. Phys. **141**, 124904 (2014).

[4] N. Frickel, R. Messing, and A. M. Schmidt, *Magneto-mechanical coupling in $CoFe_2O_4$-linked PAAm ferrohydrogels*, J. Mater. Chem. **21**, 8466 (2011).

Tunable morphologies of magnetic particles in liquid crystals

Stavros D. Peroukidis, Sabine H. L. Klapp

Institute of theoretical Physics, Secr. EW 7-1, Technical University of Berlin, Hardenbergstr. 36, D-10623 Berlin, Germany

Suspensions of magnetic nanoparticles (MNP) in liquid crystalline (LC) matrices, i.e LC-MNP hybdrid systems [1], is a non-trivial avenue for obtaining materials with programmable and controllable functions. New interest on such systems was stimulated by the recent discovery of spontaneous magnetic ordering in a hybrid system of large, micron-sized magnetic plates embedded in a low molar mass nematic LC [1]. In the present work we focus on the opposite case of small MNPs in LC matrices, where the sizes are comparable. An example of such systems are lyotropic suspensions of colloid pigment rods and magnetite MNPs [2] which have been recently studied.

To explore these type of systems we here employ canonical Monte Carlo simulations and Molecular dynamics simulations of a simple binary model system consisting of anisotropic Gay-Berne (GB) rod particles [3] and MNPs, represented as dipolar soft repulsive spheres (DSS), i.e., spheres with an embedded point dipole moment μ_i in their center [4]. The length (l)-to-width (σ) ratio of the rods is set to $\frac{l}{\sigma}=3$. The dipolar spheres have diameter σ_s. We focus on systems with comparable sizes, i.e $0.25\sigma \le \sigma_s \le 2.0\sigma$.

Initially, we examine GB-DSS mixtures with relative small DSS $\sigma_s = 0.25\sigma$. This system exhibits Isotropic (I), uniaxial Nematic (N_u) and smectic-B

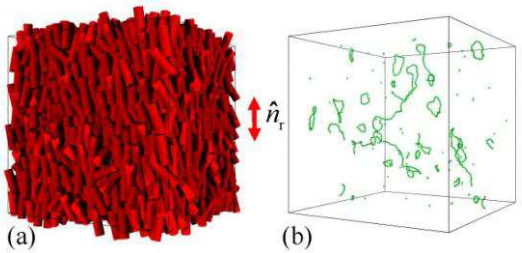

Figure. 1. Representative simulation snapshots for mixtures with $\sigma_s = 0.25\sigma$ in the uniaxial nematic (N_u) state for $\lambda = \mu^2/kT\sigma_s^2 = 7.5$. In (b) only the MNPs are shown for clarity. The director of rods $\hat{n}_r$ is also indicated.

(SmB) phases. In this system the magnetic particles self-assembly into clusters (such as rings and ferromagnetic chains). The most important finding is that the LC matrix induces orientational order to these clusters (see Fig. 1).

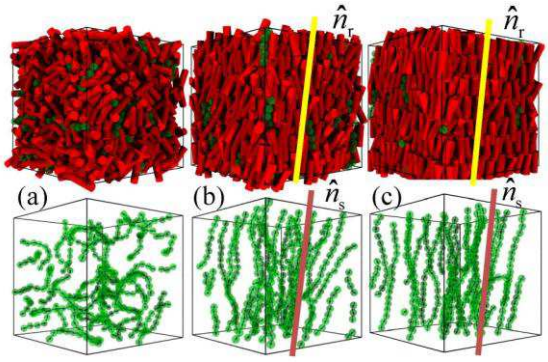

Figure 2. Representative simulation snapshots for mixtures with $\sigma_s = 1.0\sigma$ in the (a) Isotropic, (b) uniaxial nematic (N_u) and (c) Smectic-B phase. In the bottom parts only the MNPs are shown for clarity. The nematic directors of the species are also indicated.

We now turn to GB-DSS mixture where the diameter of the spheres is equal to the width of the rods ($\sigma_s = 1.0\sigma$) [4]. This system also exhibits I, N_u and SmB phases; nevertheless, the morphology of the DSS particles within the phases is completely different in comparison to the previous system. In the I-state, the DSS particles self-assemble into isotropic networks of wormlike chains (see Fig. 2a). Remarkably, in the N_u and SmB states the ferromagnetic chains spontaneously align along the LC director $\hat{n}_r$ (see Fig. 2b-c). Overall, the ferromagnetic chains are randomly arranged 'up' or 'down' and the system does not exhibit a net magnetization.

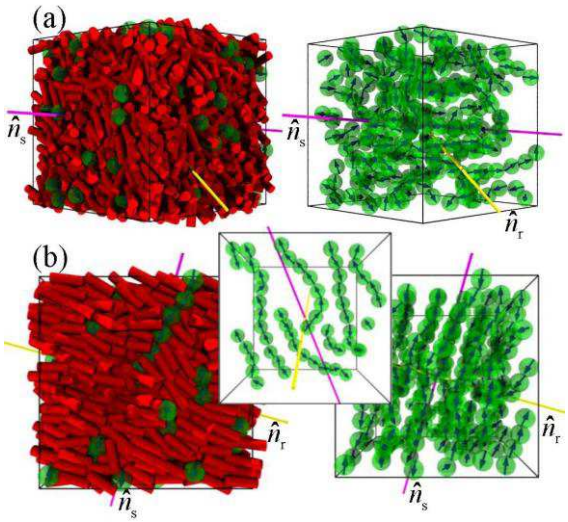

Figure 3. Representative simulation snapshots for mixtures with $\sigma_s = 2.0\sigma$: a) biaxial nematic (N_b) state and b) biaxial lamellar (L_b) state. On the right sides only the MNPs are shown for clarity. Part b) additionally includes a snapshot of the structure in one dipolar layer. The directors are indicated by thick lines.

Intriguing results obtained for a GB-DSS mixture with relatively large diameter of DSS, $\sigma_s = 2.0\sigma$ [4]. This system exhibits spontaneously biaxial nematic ordering in which, on average, the director $\hat{n}_r$ of the rods is perpendicular to the director $\hat{n}_s$ of the DSS particles (see Fig. 3). In the biaxial Lamellar L_b-state the ferromagnetic chains align, on average, perpendicularly to the director $\hat{n}_r$, and are arranged into an antiparallel manner resulting no net magnetization.

In conclusion, we have observed (i) spontaneous formation of clusters of magnetic particles, (ii) formation of ferromagnetic chains, yielding an uniaxially ordered hybrid without net magnetization but enhanced ordering of the LC matrix, and (ii) biaxial nematic and lamellar phases, where the magnetic particles arrange into chains oriented perpendicular to the LC director. Due to the magnetic component, both the uniaxial and biaxial ordered 'hybrids' possess strong anisotropic sensitivity to external magnetic field.

Acknowledgments
We thank R. Stannarius, S. Odenbach, A. Eremin and K. May for stimulating discussions. This research has been financed by DFG-Priority Programme 1681 ‘field controlled particle matrix interactions: synthesis multiscale modeling and application of magnetic hybrid materials’.

References

[1] A. Mertelj, D. Lisjak, M. Drofenik and M. Copic, et. al., Nature, **504**, 237 (2013)

[2] Private communication with R.Stannarius group.

[3] D. J. Cleaver, C. M. Care, M. P. Allen, and M. P. Neal, Phys. Rev. E, **54**, 559 (1996).

[4] S. D. Peroukidis and S. H.L .Klapp, arXiv:1503.08277 (2015); S. D. Peroukidis, K. Lichtner and S. H. L.Klapp, arXiv:1504.04161 (2015).

Flow cytometry for intracellular SPION quantification: Specificity and sensitivity in comparison with spectroscopic methods

RP Friedrich[1], C Janko[1], M Pöttler[1], P Tripal[1], J Zaloga[1], I Cicha[1], S Dürr[1,2], J Nowak[3], S Odenbach[3], I Slabu[4], M Liebl[4], L Trahms[4], M Stapf[5], I Hilger[5], S Lyer [1], C Alexiou[1*]

[1] *University Hospital Erlangen, Department of Otorhinolaryngology, Head and Neck Surgery, Section for Experimental Oncology and Nanomedicine (SEON), Glückstr. 10A, 91054 Erlangen.*
[2] *University Hospital Erlangen, Department of Otorhinolaryngology, Head and Neck Surgery, Section of Phoniatrics and Pediatric Audiology, Bohlenplatz 21, 91054 Erlangen.*
[3] *Technische Universität Dresden, Chair of Magnetofluiddynamics, Measuring and Automation Technology, George-Bähr-Str. 3, 01062 Dresden.*
[4] *Physikalisch-Technische Bundesanstalt (PTB) Berlin, Medical Physics and Metrological Information Technology, Biosignals, Biomagnetism, Abbestr. 2-12, 10587 Berlin.*
[5] *University Hospital Jena, Department of Radiology, Division of Diagnostic and Interventional Radiology, Experimental Radiology, Erlanger Allee 101, 07747 Jena.*

Background

Due to their special physicochemical properties, iron nanoparticles offer new promising possibilities for biomedical applications. For bench to bedside translation of SPIONs, safety issues have to be comprehensively clarified. To understand concentration-dependent nanoparticle-mediated toxicity, the exact quantification of intracellular SPIONs by reliable methods is of great importance.

Results

In the present study, we compared three different SPION quantification methods (ultraviolet spectrophotometry (UVS), magnetic particle spectroscopy (MPS), atomic adsorption spectroscopy (AAS)) and discussed the shortcomings and advantages of each method. Moreover, we used those results to evaluate the possibility to use flow cytometric technique to determine the cellular SPION content. For this purpose, we correlated the side scatter (SSc) data received from flow cytometry with the actual cellular SPION amount.

We showed that flow cytometry provides a rapid and reliable method to assess the cellular SPION content (Table 1).

quantification method	detection threshold unit (Ø + 3σ)	SEON^{LA}	SEON^{LA-BSA}	Rienso®
UVS	[μg_{Fe}/ml]	4.47	4.74	4.03
MPS	[μg_{Fe}/ml]	0.49	0.31	2.52
AAS	[μg_{Fe}/ml]	0.56	0.56	0.56
SSc	[%]	110.48	109.16	112.11

Table 1 Detection threshold for the UVS, MPS and ASS techniques with SPION-containing cell lysates indicated as μg_{Fe}/ml cell lysate. The detection threshold for SSc analysis is indicated in percentage compared to SSc data of untreated cells. The thresholds for UVS, MPS and SSc is dependent on the SPION nature, whereas ASS, a method quantifying elementary iron, is not. The determinations of the detection threshold were achieved using the 3σ criteria.

Our data also demonstrate that internalization of iron oxide nanoparticles in human umbilical vein endothelial cells is strongly dependent to the SPION type and results in a dose-dependent increase of toxicity (Fig. 1).

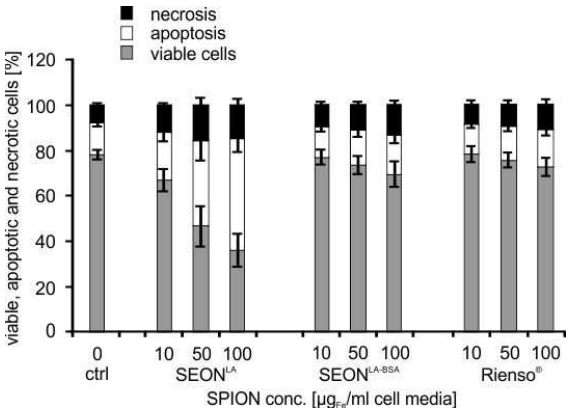

Figure 1 Association of cellular uptake with toxicity of SPIONs. HUVECs were incubated for 48 h with different amounts of SPIONs and cytotoxicity was analyzed by flow cytometry. Cell viability determined by annexin V/propidium iodide staining. Percentages of necrotic (PI+), apoptotic (Ax+, PI-) and viable cells (Ax-, PI-) are shown. Data are presented as mean standard error; n=3 with sample triplicates. The results were normalized untreated control cells, set to 100%

Thus, treatment with lauric acid (LA) coated SPIONs ($SEON^{LA}$) resulted in a significant increase in the intensity of SSc and toxicity, whereas $SEON^{LA}$ with an additional protein corona formed by bovine serum albumin ($SEON^{LA\text{-}BSA}$) and commercially available Rienso® particles showed only a minimal increase in both SSc intensity and cellular toxicity. The increase of the SSc was in accordance with the measurements of the SPION content by the AAS reference method.

Summary

Our data revealed that flow cytometry analysis can be used for the estimation of uptake of SPIONs by mammalian cells and provides a fast tool for scientists to evaluate the safety of nanoparticle products.

Acknowledgments

Statements of funding: This study was supported by the Deutsche Forschungsgemeinschaft (DFG: SPP1681 (AL 552/5-1, TR 408/8-1), OD 18/23-1, HI 698/7-4, TR 408/4-3, CI162/2-1), by the Bavarian State Ministry for Environment and Consumer Protection, and the DFG Cluster of Excellence – Engineering of Advanced Materials (EAM).

Coated ferromagnetic nickel nanorods affect cell vitality and intracellular signalling

A.-K. Schmidt[1], C. Gräfe[1], F. Krämer[2], K. Birster[2], M. Gratz[2], A. Tschöpe[2], A. Hochhaus[1], J. H. Clement[1]

[1] Klinik für Innere Medizin II, Abteilung Hämatologie und Internistische Onkologie, Universitätsklinikum Jena, 07747 Jena, Germany; ann-kathrin.schmidt@med.uni-jena.de; joachim.clement@med.uni-jena.de
[2] Experimentalphysik, Universität des Saarlandes, 66123 Saarbrücken, Germany

Introduction

Magnetic materials with a high magnetisation come into scope of biomedical research. There have been several attempts to use nickel nanoparticles in biomedicine, for example as drug or gene delivery systems [1, 2]. The low biocompatibility of nickel ions makes a tight coating indispensable. We investigate the effects of coated nickel nanorods on cell viability and intracellular signalling of human brain microvascular endothelial cells (HBMEC) which are a commonly used model for the human blood brain barrier [3].

Methods

HBMEC were cultivated with RPMI1640 supplemented with 10% fetal calf serum and 1% Penicillin/Streptomycin in a humidified incubator at 37°C and 5% CO_2. The cells were incubated with different concentrations of gelatine, polyvinylpyrrolidone (PVP), SiO_2, and SiO_2-rhodamine coated nickel (Ni) nanorods (Figure 1), respectively.
The nanorods were synthesised by the AAO-template method and transferred into colloidal suspension by dissolution of the template in a dilute aqueous NaOH solution to which PVP was added as surfactant [4]. Gelatine coating was obtained by spontaneous adsorption after mixing the nanorod colloid with a gelatine sol. The silica encapsulation was realised by a Stöber process carried out in the presence of PVP coated nanorods [5, 6, 7].

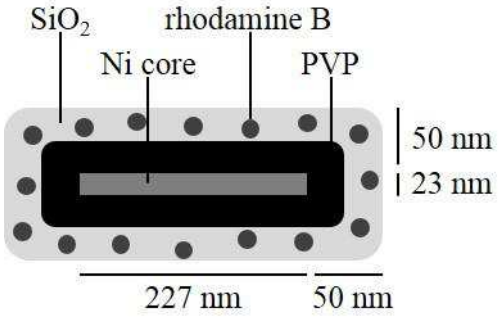

Figure 1: Schematic representation of SiO_2-rhodamine coated nickel nanorods.

The cellular uptake was studied with confocal laser scanning microscopy. PrestoBlue® Cell Viability Assay was performed to determine the overall cytotoxic effects of the nanorods on HBMEC. The influence on pro-survival and stress-associated signalling cascades involving AKT, GSK-3β, and MAP kinases was analysed by Western blotting.

Results

At first we extended our vitality studies. We reported earlier that SiO_2 coated Ni nanorods did not affect the vitality of HBMEC up to a concentration of 260 ng/cm^2. Increasing the concentration up to 25 µg/cm^2 led to a continuous reduction of cell vitality to 40% of control. Gelatine and polyvinylpyrrolidone coated nanoparticles did not affect cell viability of HBMEC (Figure 2). Therefore, we used low concentrations of SiO_2-rhodamine coated Ni nanorods for cell interaction studies and PVP coated Ni nanorods for intracellular signalling analyses.

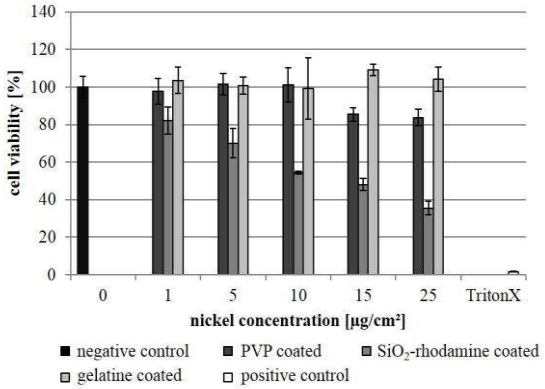

Figure 2: PrestoBlue® Cell Viability Assay was performed after 3h of incubation with the indicated concentrations of SiO_2-rhodamine, polyvinylpyrrolidone (PVP), and gelatine coated Ni nanorods. Data are expressed as percentage of untreated control. Means ± SDV of four replicates are shown.

Next, we investigated the time course of Ni nanorod-cell interaction by applying 1.5 µg/cm^2 Ni nanorods to HBMEC. Already after 30 minutes Ni nanorods could be detected within the cells by confocal laser scanning microscopy. The amount of incorporated nanorods increased continuously over time. During that interaction no morphological changes of the cells could be observed. Western blot analysis revealed that intracellular signalling cascades were influenced by nickel nanorods. Rising concentrations of PVP coated nickel nanorods caused an increase of activation of AKT and the MAP kinase p38.

Conclusion

Coated nickel nanorods affect the viability of HBMEC in dependence of the coating, the concentration, and the incubation time. The internalisation of Ni nanorods occurs rapidly after application to the cell monolayers. The interaction and internalisation of Ni nanorods activates survival and stress-associated pathways, especially the AKT signalling cascade. Next, long-term effects on cell physiology as well as AKT down-stream targets need to be considered.

Acknowledgments

This work was supported by the DFG high priority program 1681 (Grants CL202/3-1 and TS62/4-1).

References

[1] Guo et al. (2009). "Study on the enhanced cellular uptake effect of daunorubicin on leukemia cells mediated via functionalized nickel nanoparticles.“ Biomed Mater 4(2): 025013.

[2] Salem et al. (2003). "Multifunctional nanorods for gene delivery." Nat Mater 2(10): 668-671.

[3] Stins et al. (2001). "Bacterial invasion and transcytosis in transfected human brain microvascular endothelial cells." Microbial Pathogenesis 30(1): 19-28.

[4] Günther et al. (2011). „Rotational Diffusion of Nickel Nanorods in Colloidal Dispersion“ J. Phys.: Condens. Matter 23: 325103.

[5] Stöber and Fink (1968). “Controlled Growth of Monodisperse Silica Spheres in the Micron Size Range”, J. Coll. Interf. Sci., 26(1):62 – 69.

[6] Hardikar and Matijevic (2000) “Coating of Nanosize Silver Particles with Silica”, J. Coll. Interf. Sci. 221(1):133 – 136.

[7] Graf et al. (2003) “A General Method To Coat Colloidal Particles with Silica”, Langmuir, 19(17):6693–6700.

Passage of SPIONs through cell layers

C. Gräfe[1], I. Slabu[2], F. Wiekhorst[2], R. Müller[3], A. Hochhaus[1], F. von Eggeling[3,4,5], L. Trahms[2], J.H. Clement[1]

[1] *Klinik für Innere Medizin II, Abteilung Hämatologie und Internistische Onkologie, Universitätsklinikum Jena, Jena, Germany; christine.graefe@med.uni-jena.de; joachim.clement@med.uni-jena.de*
[2] *Physikalisch-Technische Bundesanstalt, Berlin, Germany*
[3] *Leibniz-Institut für Photonische Technologien, Jena, Germany*
[4] *Klinik für Hals-, Nasen-, Ohrenheilkunde, Universitätsklinikum Jena, Jena, Germany*
[5] *Institut für Physikalische Chemie, Friedrich-Schiller-Universität Jena, Jena, Germany*

Introduction

Based on their remarkable and unique properties superparamagnetic iron oxide nanoparticles (SPIONs) have been moved into the focus of biomedicine [1,2]. The introduction of SPIONs into a biological system commonly means a direct interaction with cellular structures, e.g. cells within the blood stream, endothelial cells lining the blood vessels or even epithelial cells in underlying tissues. For a reasonable assessment of SPION interactions with biological environment not only cytotoxicity but also cellular activity studies including how SPIONs cross biological barriers must be studied in detail.

The aim of our project is to establish a standardized *in vitro* test system to investigate and understand the passage of coated SPIONs through cell layers driven by magnetic forces. Of special interest is the interaction with the extracellular matrix, the cell membrane as well as intracellular lipid bilayers, e.g. endosomal/lysosomal, mitochondrial or nuclear membranes. Finally, the consequences of such SPION interactions on protein corona formation and cellular import and export are of interest.

Materials and Methods

We used human brain microvascular endothelial cells (HBMEC) to establish a cellular monolayer on the transwell system with an optimal pore size of 3 µm allowing NP permeation into the lower compartment (Figure 1). The tightness of the cell layer was evaluated by measuring the transendothelial electrical resistance (TEER), sodium fluorescein (NaFl) permeability assays, and immunofluorescent staining of tight junction protein *zonula occludens* (ZO-) 1. Starch-coated fluidMAG-D (chemicell GmbH, Berlin) was used for incubation experiments as earlier studies revealed good biocompatibility of these SPIONs [3,4]. Magnetic particle spectroscopy (MPS) [5] was used to exactly quantify SPION-associated iron.

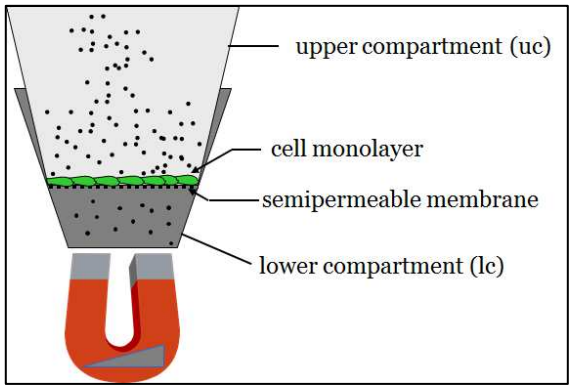

Figure 1: Scheme on experimental setup.

Cells were incubated with fluidMAG-D in a concentration range from 25 to 100 µg/cm^2 in the presence of 10 % fetal calf serum (FCS). The first 30 min of incubation time were carried out on top of a permanent magnet (350 mT at the surface, field gradient at the used distance from the magnet: 10 – 15 T/m) whereupon the magnet was removed and incubation time was completed without the influence of the external magnetic field. All sections including the upper compartment, membrane/cells, and the lower compartment were sampled and analysed by MPS. For this, the third harmonics of the MPS spectra were normalized to the

moment of a SPION reference sample of known iron amount.

Results and Discussion

First we confirm the accurate tightness of the HBMEC monolayer. TEER, molecular NaFl permeability, and ZO-1 localization are affected by the cell medium composition. Conditioned medium enhanced cell-cell contacts and FCS strongly increase TEER and reduce sodium fluorescein permeability.

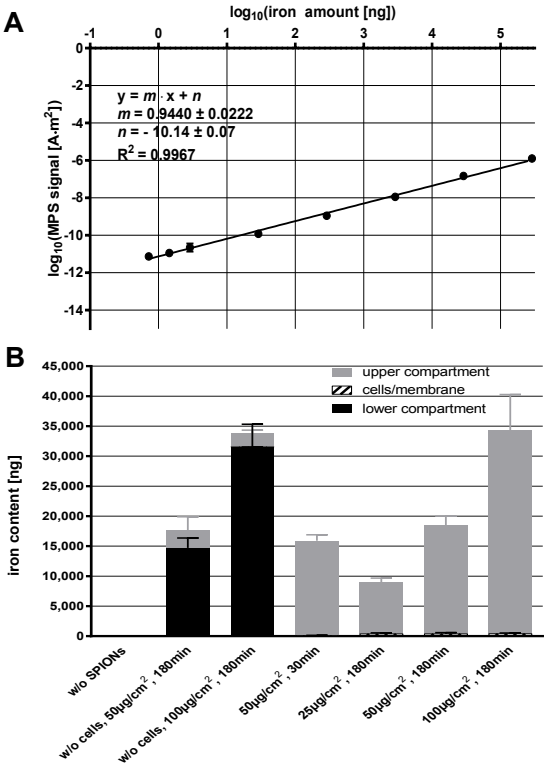

Figure 2: SPION-associated iron quantification by magnetic particle spectroscopy (MPS)*. Standard curve of MPS signals obtained from fluidMAG-D dilution series (A). Compartment-specific iron recovery upon indicated incubation conditions (B).*

MPS data obtained from SPION dilution series indicate excellent correlation between MPS signal and iron amount (Figure 2A) with a high level of sensitivity down to 1ng of iron.Further iron quantification data summarized in figure 2B indicate that SPIONs easily traverse cell-free membranes whereas the presence of cells on the membrane nearly completely prevents SPION crossing confirming high cell layer tightness. Nevertheless, low but significantly increased iron contents can be detected within the lower compartment upon 180min of incubation representing about 0.03% of total iron yield. The HBMEC monolayer contains roughly 2% of the applied iron amount. After a short-term incubation (30 min) the detectable iron content is below the detection limit indicating that SPIONs need some time to attach to the cell surface and then traverse the cellular barrier by transcytosis rather than via intercellular gaps. The magnetic enrichment of these transcytosed SPIONs will enable a detailed analysis of SPION surface regarding protein corona and phospholipid membrane contents. In consequence these studies permit detailed information on cellular interaction and processing. These results encourage us to use this experimental setting for further cell-nanoparticle interaction studies where a variety of particles can be tested in a standardized manner. Thus, systematic and reliable nanoparticle assessment contributes to the development of tailor-made and safe SPIONs for intended purposes.

Conclusion

The presented workflow seems appropriate for further precise SPION quantifications during nanoparticle-cell-interaction studies using the combination of the *in vitro* transwell system with magnetic particle spectroscopy quantification.

Acknowledgements

The perfect technical assistance of Cornelia Jörke is highly acknowledged. This work was supported by Deutsche Forschungsgemeinschaft (DFG) in the framework of the priority program 1681 (FKZ: CL202/3-1; TR408/8-1; MU2382/4-1) and KFO 213 (TR408/5-3).

References

[1] S. Dutz, J.H. Clement, D. Eberbeck, T. Gelbrich, R. Hergt, R. Müller, J. Wotschadlo, M. Zeisberger, *J. Magn. Magn. Mater.* **2009**, *321, 1501-1504*.

[2] J Estelrich, E. Escribano, J. Queralt, M.A. Busquets, *Int. J. Mol. Sci.***2015**, *4, 8070-8101*

[3] A. Theumer*, C. Gräfe*, F. Bähring, C. Bergemann, A. Hochhaus, J. H. Clement, *JMMM* **2014**, *380, 27-33*.

[4] F. Bähring, F. Schlenk, J. Wotschadlo, N. Buske, T. Liebert, C. Bergemann, T. Heinze, A. Hochhaus, D. Fischer, J.H. Clement, *IEEE T. Magn.* **2013**, *49, 383-388*.

[5] F. Wiekhorst, U. Steinhoff, D. Eberbeck, L. Trahms, Pharm. Res. **2012** *5, 1189-1202*

List of participants

Ingo Appel
Karlsruhe Institute of Technology
ingo.appel@kit.edu

Kira Arndt
Universität Rostock
kira.arndt@uni-rostock.de

Abdolhamid Attaran
TU Dresden
Abdolhamid.Attaran@tu-dresden.de

Dr. Günter K. Auernhammer
Max Planck Institute for Polymer Research
auhammer@mpip-mainz.mpg.de

Dr. Silke Behrens
Karlsruhe Institute of Technology
silke.behrens@kit.edu

Dr. Philipp Bender
Universidad de Cantabria
philipp.bender@unican.es

Kerstin Birster
Universität des Saarlandes
k.birster@nano.uni-saarland.de

Dr. Dmitry Borin
TU Dresden
dmitry.borin@tu-dresden.de

Prof. Dr. Helmut R. Brand
Universität Bayreuth
brand@uni-bayreuth.de

Norbert Buske
MagneticFluids
n.buske@magneticfluids.de

Dr. Joachim H. Clement
Universitätsklinikum Jena
joachim.clement@med.uni-jena.de

Annelies Coene
Ghent University
annelies.coene@ugent.be

Peet Cremer
Heinrich-Heine-Universität Düsseldorf
pcremer@thphy.uni-duesseldorf.de

Johanna Demut
Universitätsklinkum Jena
johanna.demut@med.uni-jena.de

Joe G. Donaldson
University of Vienna
joe.donaldson@univie.ac.at

Dr. Silvio Dutz
TU Ilmenau
silvio.dutz@tu-ilmenau.de

Dr. Dietmar Eberbeck
Physikalisch-Technische Bundesanstalt Berlin
dietmar.eberbeck@ptb.de

Dr. Birgit Fischer
Universität Hamburg
birgit.fischer@chemie.uni-hamburg.de

Christine Gräfe
Universitätsklinikum Jena
christine.graefe@med.uni-jena.de

Thomas Gundermann
TU Dresden
thomas.gundermann@tu-dresden.de

Dr. Dirk Heinrich
TU Berlin
dhein@physik.tu-berlin.de

Shilin Huang
Max Planck Institute for Polymer Research
huangs@mpip-mainz.mpg.de

Dr. Markus Kästner
TU Dresden
markus.kaestner@tu-dresden.de

Joachim Landers
University of Duisburg-Essen
joachim.landers@uni-due.de

Julia Linke
TU Dresden
julia.linke@tu-dresden.de

Dr. Stefan Lyer
University Hospital Erlangen
stefan.lyer@uk-erlangen.de

Sarah Metzke
TU Berlin
s.metzke@tu-berlin.de

Johannes Nowak
TU Dresden
johannes.nowak@tu-dresden.de

Giorgio Pessot
Heinrich-Heine-Universität Düsseldorf
giorgpess@thphy.uni-duesseldorf.de

Dr. Oliver Posth
Physikalisch-Technische Bundesanstalt
oliver.posth@ptb.de

Dr. Richter Reinhard
Universität Bayreuth
reinhard.richter@uni-bayreuth.de

Eric Roeben
Universität zu Köln
eroeben@uni-koeln.de

Malte Schümann
TU Dresden
Malte.Schuemann@tu-dresden.de

Michael Koof
Universität Rostock
michael.koof@uni-rostock.de

Jonathan Leliaert
Ghent University
jonathan.leliaert@ugent.be

Dr. Frank Ludwig
TU Braunschweig
f.ludwig@tu-bs.de

Jasmin Matuszak
University Hospital Erlangen
jasmin_matuszak@uk-erlangen.de

Dr. Robert Müller
Leibniz-Institut für Photonische Technologien
robert.mueller@ipht-jena.de

Prof. Dr. Stefan Odenbach
TU Dresden
stefan.odenbach@tu-dresden.de

Prof. Dr. Harald Pleiner
Max Planck Institute for Polymer Research
pleiner@mpip-mainz.mpg.de

Dr. Helene Rahn
TU Dresden
Helene.Rahn@tu-dresden.de

Hilke Remmer
TU Branschweig
h.remmer@tu-bs.de

Ann-Kathrin Schmidt
Universitätsklinikum Jena
ann-kathrin.schmidt@med.uni-jena.de

Ahmad Shaaban
Universität zu Köln
ahmad.shaaban@uni-koeln.de

Romy Sandig
TU Ilmenau
romy.sandig@tu-ilmenau.de

Julian Seifert
Universität Rostock
julian.seifert@uni-rostock.de

Erik Siebert
TU Dresden
erik.siebert@tu-dresden.de

Christian Spieler
TU Dresden
Christian.Spieler@tu-dresden.de

Lisa Sprenger
TU Dresden Chair of Magnetofluiddynamics Measuring and Automation Technology
Lisa.Sprenger@tu-dresden.de

Dr. Uwe Steinhoff
Physikalisch-Technische Bundesanstalt
uwe.steinhoff@ptb.de

René Steinmeier
Volkswagen AG
rene.steinmeier@volkswagen.de

Andreas Tschöpe
Universität des Saarlandes
a.tschoepe@nano.uni-saarland.de

Harald Unterweger
ENT Clinic Erlangen
harald.unterweger@uk-erlangen.de

Dr. Tatiana Volkova
TU Ilmenau
Tatiana.volkova@tu-ilmenau.de

Prof. Dr. Joachim Wagner
Universität Rostock
joachim.wagner@uni-rostock.de

Prof. Dr. Thomas Wallmersperger
TU Dresden
thomas.wallmersperger@tu-dresden.de

Andreas Weidner
TU Ilmenau
andreas.weidner@tu-ilmenau.de

Emilia Wisotzki
Leibniz Institute of Surface Modification (IOM)
emilia.wisotzki@iom-leipzig.de

Marcus Witt
TU Berlin
m.witt@tu-berlin.de

Mengbo Zhou
Universität Jena
mengbo.zhou@uni-jena.de

Falko Ziegert
Universität Rostock
falko.ziegert@uni-rostock.de

Dr. Sabina Ziemian
Bayer Pharma AG
sabina.ziemian@bayer.com